MODELING PERFORMANCE OF HORIZONTAL, UNDULATING, AND MULTILATERAL WELLS

A Dissertation

by

RUNGTIP KAMKOM

Submitted to the Office of Graduate Studies of
Texas A&M University
in partial fulfillment of the requirements for the degree of

DOCTOR OF PHILOSOPHY

August 2007

Major Subject: Petroleum Engineering

MODELING PERFORMANCE OF HORIZONTAL, UNDULATING,

AND MULTILATERAL WELLS

A Dissertation

by

RUNGTIP KAMKOM

Submitted to the Office of Graduate Studies of
Texas A&M University
in partial fulfillment of the requirements for the degree of

DOCTOR OF PHILOSOPHY

Approved by:

Chair of Committee,	Ding Zhu
Committee Members,	A. Daniel Hill
	Akhil Datta-Gupta
	J. Eric Bickel
Head of Department,	Stephen A. Holditch

August 2007

Major Subject: Petroleum Engineering

ABSTRACT

Modeling Performance of Horizontal, Undulating, and Multilateral Wells.

(August 2007)

Rungtip Kamkom, B.Eng., King Mongkut's University of Technology Thonburi;

M.S., New York Institute of Technology;

M.S., University of Texas at Austin

Chair of Advisory Committee: Dr. Ding Zhu

Horizontal, undulating, and multilateral wells are relatively new alternatives in field development because they can increase the productivity per well and reduce the cost of field development. Because the feasibility of these wells may not be valid in some reservoirs, well performance should be verified before making decisions. Undulation is usually associated to horizontal wells with some degrees. Existing inflow performance models do not account for the undulation of the well, which can cause significant error and economic loss. Moreover, some of the inflow models ignore pressure drop along the lateral, which is definitely not true in high production and long lateral wells.

The inflow performance models of horizontal, undulating, and multilateral wells are developed in this study. The models can be divided into two main categories: the closed form model and the line source model. The closed form model applies for relatively low vertical permeability formations for the single-phase system and two-phase system. The model is flexible and easy to apply with reasonable accuracy. The line source model does not have any restrictions with permeability. The model applies for single-phase system. The model is very accurate and easy to use. Both models can be applied to various well trajectories with realizable accuracy. As a result of this study, the well performance of unconventional well trajectories can be predicted and optimized.

DEDICATION

To my parents, Vilai and Choochai Kamkom

To my brother, Tamrong and Theera Kamkom

To my husband, Terapat Apichartthabrut

ACKNOWLEDGMENTS

Although this dissertation would not have been possible without the help of many people, my first gratitude would go to my adviser, Dr. Ding Zhu. I would like to express my sincere appreciation to Dr. Ding Zhu for giving me the opportunity to pursue my Ph.D. at Texas A&M University. I am grateful to her commitment and encouragement throughout my study. Her guidance, patience, and generosity made me where I am today.

My truthful gratitude is extended to my committee members, Dr. A. Daniel Hill, Dr. Akhil Datta-Gupta and Dr. J. Eric Bickel for their suggestions and comments on my dissertation. I would like to especially thank Dr. A. Daniel Hill for his valuable advice and his generosity. I also thank Dr. Christine Ehlig-Economides for her precious time and comments.

This degree and dissertation could not be completed without my husband, Terapat Apichartthabrut, who always loved and supported me. I deeply appreciate his dedication and time during my graduate study. I cannot imagine how I could have graduated without him, and he definitely deserves this award as much as I do.

I also would like thank my colleagues, Maysam Pournik, Weibo Sui and Keita Yoshioka for their friendship and help during my graduate study.

Finally, my gratitude goes to my parents, Vilai and Choochai Kamkom, for their devotion and love.

TABLE OF CONTENTS

LIST OF TABLES

LIST OF FIGURES

CHAPTER I

INTRODUCTION

1.1 Background

Horizontal wells, undulating wells, and multilateral wells are relatively new technologies in oil and gas field developments. Their main advantages include increasing the productivity per well, accessing the unconventional resources, and reducing the number of well needed and thereby reducing the cost of field development. However, because the complexity involves both reservoirs and well structures, and also because of the higher cost of drilling and completion of these wells, well performance should be studied carefully before making decisions. Well performance models are very essential in many activities such as well design, production optimization, field development, and reservoir management. A reliable and accurate inflow performance model is very crucial for these tasks.

The methodologies used to analyze well productivity are divided in two main approaches: numerical simulation and analytical solution. The numerical method usually requires intensive input data to describe the reservoir/well system, and is a time-consuming procedure. Refined grids are usually needed to capture the well trajectory and well location, particularly for complex well structures. In most numerical simulation models, the wellbore pressure drop is neglected. For complex well applications, the wellbore pressure drop often becomes a critical factor for well performance. The models may provide misleading information when the wellbore pressure drop is not considered.

Analytical well performance models have been developed for vertical wells, horizontal wells, and slanted wells. With some assumptions, these models present explicit relationships between a flow rate and a wellbore flowing pressure. The models are much easier to apply compared with numerical models. Wellbore pressure drop can be included by coupling inflow models with wellbore flow models. However, the actual

---

This dissertation follows the style of the *SPE Journal*.

reservoir and well structures in reality are usually much more complex than the assumptions made in the closed form models. The closed form models may have some errors, and sometimes the error can be significant. For example, most horizontal well models assume that the horizontal wellbore is perfectly horizontal. Actual horizontal wells are not perfectly horizontal as a result of a lack of sufficient drilling control or varying formation structures. Using horizontal well models to evaluate the performance of intensive undulating well may result in significant deviation.

The main purpose of this dissertation is to predict and optimize the well performance of unconventional well structures including horizontal wells, undulating wells, and multilateral wells. It also presents models and effective procedures to evaluate well performance. The new procedures reduce the limitation of the existing model and make the model more practical. For instance, well trajectories can be undulated and reservoir boundary conditions can be steady-state condition, pseudo-steady-state condition or mixed boundary condition. As a result of this dissertation, the accuracy of performance models of horizontal wells, undulating wells, and multilateral wells is improved and the models will be more applicable in various well trajectories. Moreover, this research presents the methodology to account for two-phase inflow performance in horizontal wells, undulating wells, and multilateral wells which eliminate the limitations of available models.

1.2 Literature Review

Many closed form models of horizontal wells have been published to evaluate the well performance. These models are usually based on either a steady-state condition or pseudosteady-state condition. The models under the steady-state condition were presented for ellipsoidal or box-shaped reservoirs. There are two well-known models for ellipsoid drainage volume. The first model is Joshi's model[1] and the second model is Economides model[2]. Joshi presented his model in 1988. He divided the three-dimensional flow problem into two two-dimensional problems to obtain the horizontal performance model. For a box-shaped reservoir, the models were presented by Bulter[3]

and Furui[4]. Although their models are derived by different methods, these models are very similar. Butler's model was obtained by applying the superposition principle and the image technique. On the other hand, Furui's model was based on the finite element model. Both of these models assume no-flow boundary at the top and the bottom of the formation, the z-direction, and constant pressure in the x-direction. For Butler's model, the model predicts the productivity of fully penetrated well and the well can be off center in the z-direction. In 2003, Furui presented a closed form model for fully penetrated horizontal well. He divided the flow to a horizontal well into two regimes, a radial flow region near the wellbore and a linear flow region away from the wellbore. The well is located in the center of the reservoir. A widely used model under the pseudosteady-state condition is Babu and Odeh's model[5]. Babu and Odeh presented the horizontal well productivity model in a box-shaped reservoir. The only limitation in their model is that the well has to be parallel to the y-axis. All of the above models are limited to a perfectly horizontal well and a single-phase reservoir.

In general horizontal well models do not account for the undulating effect of well trajectories which is not the case in reality. Normally, a horizontal well is not perfectly horizontal. Almost every well has a certain degree of undulation in wellbore trajectory. Many studies[6-8] show that the undulating effect should be considered, especially when the degree of undulation is intensive. Goktas and Ertekin[6] showed that the pressure responses of wells with intensive undulation deviate from the responses of horizontal wells. They also noted that the pressure drop along the wellbore in high production well should be considered in order to improve the accuracy of the evaluation of well performance. Additionally, the study of Al-Mohannadi[7] *et al*. confirmed that when the degree of undulation is not severe, the pressure responses of the undulating well agree very well with those of the horizontal well. On the other hand, when the well is extremely undulating, the effective well length is significantly longer than that from the straight wellbore length, which results in the pressure responses of undulating wells to differ from the pressure responses of horizontal wells. Azar-Nejad *et al.*[8] also showed that applying the horizontal well model to an undulating well may create significant

error. These previous studies showed that the wellbore performance model of an intensive undulating well is necessary for evaluating the well performance.

1.3 Objectives

The objective of this study is to develop systematic analytical well performance models that can be used

- To predict the well performance of horizontal wells, undulating wells, and multilateral wells in anisotropic formations under different boundary condition for single-phase oil, single-phase gas and two-phase oil and gas reservoir.
- To study the effects of well structure on well performance and productivity.
- To optimize well design for maximum well performance in different reservoir conditions.

1.4 Organization of the Dissertation

The dissertation is divided into six chapters. Chapter I outlines the dissertation with the research background, the literature review, and the objectives. The dissertation outline gives a brief overview of the dissertation. The literature review provides the status of the research that is available relating to this subject. The objectives list the intent and the organization of the dissertation.

In Chapter II, the horizontal well performance models are reviewed and summarized in a systematic way. The intent of this chapter is to review the available horizontal well models for different flow systems under varieties of reservoir boundary conditions. The models were for single-phase oil, single-phase gas, and two-phase oil and gas reservoirs. For each fluid flow system, the models were investigated for steady-state and pseudosteady-state condition. A method to account for the pressure effect along the wellbore is presented.

Chapter III presents the methodology used to apply the line source solution to estimate the inflow performance of a variety of well trajectories in a single-phase

reservoir. The reservoir is considered homogeneous and it can be either isotropic or anisotropic. The initial boundary condition is constant pressure in the reservoir. The outer boundary condition can be steady-state, pseudosteady state or mixed. For the inner boundary condition, uniform flux, infinite conductivity or finite conductivity can be used.

Chapter IV introduces models for undulating well performance. Two approaches are discussed for performance of undulating wells. The first model is an analytical approach that applies a modified vertical well model along with a slanted skin model, and a shape factor. The application using the line source solution to model on undulating well is presented. After that the undulating well performance obtained by the closed form model is compared with that obtained using the line source model.

Chapter V discusses multilateral well performance. The first section presents the methodology used for a horizontal well model along with assumptions to evaluate multilateral well performance for single-phase and two-phase reservoirs. The second section shows the procedure for applying the line source solution to model multilateral well performance. This application can predict the performance of any type of multilateral well trajectories.

The last chapter, Chapter VI, presents conclusions and recommendations from the research.

CHAPTER II

CLOSED FORM MODELS FOR HORIZONTAL WELLS

Many horizontal well models[1-5, 9-10] have been published under different boundary condition assumptions. In general, these assumptions define the applications of models. In order to apply models properly, these assumptions should be understood clearly. In this chapter, we review horizontal well performance models and modify the horizontal performance model under steady-state condition for single-phase oil wells. We also present gas inflow performance models for horizontal wells under steady-state and pseudosteady-state conditions. Then the models are summarized in the systematic table for horizontal well performance. In addition to the coupling model of wellbore performance and wellbore flow, the effect of wellbore pressure drop on horizontal well performance is also addressed.

2.1 Single-Phase Oil Wells

Although there have been horizontal well models presented for undersaturated oil reservoirs[1-5], the applications of these models are different depending on reservoir boundary conditions. The distinctions of each model should be clarified so each model can be used properly.

2.1.1 Transient Flow Equation

The transient flow in a horizontal well is divided into 4 periods, early time radial flow, intermediate time linear flow, late time radial flow, and late time linear flow. Some periods may not occur in some cases. For example, if the ratio of well length to drainage area is very low, intermediate time linear flow may not occur because the horizontal well acts like a point sink, thus, the flow will be late time radial flow instead[9].

The early time radial flow occurs before the flow reach both top and bottom boundaries. After the top and the bottom boundaries have been encountered, the flow becomes intermediate time linear flow unless the well length is relatively short comparing with drainage area. The late time radial flow occurs if the drainage area is relatively large comparing with the well length. Finally, after all boundaries have been reached, the flow is in the late time linear flow. Goode and Thambynayagam[10] presented the transient flow models of horizontal wells in 1987. The original work was done for a well test purpose. The models are based on uniform production along horizontal wells. The models were presented for both drawdown test and build up test. Their model has been used widely to analyze the pressure transient in horizontal wells. In 1994, Yildiz and Ozkan[11] presented the pressure transient model for non-uniform production along horizontal wells. The model is useful in many applications, one of them is when the damage skin varies along a horizontal well, and the productivity index is not a constant. With fully appreciation of the value of transient flow models, well testing, and other applications, for longer term production, we focus on the models at steady-state and pseudosteady-state conditions in this study.

2.1.2 Steady-State Condition

Joshi published the first horizontal well performance model in SPE literature 1988, and the model is still commonly used today in the industry. After Joshi's work, several models were developed to improve the method of estimating production rate for horizontal wells under the steady-state condition. The model developed by Furui *et al*. assumes that the flow regime of a horizontal well can be divided into two parts, the radial flow part around the wellbore, and the liner flow part away from the wellbore. The total pressure drop is the sum of the pressure drops in these two regions. The concept is demonstrated in Fig. 2.1. This model can be coupled with a wellbore pressure drop model to estimate the pressure drop along horizontal wells, which have been proven to be the important issue in horizontal well production. Furui *et al*.'s model describes the relationship between flow rate and pressure drawdown as shown in Eq. 2.1

$$q_o = \frac{k_{eq}L(p_e - p_{wf})}{141.2B_o\mu_o\left(ln\left[\frac{hI_{ani}}{r_w(I_{ani}+1)}\right] + \frac{\pi y_b}{hI_{ani}} - 1.224 + s\right)} \qquad (2.1)$$

where k_{eq} is defined as $\sqrt{k_H k_V}$.
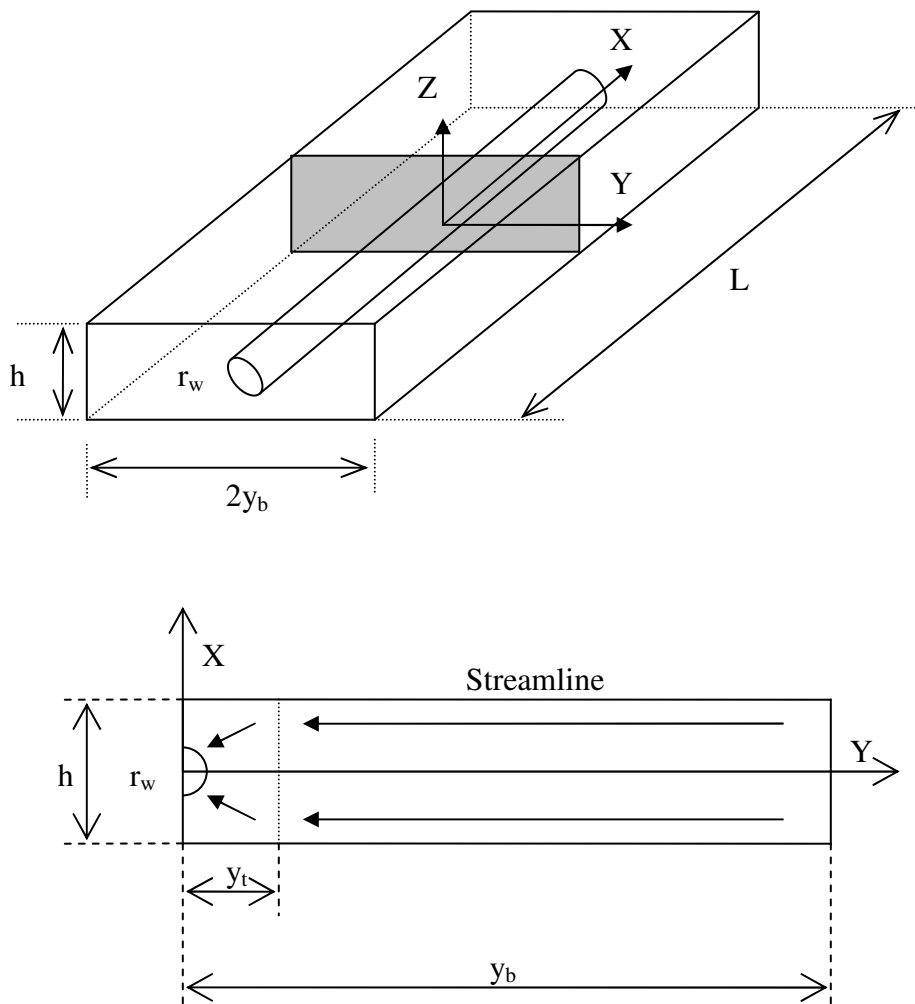
Fig. 2.1 Geometry model for steady-state flow equation.

One weakness of this model is that the model only applies for fully penetrating horizontal wells. In other words, the wellbore length is set equal to the drainage length in the model. This greatly limits the model applications since horizontal wells are rarely drilled fully penetrating. When implement the model to estimate the production rate, the reservoir beyond the wellbore length is assumed to be non-producing, which results in underestimating well performance of partial penetrating wells.

To improve the model, we modify Furui *et al.*'s model by adding a partial penetrated skin factor to account for partial penetration. A partial penetrated skin factor calculation for horizontal wells in a box-shaped reservoir was presented by Babu and Odeh's model. Directly adapting the partial penetration skin factor, the steady-state flow equation with the modification for partially penetrating wells can be expressed as

$$q_o = \frac{k_{eq}b(p_e - p_{wf})}{141.2B_o\mu_o\left(ln\left[\frac{hI_{ani}}{r_w(I_{ani}+1)}\right] + \frac{\pi y_b}{hI_{ani}} - 1.224 + s + s_R\right)} \qquad (2.2)$$

where, s_R is partial penetrated skin factor and b is the reservoir drainage dimension along the horizontal well direction. We realize that Babu and Odeh's model was developed for pseudosteady-state condition. In order to add the skin to the inflow equation under steady-state condition, we need to validate the approach first. The modified Furui *et al.*'s model is compared with the line source model (Appendix A) for steady-state flow. The comparison   for horizontal well under a wide range of parameters is shown in Fig. 2.2.
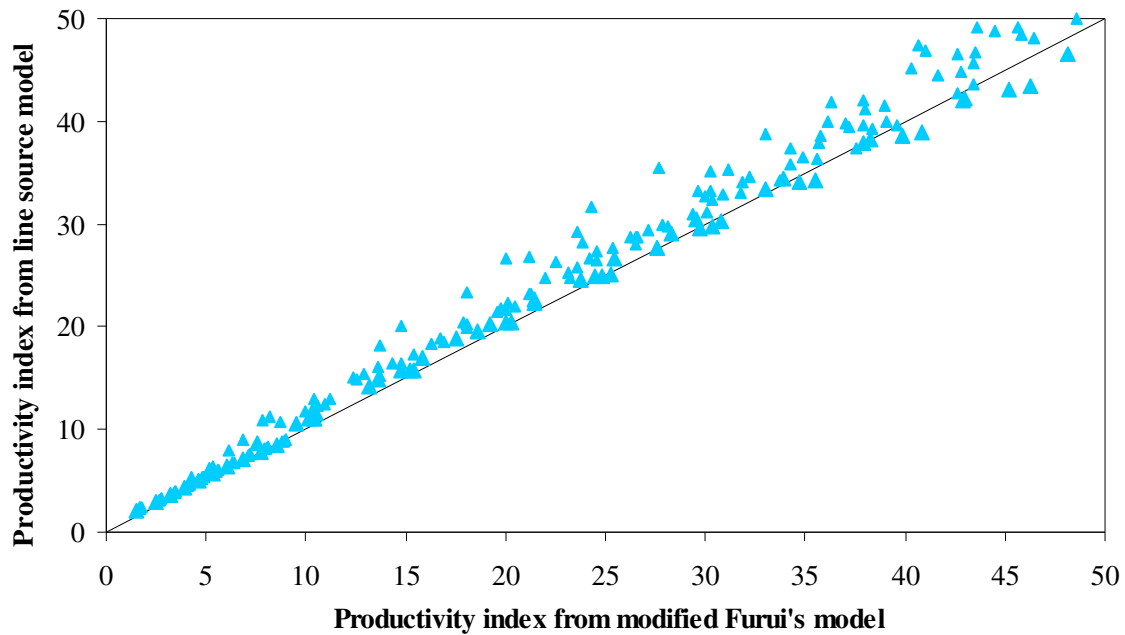
Fig. 2.2 Validation modified Furui's model with line source solution.

The comparison shows that the productivity index obtained by the line source model is almost the same as the productivity index obtained by the modified Furui *et al*.'s model (Eq. 2.2), indicating that in general the modified Furui *et al*.'s model can be used to predict the horizontal well for non-fully penetrating wells under steady-state condition.

It is noticed that for certain conditions, the results from the modified Furui *et al*.'s model deviate from the line source model at high productivity index. After analyzing the condition that the deviation occurs, we recognize that the deviation mainly relates to the length of horizontal wells and anisotropic ratios. Thus, we compare the productivity index calculated by the line source model with that by Eq. 2.2 at different anisotropic ratios and different well lengths; the results are shown in Fig. 2.3.

Fig. 2.3 shows that when a reservoir is anisotropic, Eq. 2.2 can be used to estimate the performance of partial penetrating horizontal wells with fair accuracy, but when a reservoir is isotropic ($k_H = k_V$), Eq. 2.2 deviates from the line source model. In addition, we also see that when the well is much shorter than the reservoir size, the

modified Furui *et al.*'s model creates error in productivity calculation. If a well penetrates 80% through isotropic reservoir, the different between the line source model and the closed form model with partial penetrated skin is less than 5%. The study shows that for the well at least 50% penetrates through the reservoir the error is less than 10% for isotropic reservoir.
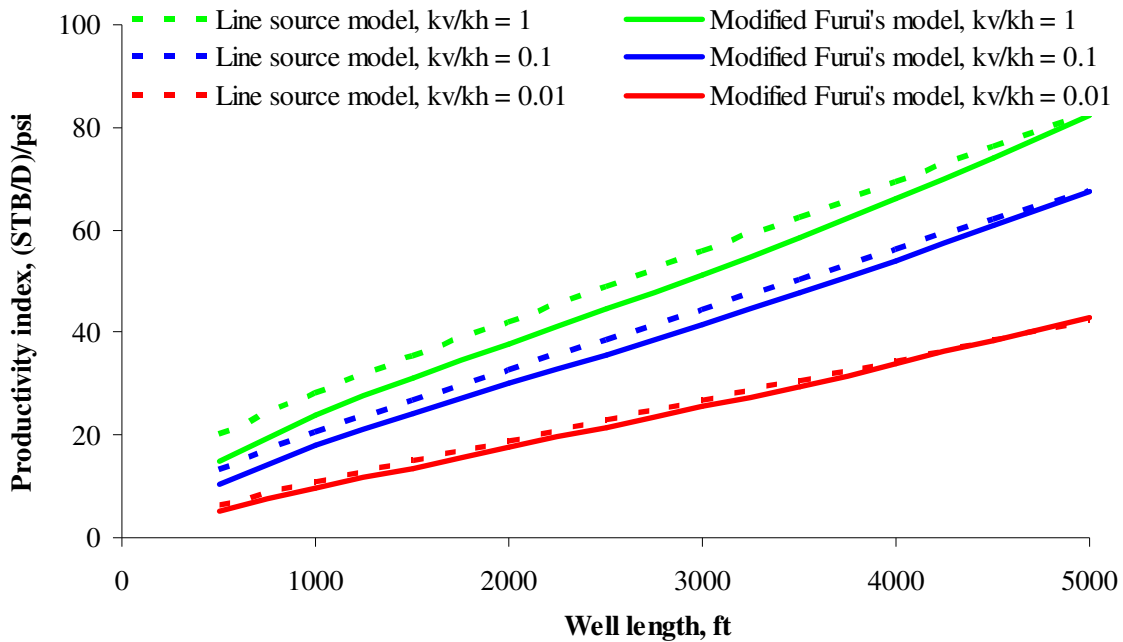
Fig. 2.3 Sensitivity study on well length and anisotropic ratio on partial penetrating well model.

2.1.3 Pseudosteady-State Condition

For pseudosteady-state flow, the most commonly used model was presented by Babu and Odeh. The horizontal well is placed parallel to one of the reservoir boundaries. The model was derived from the line source solution of single-phase oil diffusivity equation

$$\nabla^2 p = \frac{\phi c_t \mu}{k} \frac{\partial p}{\partial t} \tag{2.3}$$

The line source solution of Eq. 2.3 as a result of a uniform constant flow rate, q_o, into a horizontal well is

$$\Delta p = \left[\frac{B_o \mu_o q_o}{\alpha L}\right] \int_0^t \int_{y_1}^{y_2} (S_x S_y S_z) dy_o d\tau \tag{2.4}$$

where $\alpha = \phi \mu c_t$ and,

$$S_x = \frac{1}{a}\left(1 + 2\sum_{n=1}^{\infty} \cos\frac{n\pi x}{a} \cos\frac{n\pi x_0}{a} \exp\left[-\frac{n^2\pi^2 k_x \tau}{\alpha a^2}\right]\right) \tag{2.5}$$

$$S_y = \frac{1}{b}\left(1 + 2\sum_{m=1}^{\infty} \cos\frac{m\pi y}{b} \cos\frac{m\pi y_0}{b} \exp\left[-\frac{m^2\pi^2 k_y \tau}{\alpha b^2}\right]\right) \tag{2.6}$$

$$S_z = \frac{1}{h}\left(1 + 2\sum_{l=1}^{\infty} \cos\frac{l\pi z}{h} \cos\frac{l\pi z_0}{h} \exp\left[-\frac{l^2\pi^2 k_z \tau}{\alpha h^2}\right]\right) \tag{2.7}$$

Babu and Odeh showed that Eq. 2.4 can be simplified to a closed form model of inflow performance relationship of horizontal wells,

$$q_o = \frac{b\sqrt{k_x k_z}(p_R - p_{wf})}{141.2 B_o \mu_o \left[ln\left(\frac{\sqrt{A}}{r_w}\right) + ln\,C_H - 0.75 + s_R + s\right]} \tag{2.8}$$

In Eq. 2.8, the shape factor, $ln(C_H)$, accounts for the position of horizontal wells. The partial penetration skin factor, s_R, accounts for partially penetrating horizontal wells. The pseudosteady-state model for single-phase oil horizontal well is flexible and easy to use because the well can be located anywhere as long as the well is parallel to the boundary of the reservoir and the well can be either fully or partially penetrating wells. With material balance, we can generate production history. The model will be used as the base to develop the pseudosteady-state equations for gas wells and two-phase flow wells in this chapter.

2.2 Single-Phase Gas Wells

Although many horizontal well performance models have been published over a decade, most of these models only apply for single-phase oil reservoirs. To obtain the horizontal well performance in gas reservoirs, we need to consider the strong dependency of gas properties, density, viscosity and compressibility, to reservoir pressures and temperature. This dependency changes the diffusivity equation from a linear equation to a non-linear relationship. To solve the equation analytically, we can replace the pressure in diffusivity equation with a pseudo-pressure function[12] to unify the diffusivity of gas and liquid. When the reservoir pressure is relatively high, the pseudo-pressure can also be replaced by the difference of squared pressure[13]. Here we derive the inflow equation for horizontal gas wells under steady-state condition, and discuss the equation for pseudosteady-state flow with analogical approach.

2.2.1 Steady-State Condition

Under steady-state condition, the flow in porous media can be directly solved by the Darcy's law because a pressure is constant at the boundary. For oil wells, Furui showed that the flow of the horizontal well can be calculated by adding the radial pressure drop around the wellbore region and the linear pressure drop on the outer region.[4] The radial flow was identified from distance $r = r_w$ to $r = r_t$ ($r_t = \left(h\sqrt{2} \right)/2$) and the linear flow is from $x = h/2$ to the outer reservoir boundary or $x = y_b$ shown in Fig. 2.1.

for radial flow, Darcy's law states,

$$q = \frac{kA}{\mu} \frac{\partial p}{\partial r} \qquad (2.9)$$

To convert the gas flow rate at the standard condition we introduce the gas formation volume factor to Eq. 2.9 and then we have

$$q_g = \frac{kA}{B_g \mu_g} \frac{\partial p}{\partial r}$$ (2.10)

From the definition of gas formation volume factor and the Real Gas law, we have

$$B_g = \frac{p_{sc}}{T_{sc} z_{sc}} \frac{Tz}{p}$$ (2.11)

Then substituting Eq. 2.11 into Eq. 2.10

$$q_g = \frac{kA}{\mu_g} \frac{T_{sc} z_{sc}}{p_{sc}} \frac{p}{Tz} \frac{\partial p}{\partial r}$$ (2.12)

For radial flow, the flow area A is $2\pi r L$, then Eq. 2.12 becomes

$$\frac{q_g T}{2k\pi r L} \partial r = \frac{T_{sc} z_{sc}}{p_{sc}} \frac{p}{z\mu_g} \partial p$$ (2.13)

Integrate Eq. 2.13 from $r = r_w$ to r $= \left(h\sqrt{2}\right)/2$

$$\int_{r_w}^{\left(h\sqrt{2}\right)/2} \frac{q_g T}{\pi r L k} \partial r = \frac{T_{sc} z_{sc}}{p_{sc}} 2 \int_{p_{wf}}^{p_{rt}} \frac{p}{z\mu_g} \partial p$$ (2.14)

With the definition of pseudo-pressure[9],

$$m(p) = 2 \int_{p_{base}}^{p} \frac{p}{z\mu_g} \partial p$$ (2.15)

Then the integral term on the right hand side of Eq. 2.14

$$2 \int_{p_{wf}}^{p_{rt}} \frac{p}{z\mu_g} \partial p = m(p_{rt}) - m(p_{wf})$$ (2.16)

Substituting Eq. 2.16 into Eq. 2.14 and integrating the left hand side of Eq. 2.14 give

$$\frac{q_g T}{\pi L k} \ln\left(\frac{h\sqrt{2}}{2r_w}\right) = \frac{T_{sc} z_{sc}}{p_{sc}} m(p_{rt}) - m(p_{wf})$$ (2.17)

Eq. 2.17 can be rearranged to

$$\left(m(p_{rt}) - m(p_{wf})\right) = q_g \frac{p_{sc}}{T_{sc} z_{sc}} \frac{T}{\pi L k} ln\left(\frac{h\sqrt{2}}{2r_w}\right) \qquad (2.18)$$

For the linear flow, the Darcy's equation is

$$q_g = \frac{kA}{\mu_g B_g} \frac{\partial p}{\partial x} \qquad (2.19)$$

Using the definition of B_g (Eq. 2.11), we have

$$q_g = \frac{kA}{\mu_g} \frac{T_{sc} z_{sc}}{p_{sc}} \frac{p}{Tz} \frac{\partial p}{\partial x} \qquad (2.20)$$

For linear flow $A = hL$, we write Eq. 2.20 as

$$\frac{q_g T}{khL} \partial x = \frac{T_{sc} z_{sc}}{p_{sc}} \frac{p}{z\mu_g} \partial p \qquad (2.21)$$

Since we only consider the linear flow from one side of the drainage area, we divide the gas flow rate by two. Then we can write Eq. 2.21 as

$$\frac{q_g T}{2khL} \partial x = \frac{T_{sc} z_{sc}}{p_{sc}} \frac{p}{z\mu_g} \partial p \qquad (2.22)$$

Integrate Eq. 2.22 for the linear flow region from $x = h/2$ to $x = y_b$,

$$\int_{h/2}^{y_b} \frac{q_g T}{khL} \partial x = \frac{T_{sc} z_{sc}}{p_{sc}} 2 \int_{p_{rt}}^{p_e} \frac{p}{z\mu_g} \partial p \qquad (2.23)$$

Considering the integral term on the right hand side of Eq. 2.23

$$2 \int_{p_{rt}}^{p_e} \frac{p}{z\mu_g} \partial p = m(p_e) - m(p_{rt}) \qquad (2.24)$$

Substituting Eq. 2.24 into Eq. 2.23 and integrating the left hand side of Eq. 2.23 give

$$\frac{q_g T}{khL}\left(y_b - \frac{h}{2}\right) = \frac{T_{sc} z_{sc}}{p_{sc}} m(p_e) - m(p_{rt}) \qquad (2.25)$$

Rearranging Eq. 2.25

$$m(p_e) - m(p_{rt}) = q_g \frac{p_{sc}}{T_{sc} z_{sc}} \frac{T}{khL}\left(y_b - \frac{h}{2}\right)$$ (2.26)

The pseudo-pressure difference as a result of uniform flow into a fully penetrating horizontal well under steady-state flow is equal to the summation of Eq. 2.18 and Eq. 2.26.

$$m(p_e) - m(p_{wf}) = q_g \frac{p_{sc}}{T_{sc} z_{sc}} \frac{1}{\pi} \frac{T}{kL}\left(ln\left(\frac{h\sqrt{2}}{2r_w}\right) + \left(\frac{y_b \pi}{h} - \frac{\pi}{2}\right)\right)$$ (2.27)

We can rewrite Eq. 2.27 as

$$\left(m(p_e) - m(p_{wf})\right) = q_g \frac{p_{sc}}{T_{sc} z_{sc}} \frac{1}{\pi} \frac{T}{kL}\left(ln\left(\frac{h}{r_w}\right) + \left(\frac{y_b \pi}{h}\right) - 1.917\right)$$ (2.28)

The damage skin factor, s, and the partial penetrated skin factor, s_R, can be add to Eq. 2.28 as discussed before, and we can write the gas inflow model for horizontal wells as,

$$q_g = \frac{kL(m(p_e) - m(p_{wf}))}{\dfrac{p_{sc}}{T_{sc} z_{sc}} \dfrac{T}{\pi}\left(ln\left(\dfrac{h}{r_w}\right) + \left(\dfrac{y_b \pi}{h}\right) - 1.917 + s_R + s\right)}$$ (2.29)

For the oil field unit, Eq. 2.29 becomes

$$q_g = \frac{kL(m(p_e) - m(p_{wf}))}{50313.4 \dfrac{p_{sc}}{T_{sc} z_{sc}} T\left(ln\left(\dfrac{h}{r_w}\right) + \left(\dfrac{y_b \pi}{h}\right) - 1.917 + s_R + s\right)}$$ (2.30)

If pressure and temperature at standard condition is 14.7 psi and 520°R respectively, we then have in the oil field unit,

$$q_g = \frac{kb(m(p_e) - m(p_{wf}))}{1422T\left(ln\left(\dfrac{h}{r_w}\right) + \left(\dfrac{y_b \pi}{h}\right) - 1.917 + s_R + s\right)}$$ (2.31)

For gas wells, the flow velocity is usually much higher than that in oil wells, especially near the wellbore. This high velocity causes additional pressure drop known as non-Darcy flow effect. This additional pressure drop is a function of flow rate, and its effect can be added to gas well inflow performance models by a Non-Darcy flow coefficient. The Non-Darcy coefficient, D, is obtained from lab experimental data or from correlations. A correlation for Non-Darcy flow for horizontal gas well[14] is

$$D = 2.22 \times 10^{-15} \frac{L\gamma_g \sqrt{k_x k_z}}{\mu_g (p_{wf})} \left[\left(\frac{\beta_d}{L^2} \right) \left(\frac{1}{r_w} - \frac{1}{r_d} \right) + \left(\frac{\beta}{L^2} \right) \left(\frac{1}{r_d} - \frac{1}{r_e} \right) \right] \qquad (2.32)$$

where, the turbulent factor for undamaged and damaged zones, β and β_d, are estimated by

$$\beta = \frac{2.6 \times 10^{10}}{\left(\sqrt{k_x k_z} \right)^{1.2}} \qquad (2.33)$$

and

$$\beta_d = \frac{2.6 \times 10^{10}}{\left(\sqrt{k_x k_z} \right)_d^{1.2}} \qquad (2.34)$$

Including the non-Darcy flow effect, Eq. 2.31 now is

$$q_g = \frac{kL(m(p_e) - m(p_{wf}))}{1424T \left(ln\left(\frac{h}{r_w} \right) + \left(\frac{y_b \pi}{h} \right) - 1.917 + s_R + s + Dq_g \right)} \qquad (2.35)$$

Eq. 2.35 is the inflow model for horizontal gas well at steady-state flow condition for isotropic reservoirs. For anisotropic reservoirs, the inflow model is

$$q_g = \frac{kL(m(p_e) - m(p_{wf}))}{1424T \left(ln\left(\frac{hI_{ani}}{r_w(I_{ani} + 1)} \right) + \left(\frac{y_b \pi}{hI_{ani}} \right) - 1.224 + s_R + s + Dq_g \right)} \qquad (2.36)$$

2.2.2 Pseudosteady-State Condition

The horizontal well performance under pseudosteady-state condition for gas wells can be derived similar to the horizontal well performance under pseudosteady-state condition for oil wells with the same initial and boundary conditions. The pseudo equation for oil wells by Babu and Odeh is shown in Eq. 2.4. For oil wells, we solve the diffusivity equation for pressure, p. For gas wells, we solve the diffusivity equation for pseudo-pressure, $m(p)$, as shown for steady-state flow. For pseudosteady-state flow, we develop a squared pressure equation instead of pseudo-pressure equation. With appropriately constant changing, the equation can be further expressed in pseudo- pressure.

From previous section, the pseudosteady-state inflow equation for horizontal oil wells (Eq. 2.4) can be expressed for gas wells with corresponding fluid properties,

$$\Delta p = \left[\frac{B_g \mu_g q_g}{\alpha L} \right] \int_0^t \int_{x_1}^{x_2} \left(S_x S_y S_z \right) dx_o d\tau \tag{2.37}$$

Substituting Eq. 2.11 into Eq. 2.37 we have

$$\Delta p = \left[\frac{Tz}{p} \frac{p_{sc}}{T_{sc} z_{sc}} \frac{\mu_g q_g}{\alpha L} \right] \int_0^t \int_{x_1}^{x_2} \left(S_x S_y S_z \right) dx_o d\tau \tag{2.38}$$

Because we solve Eq. 2.38 under isothermal system, we can use B_g that is evaluated at an average pressure,

$$\Delta p = \left[\frac{T\bar{z}}{\bar{p}} \frac{p_{sc}}{T_{sc} z_{sc}} \frac{\mu_g q_g}{\alpha L} \right] \int_0^t \int_{x_1}^{x_2} \left(S_x S_y S_z \right) dx_o d\tau \tag{2.39}$$

The average pressure used in Eq. 2.39 can be estimated in different ways. The simplest one is to assume a linear distribution of pressure in the formation between the wellbore and the drainage boundary, the average pressure can be calculated by

$$\bar{p} = \frac{\left(p_i + p_{wf} \right)}{2} \tag{2.40}$$

Substituting Eq. 2.40 into Eq. 2.39 and rearranging,

$$\Delta p = \left[\frac{T\bar{z}}{(p_i + p_{wf})} \frac{p_{sc}}{T_{sc} z_{sc}} \frac{\mu_g q_g}{\alpha L} \right]_0^t \int_{x_1}^{x_2} \left(S_x S_y S_z \right) dx_o d\tau \qquad (2.41)$$

Easily, Eq. 2.41 can be rewritten as

$$\left(p_i^2 - p_{wf}^2 \right) = \left[2 T\bar{z} \frac{p_{sc}}{T_{sc} z_{sc}} \frac{\mu_g q_g}{\alpha L} \right]_0^t \int_{x_1}^{x_2} \left(S_x S_y S_z \right) dx_o d\tau \qquad (2.42)$$

S_x, S_y, and S_z are presented in Eq. 2.5 to Eq. 2.7 respectively. If we assume the geometry terms in the above equation, S_x, S_y, and S_z are independent to pressure, comparing Eq. 2.41 with Eq. 2.4 and Eq. 2.8, the solution of Eq. 2.41 can be written as,

$$q_g = \frac{b\sqrt{k_x k_z} \left(p_R^2 - p_{wf}^2 \right)}{141.2 \bar{z} \bar{\mu}_g T \frac{2 p_{sc}}{T_{sc} z_{sc}} \left[ln\left(\frac{\sqrt{A}}{r_w} \right) + ln C_H - 0.75 + s_R + s \right]} \qquad (2.43)$$

In oil field unit, the gas rate is in Mscf/day. We can convert STB/day to Mscf/day by

$$q_g = \frac{1}{141.2} \frac{bbl}{day} \frac{5.615 ft^3}{bbl} \frac{Mscf}{1000 ft^3} = \frac{1}{25146.93} \qquad (2.44)$$

Substituting the constant in Eq. 2.44 into Eq. 2.43 gives

$$q_g = \frac{b\sqrt{k_x k_z} \left(p_R^2 - p_{wf}^2 \right)}{25146.93 \bar{z} \bar{\mu}_g T \frac{2 p_{sc}}{T_{sc} z_{sc}} \left[ln\left(\frac{\sqrt{A}}{r_w} \right) + ln C_H - 0.75 + s_R + s \right]} \qquad (2.45)$$

If the standard pressure is 14.7 psi and the standard temperature is 520°R. Eq. 2.45 becomes

$$q_g = \frac{b\sqrt{k_x k_z} \left(p_R^2 - p_{wf}^2 \right)}{1422 \bar{z} \bar{\mu}_g T \left[ln\left(\frac{\sqrt{A}}{r_w} \right) + ln C_H - 0.75 + s_R + s \right]} \qquad (2.46)$$

Then we add non-Darcy flow effect to Eq. 2.46 and the equation becomes

$$q_g = \frac{b\sqrt{k_x k_z}\left(p_R^2 - p_{wf}^2\right)}{1422\overline{z}\overline{\mu}_g T\left[ln\left(\frac{\sqrt{A}}{r_w}\right) + ln\,C_H - 0.75 + s_R + s + Dq_g\right]} \tag{2.47}$$

Eq. 2.47 is the inflow performance model of horizontal gas wells under pseudosteady-state condition. This equation can be used to predict the performance of a horizontal gas well in a close box-shaped reservoir. Analogically to the discussion for the steady-state gas flow equation, Eq. 2.47 can be expressed in the pseudo-pressure term as (add equation)

$$q_g = \frac{b\sqrt{k_x k_z}\left(m(p_R) - m(p_{wf})\right)}{1422T\left[ln\left(\frac{\sqrt{A}}{r_w}\right) + ln\,C_H - 0.75 + s_R + s + Dq_g\right]} \tag{2.48}$$

The closed form model for gas well IPR (Eq. 2.48) gives the agreed results when the bottomhole flow pressure, p_{wf}, is not too low compared with the numerical simulation results. Fig. 2.4 shows a comparison between these results. From the plots, we can see that the analytical results slightly deviate at high flow rate or at low flowing bottomhole pressures. For example, at 10% recovery factor and a reservoir pressure of 5152 psi, if the well is produced at 3500 psi drawdown, the closed form model gives 14% difference comparing with the simulation result at the same condition. However, when the drawdown is below 1400 psi, the closed form model and the simulation model predict the same production performance. At 20% recovery factor and a reservoir pressure of 4023 psi, the analytical results match the simulation results when the pressure drawdown is below 1200 psi.
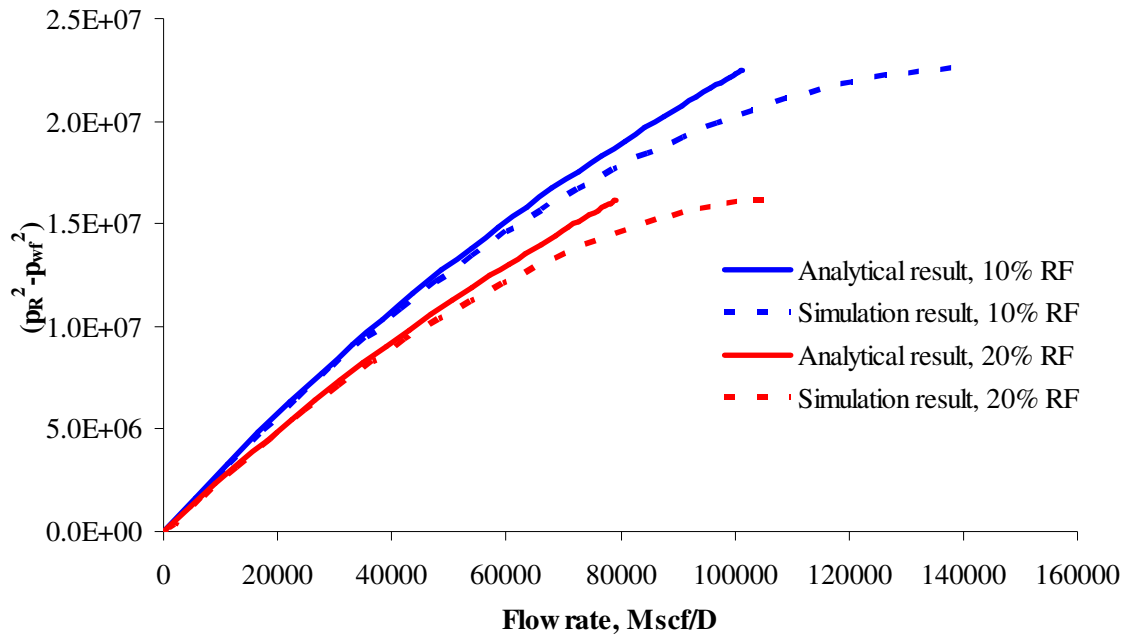
Fig. 2.4 Horizontal gas well performance.

2.3 Two-Phase Reservoirs

For two-phase flow wells, horizontal well performance is predicted by using correlations. The closed form model for two-phase flow is very difficult to derive because of the complexity of the relative permeability. One of the two-phase inflow correlations, which has been used successfully to estimate the inflow performance of two-phase vertical wells is Vogel's correlation[15]. The same idea will be used to estimate the two-phase inflow performance of horizontal wells with some modifications. The main modification uses a horizontal well model to calculate the maximum flow potential. For horizontal well, the maximum flow potential is estimated as,

For $\left(p_R < p_b \right)$

$$q_{o,max} = \frac{J p_R}{1.8} \qquad (2.49)$$

for $\left(p_R > p_b \right)$ and $\left(p_{wf} < p_b \right)$

$$q_V = \frac{Jp_b}{1.8} \qquad (2.50)$$

where

$$J_o = \frac{b\sqrt{k_y k_z}}{141.2 B_o \mu_o \left[ln\left(\frac{\sqrt{A}}{r_w}\right) + ln\, C_H - 0.75 + s_R + s \right]} \qquad (2.51)$$

After we know the maximum flow potential of horizontal wells, we can apply this number to the correlation to estimate the two-phase flow performance of horizontal wells.

2.4 Systematic Table for Horizontal Well Inflow Performance

In this section we create a systematic table of horizontal wellbore performance models. The horizontal well performance table is shown in Table 2.1.

Table 2.1   **Horizontal well performance models in different boundary conditions and fluid systems**

Reservoir Conditions	Transient Flow	Steady-State	Pseudosteady-State
Oil Reservoirs	Available	Available	Available
Gas Reservoirs	-	Available	Available
Two-Phase reservoir	-	-	Available

2.5 Wellbore Pressure Drop

The wellbore pressure in horizontal wells is one of the important factors in well performance evaluation. Usually the pressure drop in horizontal wellbores is mainly from hydrostatic pressure drop. Although in general we do not consider the hydrostatic

pressure in horizontal wells, the pressure drop along a horizontal wellbore can be high because of the frictional pressure drop term. The frictional pressure drop along the wellbore depends mainly on the flow rate, the length of the well, and the wellbore diameter. Thus for a long horizontal well with high flow rate and/or small wellbore diameter, the pressure drop along the wellbore can be significant and will affect the performance of horizontal wells.

2.5.1 Coupled Model

The wellbore pressure drop along horizontal wells is evaluated by coupling the wellbore performance model with the wellbore pressure drop model. To couple these models, we need to divide the well and the reservoir into several segments as shown Fig. 2.5. Then, we estimate the productivity index, J, of each segment. After we know the productivity index in every segment, we start the calculation from the toe segment or segment number N.
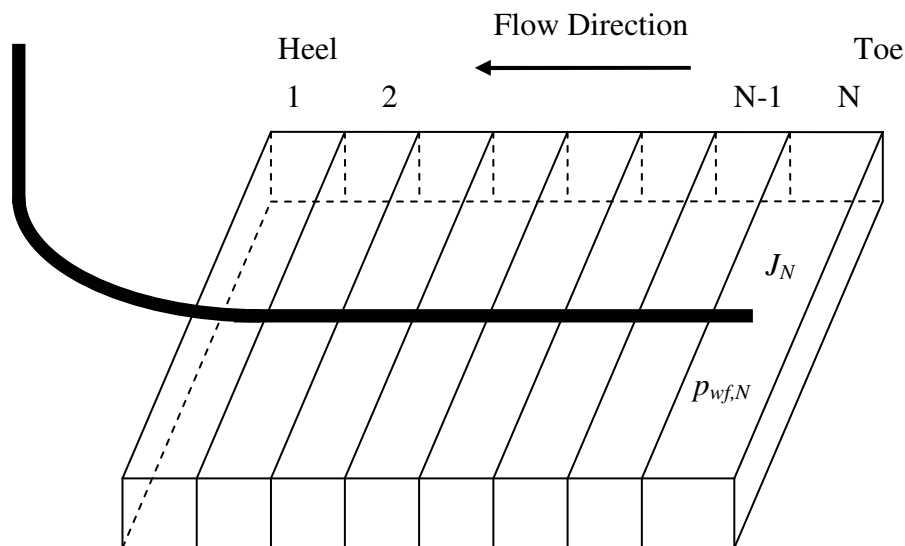
Fig. 2.5 Reservoir and wellbore geometry for coupling process.

In order to determine the flow rate into the segment N, we have to assume the wellbore pressure in the segment N, $p_{wf,N}$. Then the flow rate into the segment N is obtained by multiplying the productivity of this segment, J_N, with the pressure drawdown of this segment, $(p_r-p_{wf,N})$, as shown in Fig. 2.6.
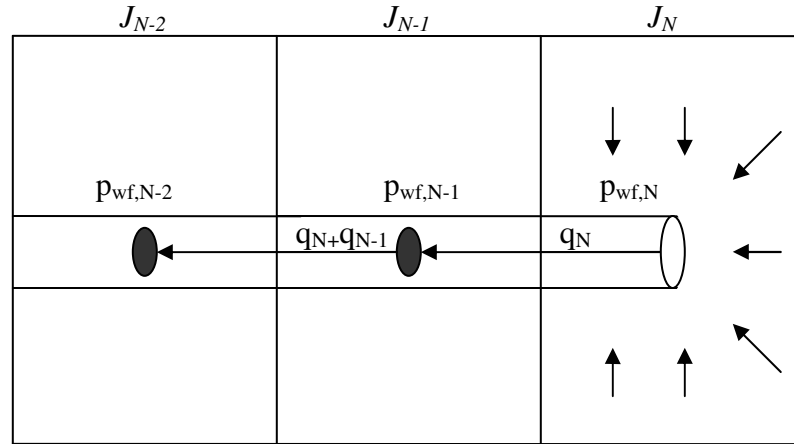
Fig. 2.6 Coupling wellbore performance model with wellbore pressure drop model.

The productivity of single-phase oil is estimated by using Eq. 2.8. For single-phase gas we compute the flow rate from Eq. 2.48. For two-phase system, we calculate the maximum flow potential and apply the correlation to evaluate the flow rate into segment N. After that, we estimate the wellbore pressure in segment N-1 by applying the wellbore pressure drop model to evaluate the pressure drop between the segments and subtract this pressure drop from the wellbore pressure in segment N, shown as,

$$p_{wf,N-1} = p_{wf,N} - \Delta p_{N-1,N} \qquad (2.52)$$

Next, we calculate the flow into segment N-1 from the productivity index and the wellbore pressure of segment N-1. After we know the inflow into segment N-1, we compute the wellbore pressure of the segment N-2 by applying the wellbore pressure drop model as shown Fig. 2.6. Then we repeat this procedure from the toe segment to the heel segment to obtain pressure profile and flow rate profile along the horizontal well.

2.5.2 Effect of Wellbore Pressure Drop

The wellbore pressure can affect the performance of horizontal wells. From the couple model, we know that the pressure profile relates to the inflow distribution along the wellbore. If the wellbore pressure drop is high, the wellbore pressure decreases rapidly from the toe to the heel. The lower the wellbore pressure, the higher the pressure drawdown. If the productivity index of every segment is the same, the flow rate will increase from the toe to the heel. When the wellbore pressure drop is comparable to the reservoir drawdown, it will affect the production distribution of horizontal wells. For example, at high pressure drop, the wellbore pressure at the toe will be higher than the pressure at the heel. The pressure drawdown at the toe will be lower, thus, we may not be able to produce from the toe as much as we produce from the heel.

A study of wellbore pressure drop in horizontal well performance is necessary to optimize horizontal well production[16]. For single-phase flow, the frictional pressure drop is estimated by

$$\Delta p_f = \frac{2 f_f \rho u^2 L}{32.17 D} \tag{2.53}$$

If we convert the unit in Eq. 2.53 to oil field unit shown as,

$$u = \frac{q}{A} = \frac{4q}{\pi D^2} \frac{bbl}{day} \frac{5.615\,ft^3}{bbl} \frac{day}{86400s} \frac{1}{ft^2} = 8.2758 \times 10^{-5} \frac{q}{D^2} \tag{2.54}$$

$$\Delta p_f = \frac{2 f_f \rho L}{32.17 D} \left(8.2758 \times 10^{-5} \frac{q}{D^2} \right)^2 \frac{ft^2}{144 in^2} \tag{2.55}$$

$$\Delta p_f = 2.9569 \times 10^{-12} \frac{f_f \rho L q^2}{D^5} \tag{2.56}$$

To compare the wellbore pressure drop with the pressure drawdown of a horizontal well, we divide Eq. 2.56 with the reservoir drawdown,

$$\frac{\Delta p_f}{\Delta p_{dd}} = \frac{2.9569\times10^{-12}\,\dfrac{f_f\,\rho L q^2}{D^5}}{\dfrac{q\mu_o}{7.08\times10^{-3}b\sqrt{k_y k_z}}\left[ln\left(\dfrac{\sqrt{A}}{r_w}\right)+ln\,C_H-0.75+s_R+s\right]} \tag{2.57}$$

Combining the constant, we have

$$\frac{\Delta p_f}{\Delta p_{dd}} = 2.0935\times10^{-14}\,\frac{f_f\,\rho L q b\sqrt{k_y k_z}}{D^5\mu_o\left[ln\left(\dfrac{\sqrt{A}}{r_w}\right)+ln\,C_H-0.75+s_R+s\right]} \tag{2.58}$$

The Reynolds number in oil field units is written as

$$N_{Re} = \frac{1.48q\rho}{12D\mu} \tag{2.59}$$

Substituting Eq. 2.59 into Eq. 2.58 gives

$$\frac{\Delta p_f}{\Delta p_{dd}} = 1.6974\times10^{-13}\,\frac{N_{Re}f_f Lb\sqrt{k_y k_z}}{D^4\left[ln\left(\dfrac{\sqrt{A}}{r_w}\right)+ln\,C_H-0.75+s_R+s\right]} \tag{2.60}$$

If we define the reservoir geometry factor as

$$F_g = \left[ln\left(\frac{\sqrt{A}}{r_w}\right)+ln\,C_H-0.75+s_R+s\right] \tag{2.61}$$

Then Eq. 2.60 becomes

$$\frac{\Delta p_f}{\Delta p_{dd}} = 1.6974\times10^{-13}\,\frac{N_{Re}f_f Lb\sqrt{k_y k_z}}{D^4 F_g} \tag{2.62}$$

Since the unit of permeability is in length square, we can define a horizontal dimensionless term as,

$$N_H = \frac{Lb\sqrt{k_y k_z}}{D^4 F_g} \tag{2.63}$$

With this horizontal dimensionless number, the pressure ratio becomes

$$\frac{\Delta p_f}{\Delta p_{dd}} = 1.6974 \times 10^{-13} f_f N_{Re} N_H \qquad\qquad (2.64)$$

Using the above equation, we can identify the conditions that wellbore pressure drop is significant and should be considered when predict well performance. The calculation is illustrated by the following example. Assume a horizontal well is located in the middle of a close box-shaped reservoir. The well length is 3500 ft with 0.25 ft wellbore radius. The reservoir width is 2000 ft, the reservoir length is 3500 ft, and the reservoir thickness is 80 ft. The oil density is 45.58 lb/ft^3 and oil viscosity is 1.16 cp. Wellbore roughness is 0.001. The reservoir is single-phase oil reservoir. We can study the effect of the wellbore pressure drop of this well by applying Eq. 2.64. The results are shown in Table 2.2.

Table 2.2   **The ratio of the wellbore pressure drop to the pressure drawdown**

k_H	k_V	Δp_{dd}	q	Couple Model, $\Delta p_f/\Delta p_{dd}$	Pressure Ratio Model, $\Delta p_f/\Delta p_{dd}$
25	2.5	200	2779	0.006	0.005
50	5	200	5573	0.022	0.020
100	1	200	5078	0.017	0.015
100	5	200	8989	0.051	0.048
100	10	200	11261	0.078	0.073
100	10	400	22464	0.146	0.139

The table shows that at the high flow rate, the pressure ratio is high. Comparing the pressure ratio obtained by the couple model with the pressure ratio obtained by Eq. 2.64 shows that Eq. 2.64 can be used to approximate the ratio of wellbore pressure drop to the drawdown pressure with reasonable results. This model should be used to calculate first. If the pressure ratio is high, meaning that the wellbore pressure drop will affect the wellbore performance, then the coupling model should be used for more detail

and accurate result. Moreover, to optimize horizontal well performance, we can use Eq. 2.64 to minimize the effect of wellbore pressure drop. From the horizontal dimensionless term, Eq. 2.63, the effect of wellbore pressure on flow rate distribution can be minimized by increasing the wellbore diameter in cases of high flow rate wells or high permeability reservoirs.

2.6 Summary

In this chapter, we study analytical horizontal well inflow performance models under different boundary conditions and fluid systems. The study covers the horizontal well performance for single-phase oil wells, for single-phase gas wells, and for two-phase flow wells under both steady-state condition and pseudosteady-state condition. For oil reservoirs, we modify a fully-penetrating horizontal well inflow performance model under steady-state condition to extend the application to partial penetrating wells. For gas reservoirs, we present the horizontal well performance model for gas wells under both steady-state and pseudosteady-state condition. After we study these horizontal well models, we create the systematic table that summarizes the horizontal well models. The wellbore pressure drop is also considered in this chapter by coupling the well performance with the wellbore pressure drop model. We also present the pressure ratio equation that can be used to monitor the effect of the wellbore pressure drop in single-phase oil horizontal. This equation is useful in understanding and optimizing horizontal well performance.

CHAPTER III

LINE SOURCE MODEL

Line source solutions have been used to solve petroleum engineering problems for a long time. The model is adapted from point source solutions of heat conduction problems. The line source solution of 3D problems is obtained by multiplying three 1D point solutions and integrating in time and along the source. To this point, the equation is too complicated and usually a numerical approach is used to obtain solutions.[17-19] We present an analytical line source solution for 2D wellbore in this chapter. The model developed here can be applied to a variety of wellbore trajectories including horizontal wells, slanted wells, undulating wells, and multilateral wells. In the first part of the chapter, we derive the analytical line source solution, and then we apply the line source solution to predict the well performance of different well trajectories. We also discuss the effect of inner boundary conditions on the flow rate and wellbore pressure profiles along the wellbore. Finally, we conduct the sensitivity study of different parameters on the flow rate distributions along the wellbore.

3.1 Mathematic Model

The diffusivity equation of a single-phase incompressible fluid is written as,

$$\nabla^2 p = \frac{\phi \mu c_t}{k} \frac{\partial p}{\partial t} \tag{3.1}$$

For an isotropic medium, we can write the diffusivity in the 3D direction as

$$k \frac{\partial^2 p}{\partial x^2} + k \frac{\partial^2 p}{\partial y^2} + k \frac{\partial^2 p}{\partial z^2} = \phi \mu c_t \frac{\partial p}{\partial t} \tag{3.2}$$

or

$$\frac{\partial^2 p}{\partial x^2} + \frac{\partial^2 p}{\partial y^2} + \frac{\partial^2 p}{\partial z^2} = \frac{\phi \mu c_t}{k} \frac{\partial p}{\partial t} \tag{3.3}$$

If the porous medium is anisotropic, then the diffusivity equation becomes

$$k_x \frac{\partial^2 p}{\partial x^2} + k_y \frac{\partial^2 p}{\partial y^2} + k_z \frac{\partial^2 p}{\partial z^2} = \phi \mu c_t \frac{\partial p}{\partial t}$$ (3.4)

To solve the flow in an anisotropic reservoir, we transform the anisotropic equation to an isotropic format through the coordinate transformation. The permeability in Eq. 3.4 is replaced by the equivalent permeability k_{eq}. The coordinate transformations are,

$$x' = \frac{x\sqrt{k_y k_z}}{k_{eq}}$$ (3.5)

$$y' = \frac{y\sqrt{k_x k_z}}{k_{eq}}$$ (3.6)

$$z' = \frac{z\sqrt{k_x k_y}}{k_{eq}}$$ (3.7)

$$k_{eq} = \sqrt[3]{k_x k_y k_z}$$ (3.8)

Substituting Eq. 3.5 – Eq. 3.8 into Eq. 3.4, we have

$$\frac{\partial^2 p}{\partial x'^2} + \frac{\partial^2 p}{\partial y'^2} + \frac{\partial^2 p}{\partial z'^2} = \frac{\phi \mu c_t}{k_{eq}} \frac{\partial p}{\partial t}$$ (3.9)

Before the transformation, the isobar in the system is elliptical away from the wellbore. With this transformation, the isobar away from the wellbore becomes circular, but the isobar around the wellbore is changed to elliptical as shown in Fig. 3.1. The concept of equivalent wellbore radius is used to solve this problem. The correct equivalent radius can be calculated from the arithmetic average of the major and minor axis of the elliptic wellbore radius.[20] The equivalent wellbore radius[21] is

Anisotropic Isobar   Transformed Anisotropic Isobar
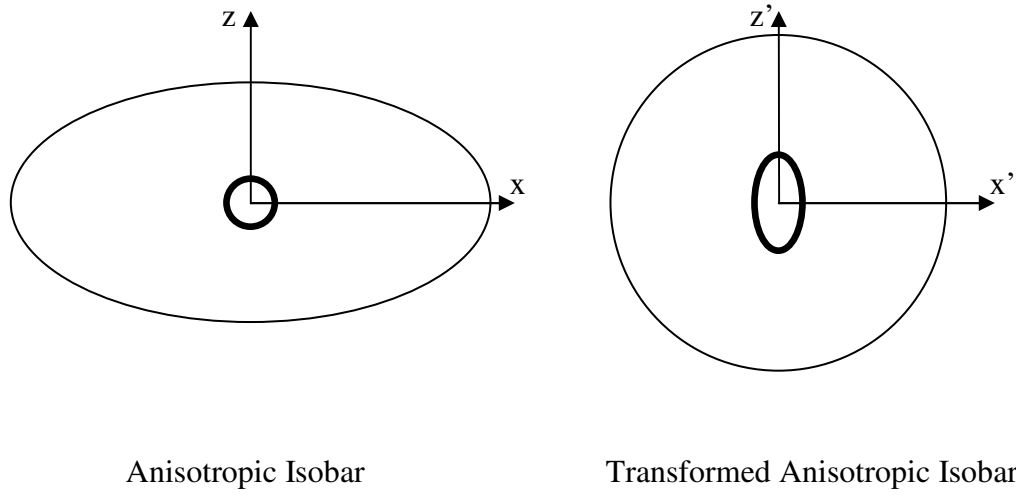
Fig. 3.1 Isobar around the wellbore in anisotropic reservoir.

$$r_{eq} = \frac{r_w}{\alpha^{1/3}} \frac{1}{2\beta} \sqrt{\left(1+\frac{\beta^2}{\gamma}\right)^2 + \left(\left(\sqrt{\frac{k_x}{k_y}}-\sqrt{\frac{k_y}{k_x}}\right)\frac{\cos\theta\cos\varphi\sin\varphi}{\gamma}\right)^2} \qquad (3.10)$$

where,

$$\alpha = \sqrt{\frac{\sqrt{k_x k_y}}{k_z}} \qquad (3.11)$$

$$\beta = \sqrt{\sqrt{\frac{k_y}{k_x}}\cos^2\varphi + \sqrt{\frac{k_x}{k_y}}\sin^2\varphi} \qquad (3.12)$$

$$\gamma = \sqrt{\cos^2\theta + \frac{k_z}{\sqrt{k_x k_y}}\beta^2\sin^2\theta} \qquad (3.13)$$

where, θ is the inclination of the well to the vertical axis and φ is azimuth of the well as shown in Fig. 3.2. Now an anisotropic medium is transformed to an isotropic medium.

Thus we can solve the flow equation of an anisotropic medium the same way as we solve that of an isotropic medium. The diffusivity equation is written as

$$\frac{\partial^2 p}{\partial x'^2} + \frac{\partial^2 p}{\partial y'^2} + \frac{\partial^2 p}{\partial z'^2} = \frac{\phi \mu c_t}{k_{eq}} \frac{\partial p}{\partial t} \tag{3.14}$$
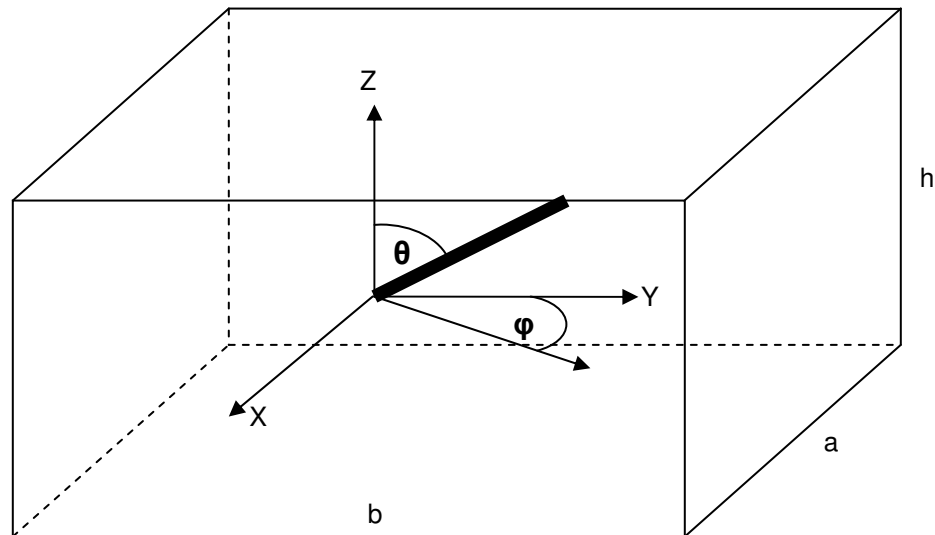
Fig. 3.2 Schematic of wellbore transformation for anisotropic reservoir. [17]

3.2 Sink/Source Technique

The flow equation of the diffusivity equation can be solved by the sink/source technique. Because the diffusivity equation is in the same format as the heat conduction problems, we can directly apply the sink/source technique to solve the flow in porous media. The solution from this technique applies to different state in the flow period, both transient flow and stabilized flow. The boundary condition of the reservoir is constant pressure, no-flow boundary or mixed, which makes the model practical to a wide range of flow problems in petroleum engineering. In this section, we present the derivation of the

analytical line source solution for 2D wellbore. The solution can be used to predict well performance of various well trajectories.

3.2.1 Instantaneous Point Source

The instantaneous Green's function in infinite slab reservoir was presented by Gringarten and Ramey[22] in 1973. This function can be applied to different flow problems in petroleum engineering. The geometries of the source function are shown in Fig. 3.3 and Green's functions for different boundary conditions in infinite slab reservoirs are shown in Table 3.1.
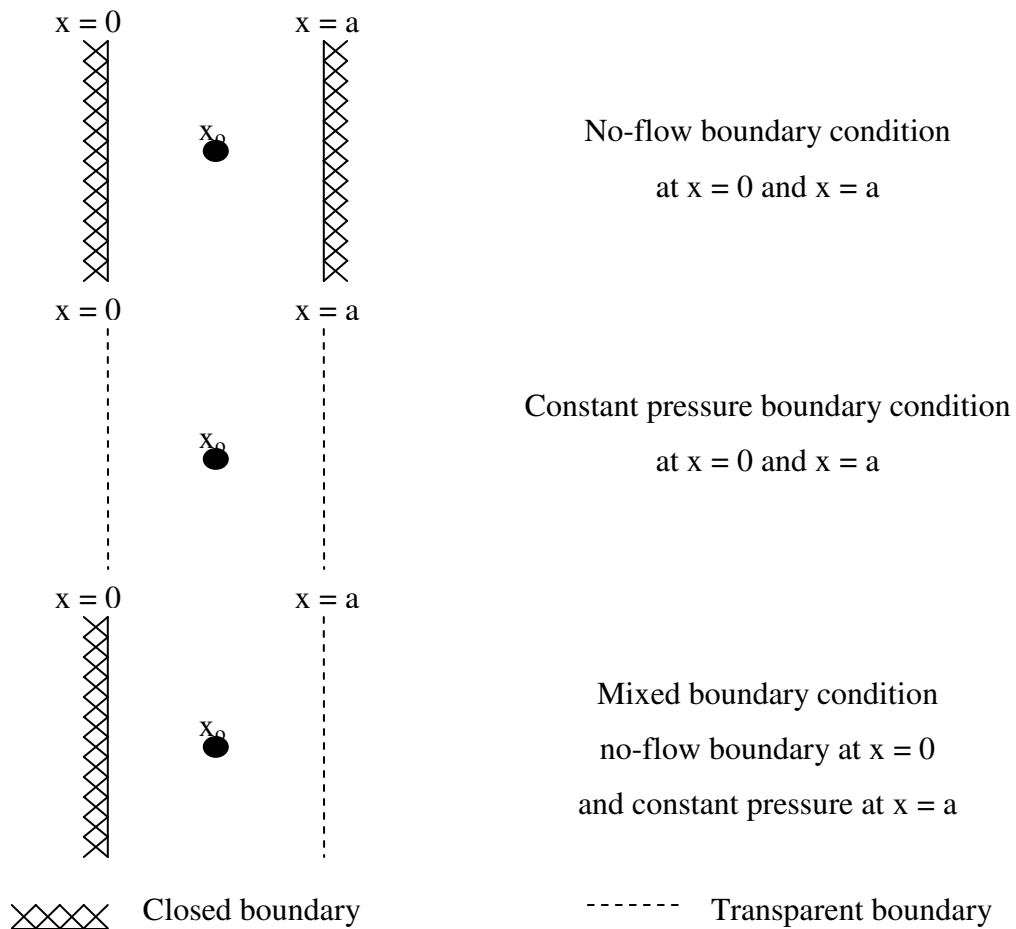
Fig. 3.3 Instantaneous Green's function.[22]

Table 3.1   Instantaneous Green's functions in 1D infinite slab reservoir

Boundary conditions	Instantaneous Green's functions
Constant pressure at x = 0 and x = a	$\dfrac{2}{a}\sum\limits_{n=1}^{\infty} \sin\dfrac{n\pi x}{a}\sin\dfrac{n\pi x_0}{a}\exp\left[-\dfrac{n^2\pi^2 k_x \tau}{\alpha a^2}\right]$
No-flow at x = 0 and x = a	$\dfrac{1}{a}\left(1+2\sum\limits_{n=1}^{\infty}\cos\dfrac{n\pi x}{a}\cos\dfrac{n\pi x_0}{a}\exp\left[-\dfrac{n^2\pi^2 k_x \tau}{\alpha a^2}\right]\right)$
No-flow at x = 0 Constant pressure at x = a	$\dfrac{2}{a}\left(\sum\limits_{n=1}^{\infty}\cos\dfrac{(2n+1)\pi x}{a}\cos\dfrac{(2n+1)\pi x_0}{a}\exp\left[-\dfrac{(2n+1)^2\pi^2 k_x \tau}{4\alpha a^2}\right]\right)$

where, $\alpha = \phi\mu c_t$.

By Newman's rule, the instantaneous Green's function in a 3D domain can be obtained by multiplying the instantaneous Green's function in each direction. In other words, the product of the three 1D solutions is the solution of the 3D problem.[23] For instance, the pressure drop as a results of a constant production, q, at a position (x_0, y_0, z_0) in a homogeneous box-shaped reservoir measured at a position (x, y, z) is readily calculated by

$$p_{init} - p(x,y,z,t) = \left[\frac{B_o\mu_o q_o}{L\alpha}\right]\left(S_x S_y S_z\right)$$ (3.15)

The boundary conditions of the reservoir can be any boundary conditions depending on the instantaneous Green's functions, S_x, S_y, S_z defined in Table 3.1. Fig. 3.4 shows the geometry of the source and the reservoir.
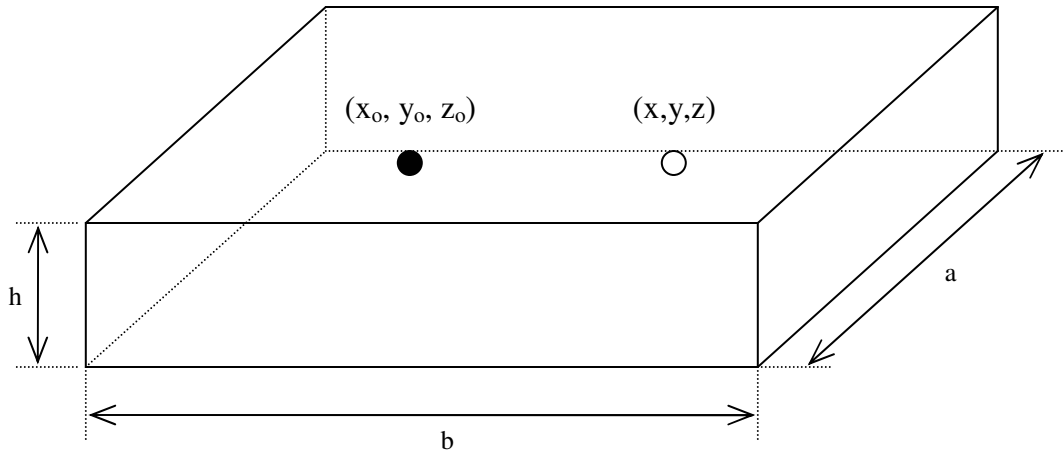
Fig. 3.4 Instantaneous point source in a box-shaped reservoir.

From all type of boundary conditions, one special case is that the reservoir is completely bounded or no-flow across the reservoir boundary, and S_x, S_y, and S_z in this case are

$$S_x = \frac{1}{a}\left(1 + 2\sum_{n=1}^{\infty} \cos\frac{n\pi x}{a}\cos\frac{n\pi x_0}{a}\exp\left[-\frac{n^2\pi^2 k_x\tau}{\alpha a^2}\right]\right) \tag{3.16}$$

$$S_y = \frac{1}{b}\left(1 + 2\sum_{m=1}^{\infty} \cos\frac{m\pi y}{b}\cos\frac{m\pi y_0}{b}\exp\left[-\frac{m^2\pi^2 k_y\tau}{\alpha b^2}\right]\right) \tag{3.17}$$

$$S_z = \frac{1}{h}\left(1 + 2\sum_{l=1}^{\infty} \cos\frac{l\pi z}{h}\cos\frac{l\pi z_0}{h}\exp\left[-\frac{l^2\pi^2 k_z\tau}{\alpha h^2}\right]\right) \tag{3.18}$$

If the reservoir is sealed at the top and the bottom boundaries and has a constant pressure at the horizontal direction, the S_x, S_y, and S_z will be

$$S_x = \frac{2}{a}\sum_{n=1}^{\infty} \sin\frac{n\pi x}{a}\sin\frac{n\pi x_0}{a}\exp\left[-\frac{n^2\pi^2 k_x\tau}{\alpha a^2}\right] \tag{3.19}$$

$$S_y = \frac{2}{b} \sum_{m=1}^{\infty} sin\frac{m\pi y}{b} \, sin\frac{m\pi y_0}{b} \, exp\left[-\frac{m^2\pi^2 k_y\tau}{\alpha b^2}\right] \tag{3.20}$$

$$S_z = \frac{1}{h}\left(1 + 2\sum_{l=1}^{\infty} cos\frac{l\pi z}{h}\,cos\frac{l\pi z_0}{h}\,exp\left[-\frac{l^2\pi^2 k_z\tau}{\alpha h^2}\right]\right) \tag{3.21}$$

3.2.2 Continuous Point Source Solution

After we obtain the instantaneous point source solution under defined boundary conditions, we integrate the instantaneous point source over a time interval to attain the continuous point source solution. The pressure drop at point (x, y, z) as a result of the continuous production or injection at point (x_0, y_0, z_0) in a homogenous box-shaped reservoir as shown in Fig. 3.4 is estimated by

$$p_{init} - p(x,y,z,t) = \int_0^t \left[\frac{B_o\mu_o q_o}{L\alpha}\right]\left(S_x S_y S_z\right)d\tau \tag{3.22}$$

The S_x, S_y, and S_z in Eq. 3.22 can be any combinations of the instantaneous Green's function depending on the interested boundary conditions.

3.2.3 Continuous Line Source Solution for 2D Wellbore

The continuous line source solution is calculated by integrating the continuous point source solution along the line. For the line source that have the initial position at (x_0,y_{01},z_{01}) and the end point at (x_0,y_{02},z_{02}), the solution of the continuous line source can be written as,

$$p_{init} - p(x,y,z,t) = \int_{(y_{01},z_{01})}^{(y_{02},z_{02})}\int_0^t \left[\frac{B_o\mu_o q_o}{L\alpha}\right]\left(S_x S_y S_z\right)d\tau dL \tag{3.23}$$

If the source is a straight line, then the source trajectory can be represented by a linear equation written as,

$$z_0 = \hat{m}y_0 + \hat{c} \tag{3.24}$$

where $\hat{m}$ is the slope of the line and $\hat{c}$ is the interception shown in Fig. 3.5.

$$y_0 = \hat{m} \, z_0 + \hat{c}$$

$$\hat{m} = \frac{z_{o2} - z_{o1}}{y_{o2} - y_{o1}}$$
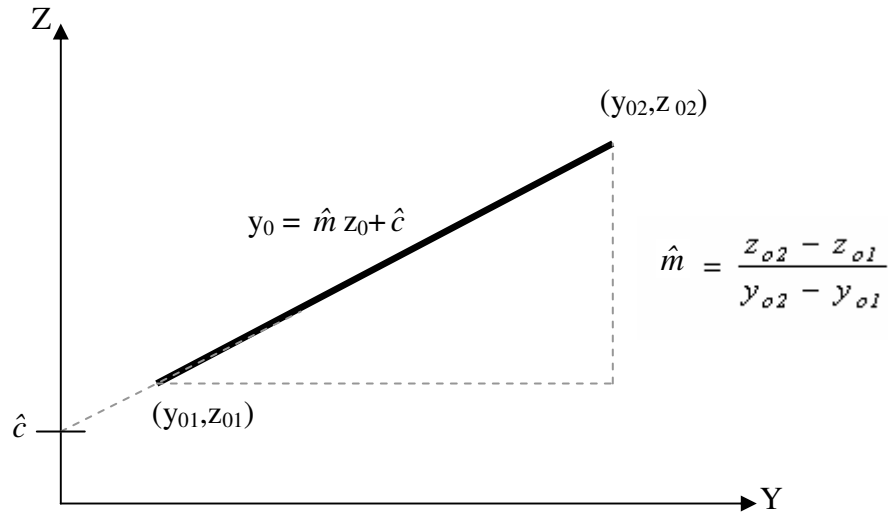
Fig. 3.5 Schematic of a straight wellbore trajectory.

The length of the line, $\hat{s}$, is calculated by

$$\hat{s} = \int_{(y_{01},z_{01})}^{(y_{02},z_{02})} dL \tag{3.25}$$

We can write the length of the line as

$$\hat{s} = \int_{y_1}^{y_2} \left(\sqrt{1 + \left(\frac{dz}{dy}\right)^2} \right) dy_0 \tag{3.26}$$

Since *(dz/dy)* is a slope of the linear function, Eq. 3.26 becomes

$$\hat{s} = \int_{y_1}^{y_2} \left(\sqrt{1 + (\hat{m})^2} \right) dy_0 \tag{3.27}$$

Combining Eq. 3.27 and Eq. 3.25, we have

$$\int_{(y_{01},z_{01})}^{(y_{02},z_{02})} dL = \int_{y_1}^{y_2} \left(\sqrt{1+(\hat{m})^2} \right) dy_0 \tag{3.28}$$

Substituting Eq. 3.28 into Eq. 3.23, we have

$$p_{init} - p(x,y,z,t) = \int_0^t \int_{y_1}^{y_2} \left[\frac{B_o \mu_o q_o}{L\alpha} \right] \left(S_x S_y S_z \right) \left(\sqrt{1+(\hat{m})^2} \right) dy_o d\tau \tag{3.29}$$

If the line source produces at a constant rate, q_o, and the slope of the line source is constant, Eq. 3.30 becomes,

$$p_{init} - p(x,y,z,t) = \left[\frac{B_o \mu_o q_o \left(\sqrt{1+(\hat{m})^2} \right)}{L\alpha} \right] \int_0^t \int_{y_1}^{y_2} \left(S_x S_y S_z \right) dy_o d\tau \tag{3.30}$$

For a homogeneous close box-shaped reservoir, the source functions are

$$S_x = \frac{1}{a} \left(1 + 2 \sum_{n=1}^{\infty} \cos \frac{n\pi x}{a} \cos \frac{n\pi x_0}{a} \exp \left[-\frac{n^2 \pi^2 k_x \tau}{\alpha a^2} \right] \right) \tag{3.31}$$

$$S_y = \frac{1}{b} \left(1 + 2 \sum_{m=1}^{\infty} \cos \frac{m\pi y}{b} \cos \frac{m\pi y_0}{b} \exp \left[-\frac{m^2 \pi^2 k_y \tau}{\alpha b^2} \right] \right) \tag{3.32}$$

$$S_z = \frac{1}{h} \left(1 + 2 \sum_{l=1}^{\infty} \cos \frac{l\pi z}{h} \cos \frac{l\pi z_0}{h} \exp \left[-\frac{l^2 \pi^2 k_z \tau}{\alpha h^2} \right] \right) \tag{3.33}$$

With individual source function, the pressure in 3D domain is calculated by substituting Eq. 3.31-Eq. 3.33 into Eq. 3.30 and integrating Eq. 3.30. The solution is

$$p_{init} - p(x,y,z,t) = \left[\frac{B_o \mu_o q_o}{abhL\alpha} \right] \sqrt{(1+\hat{m}^2)}$$

$$\left\{ (y_2 - y_1)t + \frac{2\alpha a^2 (y_2 - y_1)}{\pi^2 k_x} \sum_{n=1}^{\infty} \cos \frac{n\pi x}{a} \cos \frac{n\pi x_0}{a} \left(1 - \exp \left[-\frac{n^2 \pi^2 k_x \tau}{\alpha a^2} \right] \right) \right.$$

$$+\frac{2\alpha b^3}{\pi^3 k_y}\sum_{m=1}^{\infty}\frac{\cos\frac{m\pi y}{b}\left(\sin\frac{m\pi y_2}{b}-\sin\frac{m\pi y_1}{b}\right)}{m^3}\left(1-exp\left[-\frac{m^2\pi^2 k_y\tau}{\alpha b^2}\right]\right)$$

$$+\frac{2\alpha h^3}{\hat{m}\pi^3 k_z}\sum_{l=1}^{\infty}\frac{\cos\frac{l\pi z}{h}\left(\sin\frac{l\pi(\hat{m}y_2+\hat{c})}{h}-\sin\frac{l\pi(\hat{m}y_1+\hat{c})}{h}\right)}{l^3}\left(1-exp\left[-\frac{l^2\pi^2 k_z\tau}{\alpha h^2}\right]\right)$$

$$+\frac{4\alpha h}{\hat{m}\pi^3}\sum_{l=1}^{\infty}\sum_{n=1}^{\infty}\frac{\cos\frac{n\pi x}{a}\cos\frac{n\pi x_0}{a}\cos\frac{l\pi z}{h}\left(\sin\frac{l\pi(\hat{m}y_2+\hat{c})}{h}-\sin\frac{l\pi(\hat{m}y_1+\hat{c})}{h}\right)}{l\left(\frac{l^2 k_z}{h^2}+\frac{n^2 k_x}{a^2}\right)}$$

$$\left(1-exp\left[-\frac{\pi^2\tau}{\alpha}\left(\frac{l^2 k_z}{h^2}+\frac{n^2 k_x}{a^2}\right)\right]\right)$$

$$+\frac{4\alpha b}{\pi^3}\sum_{m=1}^{\infty}\sum_{n=1}^{\infty}\frac{\cos\frac{n\pi x}{a}\cos\frac{n\pi x_0}{a}\cos\frac{m\pi y}{b}\left(\sin\frac{m\pi y_2}{b}-\sin\frac{m\pi y_1}{b}\right)}{m\left(\frac{m^2 k_y}{b^2}+\frac{n^2 k_x}{a^2}\right)}$$

$$\left(1-exp\left[-\frac{\pi^2\tau}{\alpha}\left(\frac{m^2 k_y}{b^2}+\frac{n^2 k_x}{a^2}\right)\right]\right)$$

$$+\frac{2\alpha bh}{\pi^2}\sum_{l=1}^{\infty}\sum_{m=1}^{\infty}\frac{\cos\frac{m\pi y}{b}\cos\frac{l\pi z}{h}}{\left(\frac{m^2 k_y}{b^2}+\frac{l^2 k_z}{h^2}\right)}\left(1-exp\left[-\frac{\pi^2\tau}{\alpha}\left(\frac{m^2 k_y}{b^2}+\frac{l^2 k_z}{h^2}\right)\right]\right)$$

$$\left\{\left[\frac{\sin\left(\frac{\pi(-hmy_2+bl(\hat{m}y_2+\hat{c}))}{bh}\right)}{-hm\pi+bl\pi\hat{m}}+\frac{\sin\left(\frac{\pi(hmy_2+bl(\hat{m}y_2+\hat{c}))}{bh}\right)}{hm\pi+bl\pi\hat{m}}\right]\right.$$

$$-\left[\frac{\sin\left(\frac{\pi\left(-hmy_1+bl(\hat{m}y_1+\hat{c})\right)}{bh}\right)}{-hm\pi+bl\pi\hat{m}}+\frac{\sin\left(\frac{\pi\left(hmy_1+bl(\hat{m}y_1+\hat{c})\right)}{bh}\right)}{hm\pi+bl\pi\hat{m}}\right]\Bigg]\Bigg\}$$

$$+\frac{4\alpha bh}{\pi^2}\sum_{l=1}^{\infty}\sum_{m=1}^{\infty}\sum_{n=1}^{\infty}\frac{\cos\dfrac{n\pi x}{a}\cos\dfrac{n\pi x_0}{a}\cos\dfrac{m\pi y}{b}\cos\dfrac{l\pi z}{h}}{\left(\dfrac{n^2 k_x}{a^2}+\dfrac{m^2 k_y}{b^2}+\dfrac{l^2 k_z}{h^2}\right)}$$

$$\Bigg\{\left[\frac{\sin\left(\frac{\pi\left(-hmy_2+bl(\hat{m}y_2+\hat{c})\right)}{bh}\right)}{-hm\pi+bl\pi\hat{m}}+\frac{\sin\left(\frac{\pi\left(hmy_2+bl(\hat{m}y_2+\hat{c})\right)}{bh}\right)}{hm\pi+bl\pi\hat{m}}\right]$$

$$-\left[\frac{\sin\left(\frac{\pi\left(-hmy_1+bl(\hat{m}y_1+\hat{c})\right)}{bh}\right)}{-hm\pi+bl\pi\hat{m}}+\frac{\sin\left(\frac{\pi\left(hmy_1+bl(\hat{m}y_1+\hat{c})\right)}{bh}\right)}{hm\pi+bl\pi\hat{m}}\right]\Bigg\}$$

$$\left(1-\exp\left[-\frac{\pi^2\tau}{\alpha}\left(\frac{n^2 k_x}{a^2}+\frac{m^2 k_y}{b^2}+\frac{l^2 k_z}{h^2}\right)\right]\right)\Bigg]\Bigg\}\Bigg\} \qquad (3.34)$$

At late time or stabilized flow, the exponential terms in Eq. 3.34 becomes zero and Eq. 3.34 reduces to

$$p_{init}-p(x,y,z,t)=\left[\frac{B_o\mu_o q_o}{abhL\alpha}\right]\sqrt{\left(1+\hat{m}^2\right)}$$

$$\Bigg\{(y_2-y_1)t+\frac{2\alpha a^2(y_2-y_1)}{\pi^2 k_x}\sum_{n=1}^{\infty}\cos\frac{n\pi x}{a}\cos\frac{n\pi x_0}{a}$$

$$+\frac{2\alpha b^3}{\pi^3 k_y}\sum_{m=1}^{\infty}\frac{\cos\dfrac{m\pi y}{b}\left(\sin\dfrac{m\pi y_2}{b}-\sin\dfrac{m\pi y_1}{b}\right)}{m^3}$$

$$+\frac{2\alpha h^3}{\hat{m}\pi^3 k_z}\sum_{l=1}^{\infty}\frac{\cos\frac{l\pi z}{h}\left(\sin\frac{l\pi(\hat{m}y_2+\hat{c})}{h}-\sin\frac{l\pi(\hat{m}y_1+\hat{c})}{h}\right)}{l^3}$$

$$+\frac{4\alpha h}{\hat{m}\pi^3}\sum_{l=1}^{\infty}\sum_{n=1}^{\infty}\frac{\cos\frac{n\pi x}{a}\cos\frac{n\pi x_0}{a}\cos\frac{l\pi z}{h}\left(\sin\frac{l\pi(\hat{m}y_2+\hat{c})}{h}-\sin\frac{l\pi(\hat{m}y_1+\hat{c})}{h}\right)}{l\left(\frac{l^2 k_z}{h^2}+\frac{n^2 k_x}{a^2}\right)}$$

$$+\frac{4\alpha b}{\pi^3}\sum_{m=1}^{\infty}\sum_{n=1}^{\infty}\frac{\cos\frac{n\pi x}{a}\cos\frac{n\pi x_0}{a}\cos\frac{m\pi y}{b}\left(\sin\frac{m\pi y_2}{b}-\sin\frac{m\pi y_1}{b}\right)}{m\left(\frac{m^2 k_y}{b^2}+\frac{n^2 k_x}{a^2}\right)}$$

$$+\frac{2\alpha bh}{\pi^2}\sum_{l=1}^{\infty}\sum_{m=1}^{\infty}\frac{\cos\frac{m\pi y}{b}\cos\frac{l\pi z}{h}}{\left(\frac{m^2 k_y}{b^2}+\frac{l^2 k_z}{h^2}\right)}$$

$$\left\{\left[\frac{\sin\left(\frac{\pi(-hmy_2+bl(\hat{m}y_2+\hat{c}))}{bh}\right)}{-hm\pi+bl\pi\hat{m}}+\frac{\sin\left(\frac{\pi(hmy_2+bl(\hat{m}y_2+\hat{c}))}{bh}\right)}{hm\pi+bl\pi\hat{m}}\right]\right.$$

$$\left.-\left[\frac{\sin\left(\frac{\pi(-hmy_1+bl(\hat{m}y_1+\hat{c}))}{bh}\right)}{-hm\pi+bl\pi\hat{m}}+\frac{\sin\left(\frac{\pi(hmy_1+bl(\hat{m}y_1+\hat{c}))}{bh}\right)}{hm\pi+bl\pi\hat{m}}\right]\right\}$$

$$+\frac{4\alpha bh}{\pi^2}\sum_{l=1}^{\infty}\sum_{m=1}^{\infty}\sum_{n=1}^{\infty}\frac{\cos\frac{n\pi x}{a}\cos\frac{n\pi x_0}{a}\cos\frac{m\pi y}{b}\cos\frac{l\pi z}{h}}{\left(\frac{n^2 k_x}{a^2}+\frac{m^2 k_y}{b^2}+\frac{l^2 k_z}{h^2}\right)}$$

$$\left\{\left[\left[\frac{sin\left(\frac{\pi\left(-hmy_2+bl(\hat{m}y_2+\hat{c})\right)}{bh}\right)}{-hm\pi+bl\pi\hat{m}}+\frac{sin\left(\frac{\pi\left(hmy_2+bl(\hat{m}y_2+\hat{c})\right)}{bh}\right)}{hm\pi+bl\pi\hat{m}}\right]\right.\right.$$

$$\left.\left.-\left[\frac{sin\left(\frac{\pi\left(-hmy_1+bl(\hat{m}y_1+\hat{c})\right)}{bh}\right)}{-hm\pi+bl\pi\hat{m}}+\frac{sin\left(\frac{\pi\left(hmy_1+bl(\hat{m}y_1+\hat{c})\right)}{bh}\right)}{hm\pi+bl\pi\hat{m}}\right]\right]\right\} \qquad (3.35)$$

Eq. 3.34 is the analytical line source solution for any time periods and Eq. 3.35 is the analytical line source solution at late time. The direction of the line source in both equations can change in the y-direction and in the z-direction. We can use these equations predict the horizontal well performance, inclined well performance or vertical well performance. By using this model along with superposition technique, we can predict the performance of undulating wells as well, and that will be discussed in Chapter IV.

3.3 Line Source Application

The line source solution is applicable to estimate the well performance. In this section we present the application of using the continuous line source to evaluate well performance. Since the diameter of a wellbore is much smaller than the dimension of reservoirs, using line source to represent a wellbore is reasonable.

To calculate the well performance, an inner boundary condition is necessary. The inner boundary condition defines the pattern of the fluid flow into the wellbore, which can be uniform flux, infinite conductivity, or finite conductivity. For the uniform flux boundary condition, the inflow distribution along the wellbore is uniform. The infinite conductivity boundary condition has the uniform pressure (no pressure drop) along the wellbore. The finite conductivity boundary condition allows wellbore pressure drop, and

the solution is obtained by coupling the line source solution with the wellbore pressure drop model presented in Chapter II.

After we defined the inner boundary condition, the well performance is calculated by specifying the wellbore pressure at the heel or specifying the total production at the surface. If the reservoir is isotropic, the wellbore pressure is evaluated at the wellbore radius. For an anisotropic reservoir, we compute the equivalent wellbore radius shown by Eq. 3.10 and the wellbore pressure is evaluated at the equivalent wellbore radius.

Z

X

Y

Flow direction

(x_o, y_{o1}, z_o) (x_o, y_{o2}, z_o)

h

a

b

p_{wf}

(x_o, y_o, z_o)

Insert
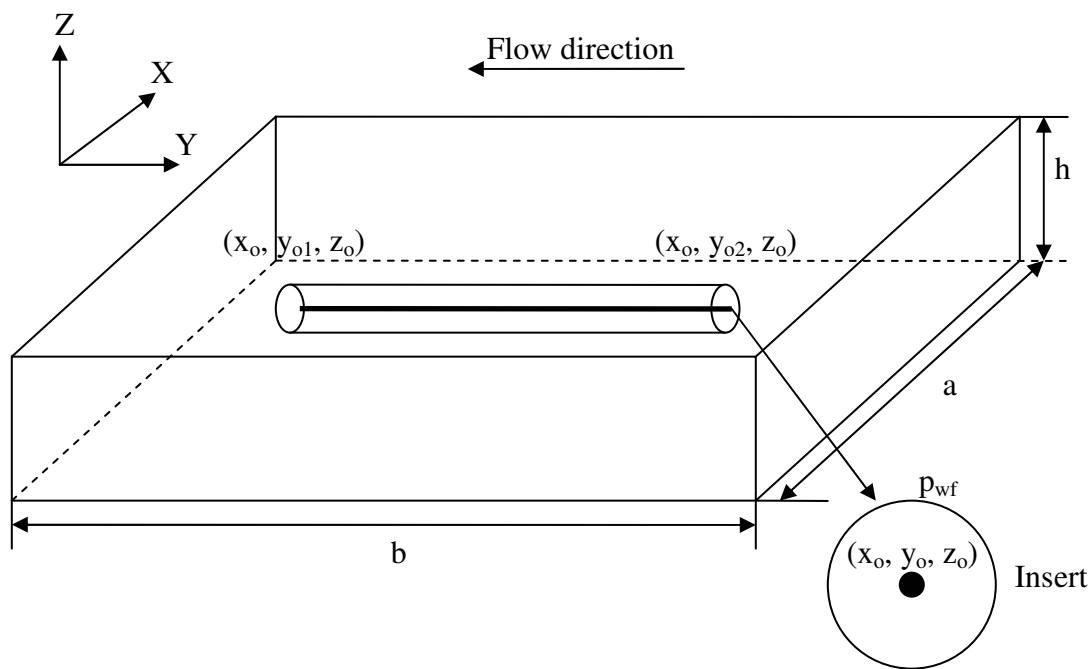
Fig. 3.6 Line source well modeling.

3.3.1 Horizontal Wells

Using the line source solution to calculate a horizontal well performance, we first define inner boundary condition. Then to count for wellbore pressure change, we divide the wellbore into N segments. Each segment connects to each other by applying the

superposition in space. By using this technique, a set of linear equation is generated and solved to predict the well performance. The pressure drop causes by a constant production flow rate, q_1, into segment 1 is evaluated on the well circumstance at the middle of every well segment, which marked as CP for the first segment in Fig. 3.7. For each segment, we have a set of N linear equations for pressure respond to the flow. With N segments, there are N set of N linear equations.
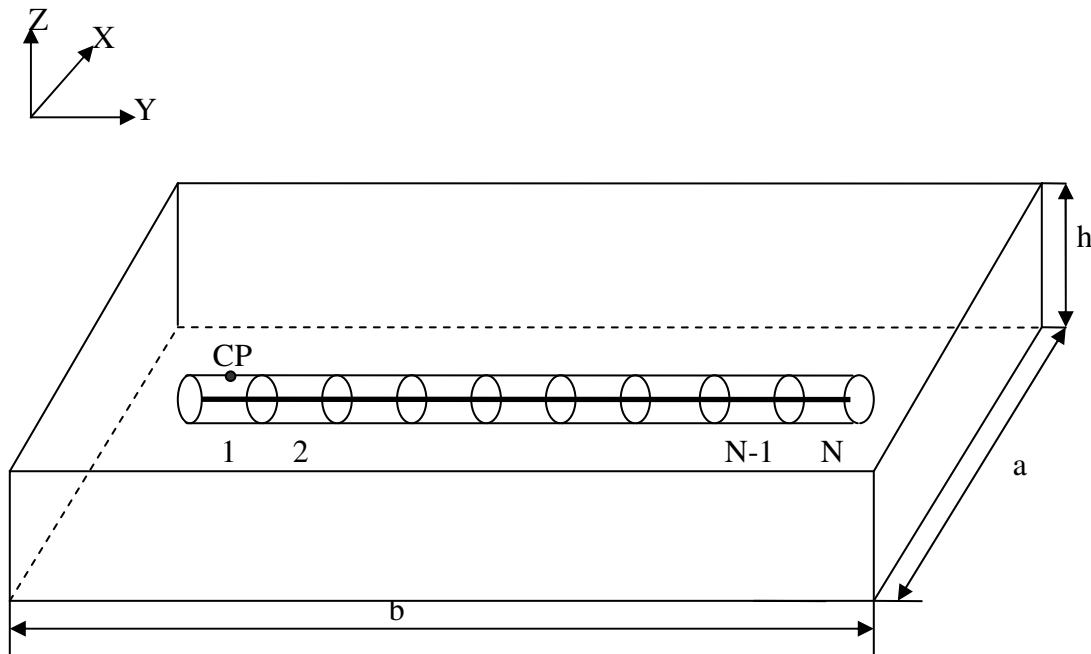
Fig. 3.7 Line source horizontal well modeling.

If we have a closed box-shaped reservoir, the performance of a horizontal well is evaluated by Eq. 3.35 for late time period. For a perfectly horizontal well, the slope, $\hat{m}$, and a constant, $\hat{c}$, are zero and the solution of Eq. 3.30 becomes

$$p_{init} - p(x, y, z, t) = \left[\frac{B_o \mu_o q_o}{abh\alpha}\right]\left\{t + \frac{2\alpha h^2}{\pi^2 k_z}\sum_{l=1}^{\infty}\frac{\cos\frac{l\pi z}{h}\cos\frac{l\pi z_0}{h}}{l^2}\right.$$

$$+ \frac{2\alpha b^3}{\pi^3 k_y (y_2 - y_1)}\sum_{m=1}^{\infty}\frac{\cos\frac{m\pi y}{b}\left[\sin\frac{m\pi y_2}{b} - \sin\frac{m\pi y_1}{b}\right]}{m^3}$$

$$+ \frac{4b\alpha}{\pi^3 (y_2 - y_1)}\sum_{m=1}^{\infty}\sum_{l=1}^{\infty}\frac{\cos\frac{l\pi z}{h}\cos\frac{l\pi z_0}{h}\cos\frac{m\pi y}{b}}{m\left(\frac{m^2 k_y}{b^2} + \frac{l^2 k_z}{h^2}\right)}\left[\sin\frac{m\pi y_2}{b} - \sin\frac{m\pi y_1}{b}\right]$$

$$+ \frac{2\alpha a^2}{\pi^2 k_x}\sum_{n=1}^{\infty}\frac{\cos\frac{n\pi x}{a}\cos\frac{n\pi x_0}{a}}{n^2}$$

$$+ \frac{4\alpha}{\pi^2}\sum_{l=1}^{\infty}\sum_{n=1}^{\infty}\frac{\cos\frac{n\pi x}{a}\cos\frac{n\pi x_0}{a}\cos\frac{l\pi z}{h}\cos\frac{l\pi z_0}{h}}{\left(\frac{l^2 k_z}{h^2} + \frac{n^2 k_x}{a^2}\right)}$$

$$+ \frac{4b\alpha}{\pi^3 (y_2 - y_1)}\sum_{m=1}^{\infty}\sum_{n=1}^{\infty}\frac{\cos\frac{n\pi x}{a}\cos\frac{n\pi x_0}{a}\cos\frac{m\pi y}{b}}{m\left(\frac{m^2 k_y}{b^2} + \frac{n^2 k_x}{a^2}\right)}\left[\sin\frac{m\pi y_2}{b} - \sin\frac{m\pi y_1}{b}\right]$$

$$+ \frac{8b\alpha}{\pi^3 (y_2 - y_1)}\sum_{l=1}^{\infty}\sum_{m=1}^{\infty}\sum_{n=1}^{\infty}\cos\frac{n\pi x}{a}\cos\frac{n\pi x_0}{a}\cos\frac{l\pi z}{h}\cos\frac{l\pi z_0}{h}\cos\frac{m\pi y}{b}$$

$$\left.\frac{\left[\sin\frac{m\pi y_2}{b} - \sin\frac{m\pi y_1}{b}\right]}{m\left(\frac{m^2 k_y}{b^2} + \frac{l^2 k_z}{h^2} + \frac{n^2 k_x}{a^2}\right)}\right\} \tag{3.36}$$

We observe that our line source solution reduces to the same results as the line source solution for a horizontal well presented by Babu and Odeh (Appendix B) validating our

line source model. For stabilized flow under pseudosteady-state condition, the average reservoir pressure can be written as

$$p_R - p_{init} = -\frac{B_o N_p}{V_p c_t} \tag{3.37}$$

Considering the drainage volume, then

$$p_{init} = p_R + \frac{B_o q_o}{abh\phi c_t} t \tag{3.38}$$

Because $\alpha = \phi \mu_o c_t$ we substitute α into Eq. 3.36 and we obtain

$$p_{init} = p_R + \frac{\mu_o B_o q_o}{abh\alpha} t \tag{3.39}$$

Substituting Eq. 3.39 into Eq. 3.36, we have

$$p_R - p(x,y,z,t) = -\frac{q_o \mu_o B_o}{abh\alpha} t + \left[\frac{q_o \mu_o B_o}{abh\alpha}\right]\left\{t + \frac{2\alpha h^2}{\pi^2 k_z}\sum_{l=1}^{\infty}\frac{\cos\dfrac{l\pi z}{h}\cos\dfrac{l\pi z_0}{h}}{l^2}\right.$$

$$+\frac{2\alpha b^3}{\pi^3 k_y (y_2 - y_1)}\sum_{m=1}^{\infty}\frac{\cos\dfrac{m\pi y}{b}\left[\sin\dfrac{m\pi y_2}{b} - \sin\dfrac{m\pi y_1}{b}\right]}{m^3}$$

$$+\frac{4b\alpha}{\pi^3 (y_2 - y_1)}\sum_{m=1}^{\infty}\sum_{l=1}^{\infty}\frac{\cos\dfrac{l\pi z}{h}\cos\dfrac{l\pi z_0}{h}\cos\dfrac{m\pi y}{b}}{m\left(\dfrac{m^2 k_y}{b^2} + \dfrac{l^2 k_z}{h^2}\right)}\left[\sin\dfrac{m\pi y_2}{b} - \sin\dfrac{m\pi y_1}{b}\right]$$

$$+\frac{2\alpha a^2}{\pi^2 k_x}\sum_{n=1}^{\infty}\frac{\cos\dfrac{n\pi x}{a}\cos\dfrac{n\pi x_0}{a}}{n^2}$$

$$+\frac{4\alpha}{\pi^2}\sum_{l=1}^{\infty}\sum_{n=1}^{\infty}\frac{\cos\dfrac{n\pi x}{a}\cos\dfrac{n\pi x_0}{a}\cos\dfrac{l\pi z}{h}\cos\dfrac{l\pi z_0}{h}}{\left(\dfrac{l^2 k_z}{h^2} + \dfrac{n^2 k_x}{a^2}\right)}$$

$$+\frac{4b\alpha}{\pi^3(y_2-y_1)}\sum_{m=1}^{\infty}\sum_{n=1}^{\infty}\frac{\cos\dfrac{n\pi x}{a}\cos\dfrac{n\pi x_0}{a}\cos\dfrac{m\pi y}{b}}{m\left(\dfrac{m^2 k_y}{b^2}+\dfrac{n^2 k_x}{a^2}\right)}\left[\sin\frac{m\pi y_2}{b}-\sin\frac{m\pi y_1}{b}\right]$$

$$+\frac{8b\alpha}{\pi^3(y_2-y_1)}\sum_{l=1}^{\infty}\sum_{m=1}^{\infty}\sum_{n=1}^{\infty}\frac{\cos\dfrac{n\pi x}{a}\cos\dfrac{n\pi x_0}{a}\cos\dfrac{l\pi z}{h}\cos\dfrac{l\pi z_0}{h}\cos\dfrac{m\pi y}{b}}{m\left(\dfrac{m^2 k_y}{b^2}+\dfrac{l^2 k_z}{h^2}+\dfrac{n^2 k_x}{a^2}\right)}$$

$$\left.\left[\sin\frac{m\pi y_2}{b}-\sin\frac{m\pi y_1}{b}\right]\right\}\tag{3.40}$$

On the right hand side of Eq. 3.40 under pseudosteady-state condition, the first and the second term becomes zero and Eq. 3.40 becomes

$$p_R-p(x,y,z,t)=\left[\frac{B_o\mu_o q_o}{abh\alpha}\right]\left\{\frac{2\alpha h^2}{\pi^2 k_z}\sum_{l=1}^{\infty}\frac{\cos\dfrac{l\pi z}{h}\cos\dfrac{l\pi z_0}{h}}{l^2}\right.$$

$$+\frac{2\alpha b^3}{\pi^3 k_y(y_2-y_1)}\sum_{m=1}^{\infty}\frac{\cos\dfrac{m\pi y}{b}\left[\sin\dfrac{m\pi y_2}{b}-\sin\dfrac{m\pi y_1}{b}\right]}{m^3}$$

$$+\frac{4b\alpha}{\pi^3(y_2-y_1)}\sum_{m=1}^{\infty}\sum_{l=1}^{\infty}\frac{\cos\dfrac{l\pi z}{h}\cos\dfrac{l\pi z_0}{h}\cos\dfrac{m\pi y}{b}}{m\left(\dfrac{m^2 k_y}{b^2}+\dfrac{l^2 k_z}{h^2}\right)}\left[\sin\frac{m\pi y_2}{b}-\sin\frac{m\pi y_1}{b}\right]$$

$$+\frac{2\alpha a^2}{\pi^2 k_x}\sum_{n=1}^{\infty}\frac{\cos\dfrac{n\pi x}{a}\cos\dfrac{n\pi x_0}{a}}{n^2}$$

$$+\frac{4\alpha}{\pi^2}\sum_{l=1}^{\infty}\sum_{n=1}^{\infty}\frac{\cos\dfrac{n\pi x}{a}\cos\dfrac{n\pi x_0}{a}\cos\dfrac{l\pi z}{h}\cos\dfrac{l\pi z_0}{h}}{\left(\dfrac{l^2 k_z}{h^2}+\dfrac{n^2 k_x}{a^2}\right)}$$

$$+\frac{4b\alpha}{\pi^3(y_2-y_1)}\sum_{m=1}^{\infty}\sum_{n=1}^{\infty}\frac{\cos\dfrac{n\pi x}{a}\cos\dfrac{n\pi x_0}{a}\cos\dfrac{m\pi y}{b}}{m\left(\dfrac{m^2 k_y}{b^2}+\dfrac{n^2 k_x}{a^2}\right)}\left[\sin\frac{m\pi y_2}{b}-\sin\frac{m\pi y_1}{b}\right]$$

$$+\frac{8b\alpha}{\pi^3(y_2-y_1)}\sum_{l=1}^{\infty}\sum_{m=1}^{\infty}\sum_{n=1}^{\infty}\frac{\cos\dfrac{n\pi x}{a}\cos\dfrac{n\pi x_0}{a}\cos\dfrac{l\pi z}{h}\cos\dfrac{l\pi z_0}{h}\cos\dfrac{m\pi y}{b}}{m\left(\dfrac{m^2 k_y}{b^2}+\dfrac{l^2 k_z}{h^2}+\dfrac{n^2 k_x}{a^2}\right)}$$

$$\left.\left[\sin\frac{m\pi y_2}{b}-\sin\frac{m\pi y_1}{b}\right]\right\} \tag{3.41}$$

In oil field unit, Eq. 3.41 becomes

$$p_R-p(x,y,z,t)=\left[\frac{887.53 B_o\mu_o q_o}{abh\alpha}\right]\left\{\frac{2\alpha h^2}{\pi^2 k_z}\sum_{l=1}^{\infty}\frac{\cos\dfrac{l\pi z}{h}\cos\dfrac{l\pi z_0}{h}}{l^2}\right.$$

$$+\frac{2\alpha b^3}{\pi^3 k_y(y_2-y_1)}\sum_{m=1}^{\infty}\frac{\cos\dfrac{m\pi y}{b}\left[\sin\dfrac{m\pi y_2}{b}-\sin\dfrac{m\pi y_1}{b}\right]}{m^3}$$

$$+\frac{4b\alpha}{\pi^3(y_2-y_1)}\sum_{m=1}^{\infty}\sum_{l=1}^{\infty}\frac{\cos\dfrac{l\pi z}{h}\cos\dfrac{l\pi z_0}{h}\cos\dfrac{m\pi y}{b}}{m\left(\dfrac{m^2 k_y}{b^2}+\dfrac{l^2 k_z}{h^2}\right)}\left[\sin\frac{m\pi y_2}{b}-\sin\frac{m\pi y_1}{b}\right]$$

$$+\frac{2\alpha a^2}{\pi^2 k_x}\sum_{n=1}^{\infty}\frac{\cos\dfrac{n\pi x}{a}\cos\dfrac{n\pi x_0}{a}}{n^2}$$

$$+\frac{4\alpha}{\pi^2}\sum_{l=1}^{\infty}\sum_{n=1}^{\infty}\frac{\cos\dfrac{n\pi x}{a}\cos\dfrac{n\pi x_0}{a}\cos\dfrac{l\pi z}{h}\cos\dfrac{l\pi z_0}{h}}{\left(\dfrac{l^2 k_z}{h^2}+\dfrac{n^2 k_x}{a^2}\right)}$$

49

$$+ \frac{4b\alpha}{\pi^3(y_2 - y_1)} \sum_{m=1}^{\infty} \sum_{n=1}^{\infty} \frac{\cos\frac{n\pi x}{a}\cos\frac{n\pi x_0}{a}\cos\frac{m\pi y}{b}}{m\left(\frac{m^2 k_y}{b^2} + \frac{n^2 k_x}{a^2}\right)} \left[\sin\frac{m\pi y_2}{b} - \sin\frac{m\pi y_1}{b}\right]$$

$$+ \frac{8b\alpha}{\pi^3(y_2 - y_1)} \sum_{l=1}^{\infty} \sum_{m=1}^{\infty} \sum_{n=1}^{\infty} \frac{\cos\frac{n\pi x}{a}\cos\frac{n\pi x_0}{a}\cos\frac{l\pi z}{h}\cos\frac{l\pi z_0}{h}\cos\frac{m\pi y}{b}}{m\left(\frac{m^2 k_y}{b^2} + \frac{l^2 k_z}{h^2} + \frac{n^2 k_x}{a^2}\right)}$$

$$\left[\sin\frac{m\pi y_2}{b} - \sin\frac{m\pi y_1}{b}\right]\Bigg\} \tag{3.42}$$

where $\alpha = 158.73\phi\mu_o c_t$

The pressure drop as a result of each wellbore segment produces at a constant rate is calculated by Eq. 3.42

$$p_R - p(x,y,z,t) = q_j F(i,j) \tag{3.43}$$

where $F(i,j)$ in Eq. 3.43 represents the right hand side of Eq. 3.42 for a constant production rate. The pressure measured at segment i as a result of the production, q_j, at segment j is evaluated by multiplying q_j with $F(i,j)$ as shown in Eq. 3.43. For the entire wellbore (N segment), we obtain a set of linear equation shown as,

$$
\begin{aligned}
q_1 F_{(1,1)} + q_2 F_{(1,2)} + q_3 F_{(1,3)} + q_4 F_{(1,4)} + \cdots + q_N F_{(1,N)} &= \Delta p_1 \\
q_1 F_{(2,1)} + q_2 F_{(2,2)} + q_3 F_{(2,3)} + q_4 F_{(2,4)} + \cdots + q_N F_{(2,N)} &= \Delta p_2 \\
q_1 F_{(3,1)} + q_2 F_{(3,2)} + q_3 F_{(3,3)} + q_4 F_{(3,4)} + \cdots + q_N F_{(3,N)} &= \Delta p_3 \\
q_1 F_{(4,1)} + q_2 F_{(4,2)} + q_3 F_{(4,3)} + q_4 F_{(4,4)} + \cdots + q_N F_{(4,N)} &= \Delta p_4 \\
\vdots & \\
q_1 F_{(N,1)} + q_2 F_{(N,2)} + q_3 F_{(N,3)} + q_4 F_{(N,4)} + \ldots + q_N F_{(N,N)} &= \Delta p_N
\end{aligned}
\tag{3.44}
$$

where, q_j is a constant flow rate flow into segment j and Δp_j is the pressure drop calculated at segment j as a result of the production into every segment. The total production from the entire wellbore is calculated by

$$\sum_{j=1}^{n} q_j = q_{total} \tag{3.45}$$

where q_{total} is the total production for every segment, or the maximum flow rate if the well constraint is constant production rate. By using the above method, we can calculate the horizontal well performance in uniform flux boundary condition, infinite boundary condition, and finite boundary condition. The well is predicted by either a constant flow rate constraint or a constant wellbore pressure constraint.

The inflow distribution along the wellbore depends on the inner boundary conditions. Each inner boundary condition implies the different well and reservoir combination. The finite conductivity inner boundary condition should be used when the flow rate is high and the infinite inner boundary condition can be applied in low flow rate well. An example of horizontal well performance under different inner boundary condition is presented here by using the input data in Table 3.2. The horizontal well is located in the middle of a box-shaped reservoir, as shown in Fig. 3.7.

The well is controlled by a constant wellbore pressure at 3000 psi. First the well is divided into 16 segments. Then we start from the toe segment or segment 16 by calculating the pressure drop at the middle of the well segment on the wellbore circumstance of every segment as a result of a constant flow rate, q_{16}, flowing into the toe segment by using Eq. 3.42. After this calculation, we will have 16 $F(i,j)$ terms (one term per segment). For segment 16 we can write $F(i,j)$ as $F(i,16)$. Then we move to the next segment which is segment 15 and repeat the same procedure but for this segment we evaluate the pressure drop as a result of a constant flow, q_{15}, flowing into segment 15 which gives another 16 $F(i,15)$. We continue this calculation to the heel segment or segment 1. At this point we will obtain totally 16 x 16 $F(i,j)$ terms. Then we use the superposition principle in space to connect the wellbore segments. From superposition principle, we acquire a set of linear equations. The series of linear equations can be written as Eq. 3.46. Then we solve this linear system by defining the inner boundary condition

Table 3.2   Well and reservoir data

Parameters	Data
Reservoir width, ft	2000
Reservoir length, ft	5000
Reservoir thickness, ft	100
Reservoir pressure, psi	4000
Horizontal permeability, md	100
Vertical permeability, md	10
Well length, ft	3000
Wellbore radius, ft	0.25
Oil formation volume factor, res bbl/STB	1
Oil viscosity, cp	1
Wellbore pressure, psi	3000

$$
\begin{aligned}
q_1 F_{(1,1)} + \quad q_2 F_{(1,2)} + \quad q_3 F_{(1,3)} + \quad q_4 F_{(1,4)} + \cdots + q_{16} F_{(1,16)} &= p_i - p_1 \\
q_1 F_{(2,1)} + \quad q_2 F_{(2,2)} + \quad q_3 F_{(2,3)} + \quad q_4 F_{(2,4)} + \cdots + q_{16} F_{(2,16)} &= p_i - p_2 \\
q_1 F_{(3,1)} + \quad q_2 F_{(3,2)} + \quad q_3 F_{(3,3)} + \quad q_4 F_{(3,4)} + \cdots + q_{16} F_{(3,16)} &= p_i - p_3 \\
q_1 F_{(4,1)} + \quad q_2 F_{(4,2)} + \quad q_3 F_{(4,3)} + \quad q_4 F_{(4,4)} + \cdots + q_{16} F_{(4,16)} &= p_i - p_4 \\
\vdots \qquad\qquad\qquad\qquad\qquad\qquad\qquad\qquad\qquad\quad & \\
q_1 F_{(16,1)} + \quad q_2 F_{(16,2)} + \quad q_3 F_{(16,3)} + \quad q_4 F_{(16,4)} + \ldots + q_{16} F_{(16,16)} &= p_i - p_{16}
\end{aligned}
\tag{3.46}
$$

For uniform flux boundary condition, we solve Eq. 3.46 by setting the flow rate into each segment to be the same ($q_i = q_{total}/16$), where i is the index of segments. Then we solve Eq. 3.45 and obtain the pressure at each segment (p_i = 3000 psi). Since the well is controlled by a constant 3000 psi wellbore pressure at the heel, p_1 = 3000 psi. We iterate by changing the total flow rate until we obtain p_1 = 3000 psi for the uniform flux boundary condition. If the inner boundary condition is infinite boundary condition, we set the wellbore pressure in every segment to be 3000 psi, and then calculate the flow

rate into each segment (q_i). For finite inner boundary condition, we have to couple the wellbore pressure drop model with Eq. 3.45 to solve for the pressure distribution.

The wellbore pressure distribution along the wellbore for uniform flux inner boundary condition is shown in Fig. 3.8. The figure shows that wellbore pressure varies along the wellbore because the productivity along the well is not constant. The productivity of horizontal wells is high when the wells are located at the middle of reservoirs because the effect of boundary is minimized. The same phenomenon applies to this case which makes the middle portion of the well have high productivity. In order to make the flow distribution uniform, the drawdown pressure of the high productivity index portion have to be low, which results in the wellbore pressure profile in w-shape. However, in general this pressure profile cannot physically happen during the wellbore flow which implies that the inflow into horizontal wells is usually not uniform. Since the well is controlled by a constant wellbore pressure at 3000 psi, the uniform flow rate is about 19.3 STB/D/ft.

For the infinite conductivity inner boundary condition, the wellbore pressure is constant at 3000 psi along the well and the productivity index is varied along the wellbore as shown in Fig. 3.9. The figure also shows that the flow rate is high at the middle of the well. With the same drawdown, the middle part produces the highest flow rate which makes the flow rate distribution in w-shape. Under uniform wellbore pressure, the flow rate along the well bore is about 18.6 STB/D/ft. The flow rate per feet of the uniform flux inner boundary condition is slightly higher than that of uniform wellbore pressure. The different is less than 4 %.

We notice that when we use uniform flux as an inner boundary condition the wellbore pressure distribution is in w-shape, but for infinite boundary condition or uniform wellbore pressure, the flow rate distribution is a w-shape distribution. Therefore, the inner boundary condition defined well pressure and flow rate distribution and it should be handled carefully.
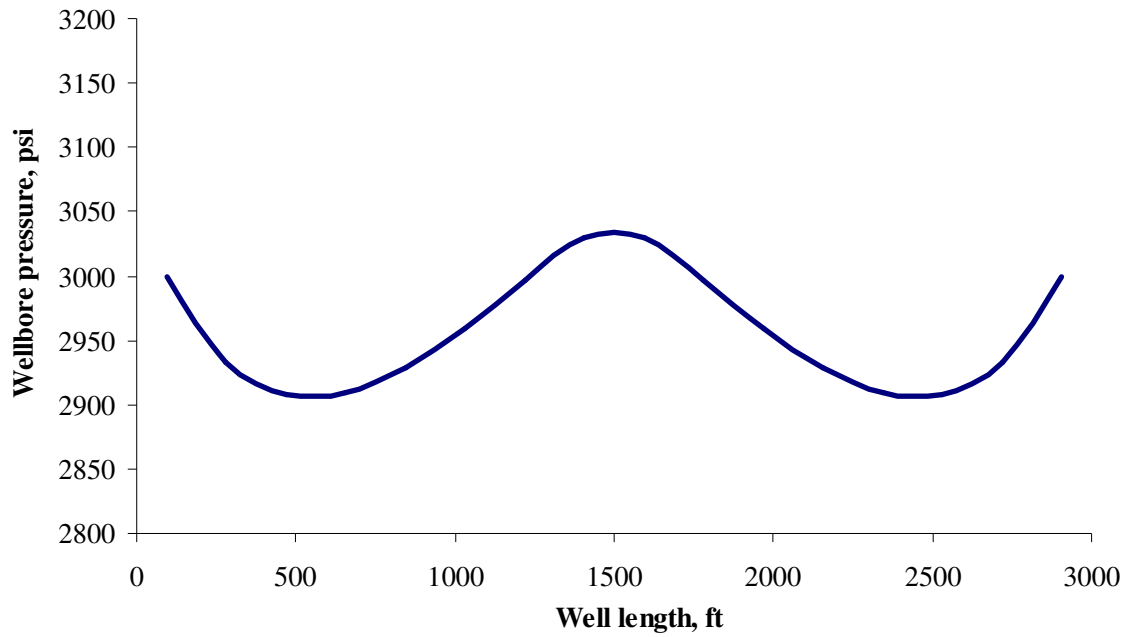
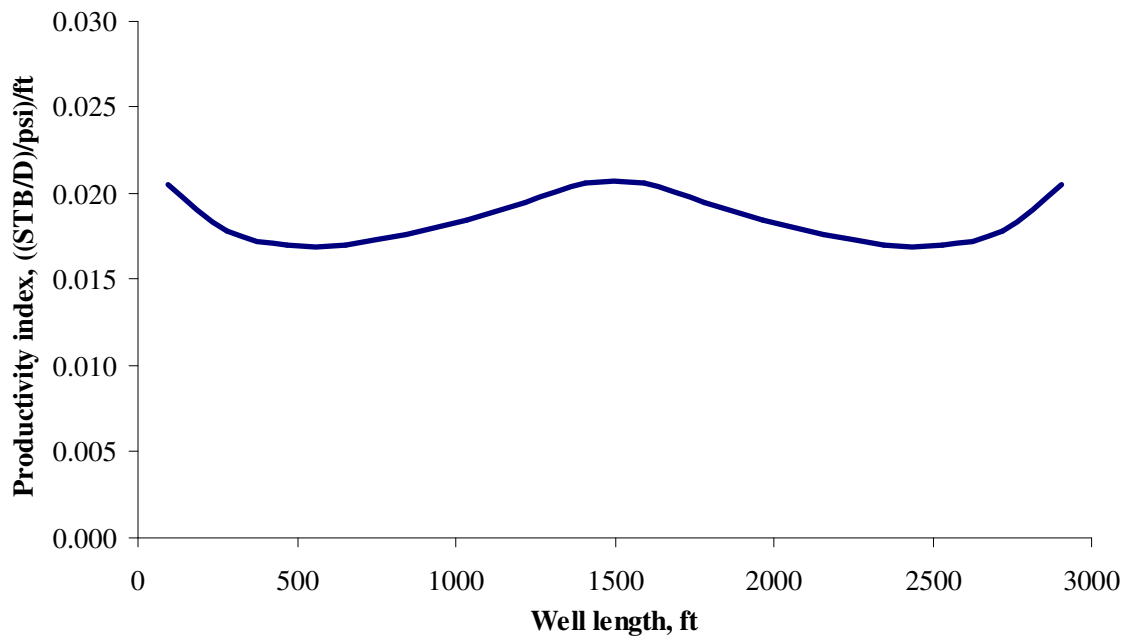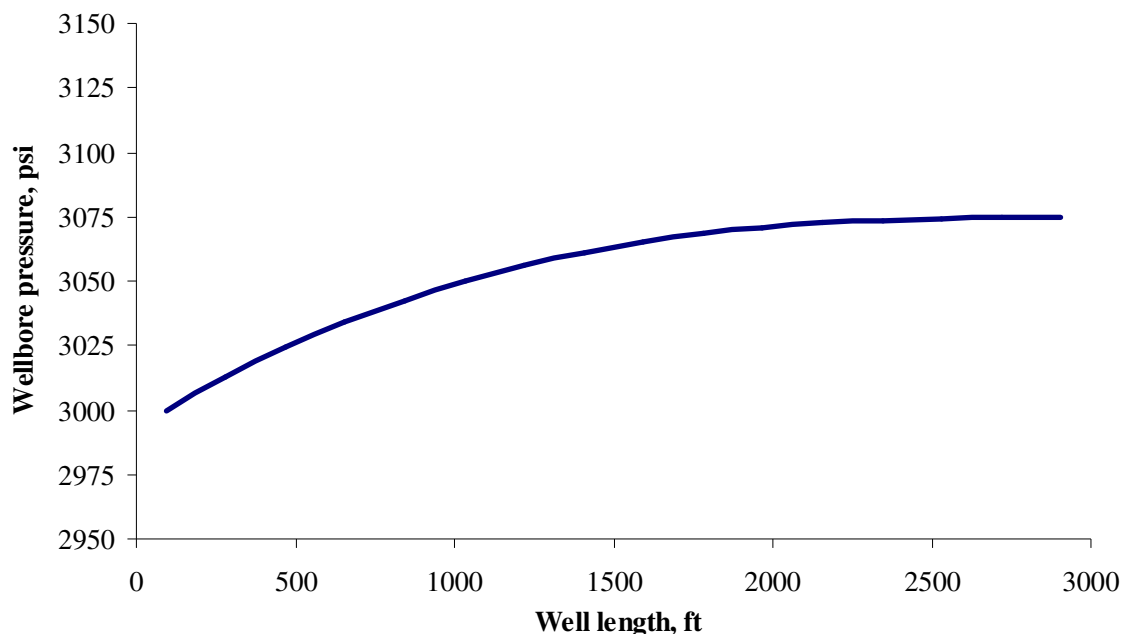**Fig. 3.8 Wellbore pressure profile of uniform flux boundary condition.**

Fig. 3.9 Productivity index profile of infinite conductivity boundary condition.

For the finite conductivity boundary condition, we first evaluate the well performance under infinite conductivity boundary condition. Then we couple the model with the wellbore pressure drop model presented in Chapter II. Since the well is controlled by a constant wellbore pressure at 3000 psi, we have to iterate the coupling model until we obtain the wellbore pressure at the heel segment equal to 3000 psi. Assuming the roughness of the wellbore is 0.01, tubing diameter is 0.5 ft, and the density of the oil is 50 lb/ft^3. The pressure profile under finite conductivity condition is shown in

Fig. 3.10. Since the well is perfectly horizontal, the pressure decreases from the toe to the heel as a result of the frictional pressure drop. The pressure drop increase as the flow rate increase from the toe to the heel. The total pressure drop along the wellbore is about 75 psi. Fig. 3.11 shows the productivity index profile along the wellbore. The flow rate profile under the finite conductivity inner boundary condition is different from that under infinite conductivity inner boundary condition because of the wellbore pressure drop.

Fig. 3.10 Pressure profile under finite conductivity inner boundary condition.

To understand the flow rate distribution along horizontal wells, we set up case studies by varying some important parameters such as anisotropic ratio, the length of the well and the reservoir thickness. The reservoir and well data for this study are shown in Table 3.2. The well is controlled by a wellbore pressure constraint at 3000 psi and the inner boundary condition is infinite conductivity boundary condition.
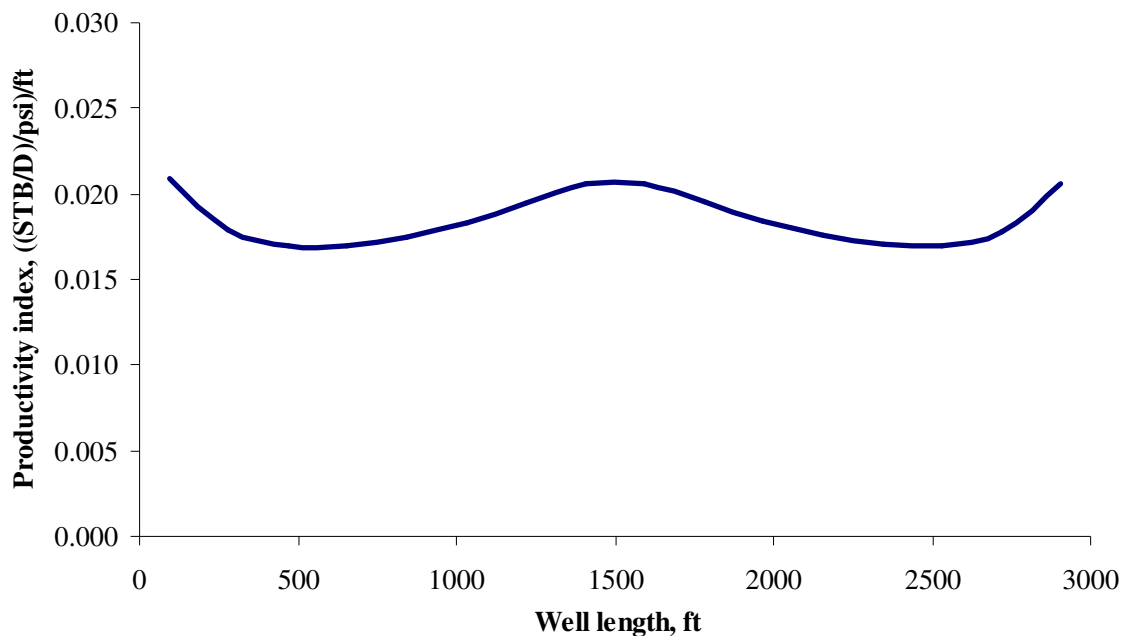
Fig. 3.11 Productivity index profile of the finite conductivity inner boundary condition.

First we study the effect of anisotropic ratio on the flow rate profile. The anisotropic ratios are set to be 0.01, 0.1, and 1. Fig. 3.12 shows the flow rate profile of the horizontal well in different anisotropic ratio reservoirs. We notice that the w-shape is flattened as the anisotropic ratio decreases. However, the distribution shape still has w-shape. The low productivity from low vertical permeability formation smoothes the shape of the distribution.
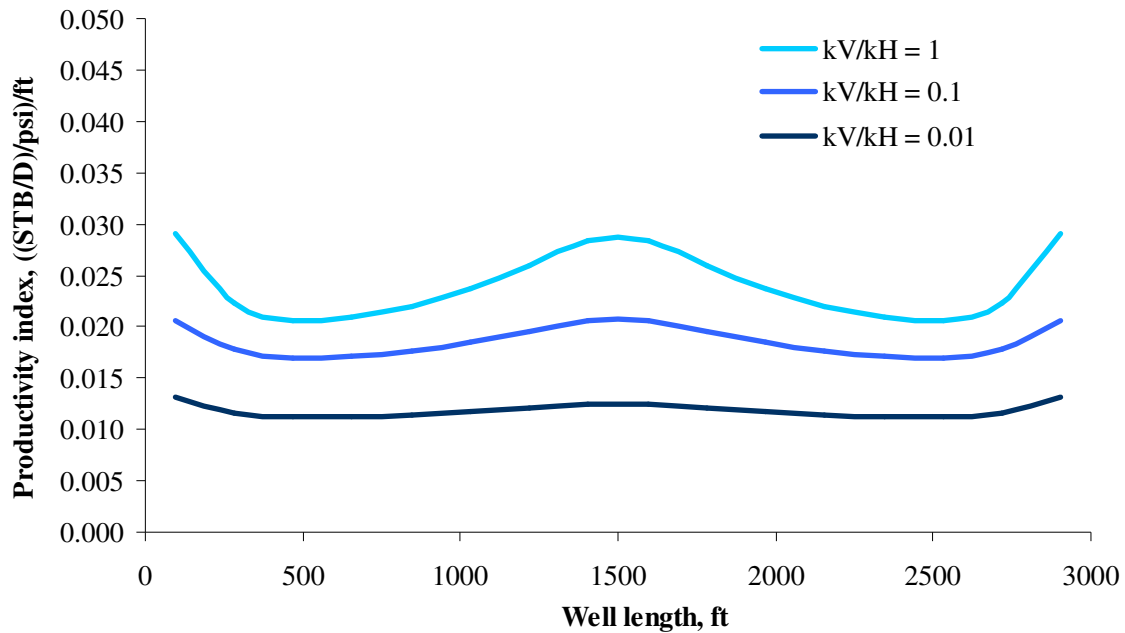
Fig. 3.12 The effect of anisotropic ratio on the productivity index profile.

Next, we study the effect of the well length. Fig. 3.13 shows the flow rate profile of the well with 1000 ft length placed at the middle of the reservoir. From Fig. 3.13, we can see that the flow rate profile of the well is a u-shape, clearly different from the flow rate profile of the well with 3000 ft long which has w-shape, as shown in Fig. 3.12. Since when the wellbore is relatively short comparing to the reservoir dimension, the toe and the heel of the well exposes to the reservoir at both ends of the well, receiving more inflow from the reservoir, which results in high production at the ends of the well. On the other hand, w-shape distribution happens when the well length is relative long comparing with the reservoir length. Therefore, the flow distribution of a horizontal well depends on the ratio of the length of a horizontal well to the reservoir length.
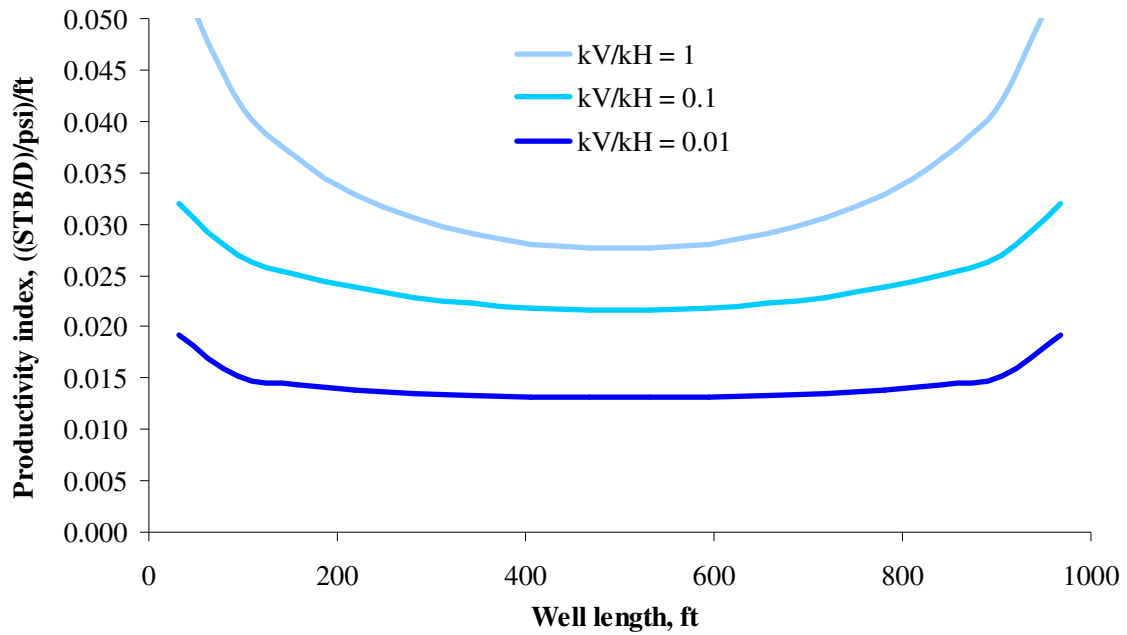
Fig. 3.13 Productivity index profile along 1000 ft wellbore.

The effect of reservoir thickness on the flow distribution along the well is shown as Fig. 3.14. The reservoir thicknesses are 25, 50, and 100 ft. The figure shows that the flow distribution along the wellbore of different reservoir thickness is almost the same for the 50 ft reservoir thickness and 100 ft reservoir thickness. However, the flow distribution is flattened for 25 ft reservoir thickness. For thin reservoir, the productivity index is low and it reduces the scale of w-shape.
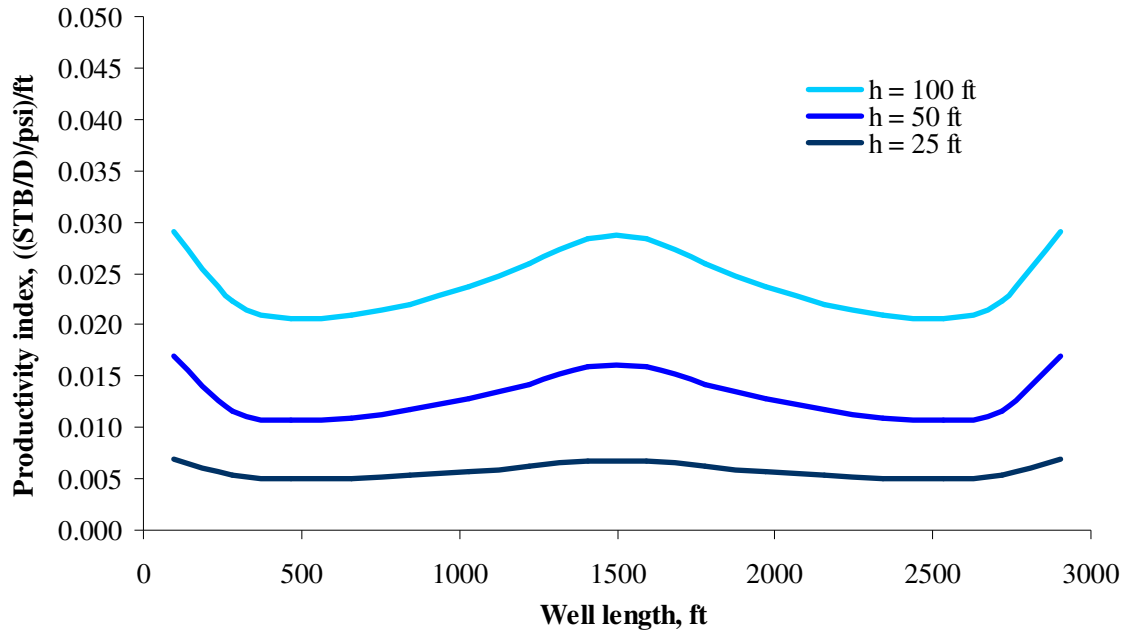
Fig. 3.14 The effect of the reservoir thickness on the productivity index profile.

In conclusion, the flow rate distribution along horizontal well depends on the ratio of the well length to the reservoir length. If this ratio is low or the well is short comparing with the reservoir length, the flow distribution is in u-shape. If the well is relatively long, then the flow distribution is in w-shape. The w-shape will be flat if the anisotropic ratio is extremely low or the reservoir is very thin.

3.3.2 Slanted Wells

The line source solution of 2D wellbore can be used to model slanted wells through Eq. 3.30. After we know the outer boundary condition, we can apply the appropriate source function to the Eq. 3.30. Then we divide the well into N segments and apply the superposition in space to connect wellbore segments. Fig. 3.15 shows the well and reservoir geometry for a slanted well by using the line source model. For a slanted well located in a close box-shape reservoir, Eq. 3.34 and Eq. 3.35 are employed to evaluate the slanted well performance.
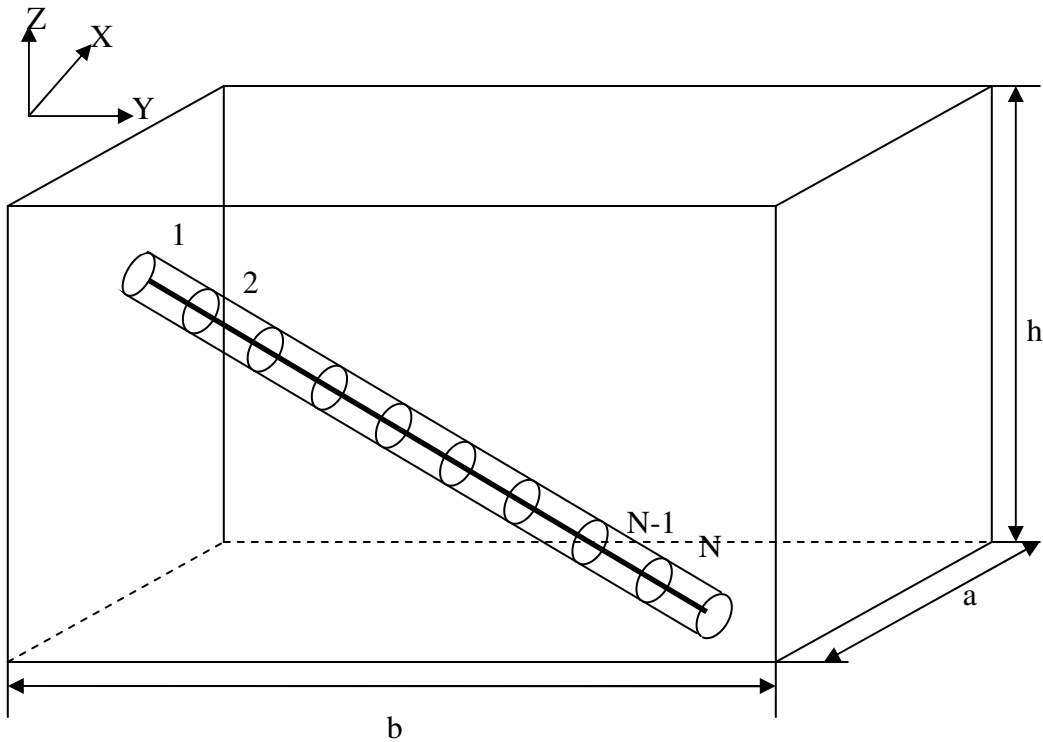
Fig. 3.15 Line source model for a slanted well.

The average reservoir pressure for stabilized flow in a sealed reservoir is calculated by Eq. 3.37. Substituting Eq. 3.39 into Eq. 3.35, we have

$$p_R - p(x,y,z,t) = \left[-\frac{\mu_o B_o q_o}{abh\alpha}t + \frac{B_o \mu_o q_o \left(\sqrt{1+(\hat{m})^2} \right)(y_2 - y_1)}{abhL\alpha}t \right]$$

$$\left[\frac{B_o \mu_o q_o \left(\sqrt{1+(\hat{m})^2} \right)}{abhL\alpha} \right] \left\{ \frac{2\alpha a^2 (y_2 - y_1)}{\pi^2 k_x} \sum_{n=1}^{\infty} cos\frac{n\pi x}{a} cos\frac{n\pi x_0}{a} \right.$$

$$+\frac{2\alpha b^3}{\pi^3 k_y}\sum_{m=1}^{\infty}\frac{\cos\dfrac{m\pi y}{b}\left(\sin\dfrac{m\pi y_2}{b}-\sin\dfrac{m\pi y_1}{b}\right)}{m^3}$$

$$+\frac{2\alpha h^3}{\hat{m}\pi^3 k_z}\sum_{l=1}^{\infty}\frac{\cos\dfrac{l\pi z}{h}\left(\sin\dfrac{l\pi(\hat{m}y_2+\hat{c})}{h}-\sin\dfrac{l\pi(\hat{m}y_1+\hat{c})}{h}\right)}{l^3}$$

$$+\frac{4\alpha h}{\hat{m}\pi^3}\sum_{l=1}^{\infty}\sum_{n=1}^{\infty}\frac{\cos\dfrac{n\pi x}{a}\cos\dfrac{n\pi x_0}{a}\cos\dfrac{l\pi z}{h}\left(\sin\dfrac{l\pi(\hat{m}y_2+\hat{c})}{h}-\sin\dfrac{l\pi(\hat{m}y_1+\hat{c})}{h}\right)}{l\left(\dfrac{l^2 k_z}{h^2}+\dfrac{n^2 k_x}{a^2}\right)}$$

$$+\frac{4\alpha b}{\pi^3}\sum_{m=1}^{\infty}\sum_{n=1}^{\infty}\frac{\cos\dfrac{n\pi x}{a}\cos\dfrac{n\pi x_0}{a}\cos\dfrac{m\pi y}{b}\left(\sin\dfrac{m\pi y_2}{b}-\sin\dfrac{m\pi y_1}{b}\right)}{m\left(\dfrac{m^2 k_y}{b^2}+\dfrac{n^2 k_x}{a^2}\right)}$$

$$+\frac{2\alpha bh}{\pi^2}\sum_{l=1}^{\infty}\sum_{m=1}^{\infty}\frac{\cos\dfrac{m\pi y}{b}\cos\dfrac{l\pi z}{h}}{\left(\dfrac{m^2 k_y}{b^2}+\dfrac{l^2 k_z}{h^2}\right)}$$

$$\left\{\left[\frac{\sin\left(\dfrac{\pi(-hmy_2+bl(\hat{m}y_2+\hat{c}))}{bh}\right)}{-hm\pi+bl\pi\hat{m}}+\frac{\sin\left(\dfrac{\pi(hmy_2+bl(\hat{m}y_2+\hat{c}))}{bh}\right)}{hm\pi+bl\pi\hat{m}}\right]\right.$$

$$\left.-\left[\frac{\sin\left(\dfrac{\pi(-hmy_1+bl(\hat{m}y_1+\hat{c}))}{bh}\right)}{-hm\pi+bl\pi\hat{m}}+\frac{\sin\left(\dfrac{\pi(hmy_1+bl(\hat{m}y_1+\hat{c}))}{bh}\right)}{hm\pi+bl\pi\hat{m}}\right]\right\}$$

$$+\frac{4\alpha bh}{\pi^2}\sum_{l=1}^{\infty}\sum_{m=1}^{\infty}\sum_{n=1}^{\infty}\frac{\cos\dfrac{n\pi x}{a}\cos\dfrac{n\pi x_0}{a}\cos\dfrac{m\pi y}{b}\cos\dfrac{l\pi z}{h}}{\left(\dfrac{n^2 k_x}{a^2}+\dfrac{m^2 k_y}{b^2}+\dfrac{l^2 k_z}{h^2}\right)}$$

$$\left\{\left[\left[\frac{sin\left(\frac{\pi\left(-hmy_2+bl(\hat{m}y_2+\hat{c})\right)}{bh}\right)}{-hm\pi+bl\pi\hat{m}}+\frac{sin\left(\frac{\pi\left(hmy_2+bl(\hat{m}y_2+\hat{c})\right)}{bh}\right)}{hm\pi+bl\pi\hat{m}}\right]\right.\right.$$

$$\left.\left.-\left[\frac{sin\left(\frac{\pi\left(-hmy_1+bl(\hat{m}y_1+\hat{c})\right)}{bh}\right)}{-hm\pi+bl\pi\hat{m}}+\frac{sin\left(\frac{\pi\left(hmy_1+bl(\hat{m}y_1+\hat{c})\right)}{bh}\right)}{hm\pi+bl\pi\hat{m}}\right]\right]\right\} \quad (3.47)$$

Considering the first parenthesis on the right hand side of Eq. 3.47, we have

$$\frac{B_o\mu_oq_o\left(\sqrt{1+(\hat{m})^2}\right)(y_2-y_1)}{abhL\alpha}t=\frac{\mu_oB_oq_o}{abh\alpha}t \quad (3.48)$$

Because $\sqrt{1+(\hat{m})^2}(y_2-y_1)=L$, Eq. 3.48 becomes zero and we can write Eq. 3.47 as,

$$p_R-p(x,y,z,t)=\left[\frac{B_o\mu_oq_o\left(\sqrt{1+(\hat{m})^2}\right)}{abhL\alpha}\right]\left\{\frac{2\alpha a^2(y_2-y_1)}{\pi^2k_x}\sum_{n=1}^{\infty}cos\frac{n\pi x}{a}cos\frac{n\pi x_0}{a}\right.$$

$$+\frac{2\alpha b^3}{\pi^3k_y}\sum_{m=1}^{\infty}\frac{cos\frac{m\pi y}{b}\left(sin\frac{m\pi y_2}{b}-sin\frac{m\pi y_1}{b}\right)}{m^3}$$

$$+\frac{2\alpha h^3}{\hat{m}\pi^3k_z}\sum_{l=1}^{\infty}\frac{cos\frac{l\pi z}{h}\left(sin\frac{l\pi(\hat{m}y_2+\hat{c})}{h}-sin\frac{l\pi(\hat{m}y_1+\hat{c})}{h}\right)}{l^3}$$

$$+\frac{4\alpha h}{\hat{m}\pi^3}\sum_{l=1}^{\infty}\sum_{n=1}^{\infty}\frac{cos\frac{n\pi x}{a}cos\frac{n\pi x_0}{a}cos\frac{l\pi z}{h}\left(sin\frac{l\pi(\hat{m}y_2+\hat{c})}{h}-sin\frac{l\pi(\hat{m}y_1+\hat{c})}{h}\right)}{l\left(\frac{l^2k_z}{h^2}+\frac{n^2k_x}{a^2}\right)}$$

$$+ \frac{4\alpha b}{\pi^3} \sum_{m=1}^{\infty} \sum_{n=1}^{\infty} \frac{\cos\dfrac{n\pi x}{a} \cos\dfrac{n\pi x_0}{a} \cos\dfrac{m\pi y}{b} \left(\sin\dfrac{m\pi y_2}{b} - \sin\dfrac{m\pi y_1}{b} \right)}{m\left(\dfrac{m^2 k_y}{b^2} + \dfrac{n^2 k_x}{a^2} \right)}$$

$$+ \frac{2\alpha bh}{\pi^2} \sum_{l=1}^{\infty} \sum_{m=1}^{\infty} \frac{\cos\dfrac{m\pi y}{b} \cos\dfrac{l\pi z}{h}}{\left(\dfrac{m^2 k_y}{b^2} + \dfrac{l^2 k_z}{h^2} \right)}$$

$$\left\{ \left[\frac{\sin\left(\dfrac{\pi(-hmy_2 + bl(\hat{m}y_2 + \hat{c}))}{bh} \right)}{-hm\pi + bl\pi\hat{m}} + \frac{\sin\left(\dfrac{\pi(hmy_2 + bl(\hat{m}y_2 + \hat{c}))}{bh} \right)}{hm\pi + bl\pi\hat{m}} \right] \right.$$

$$\left. - \left[\frac{\sin\left(\dfrac{\pi(-hmy_1 + bl(\hat{m}y_1 + \hat{c}))}{bh} \right)}{-hm\pi + bl\pi\hat{m}} + \frac{\sin\left(\dfrac{\pi(hmy_1 + bl(\hat{m}y_1 + \hat{c}))}{bh} \right)}{hm\pi + bl\pi\hat{m}} \right] \right\}$$

$$+ \frac{4\alpha bh}{\pi^2} \sum_{l=1}^{\infty} \sum_{m=1}^{\infty} \sum_{n=1}^{\infty} \frac{\cos\dfrac{n\pi x}{a} \cos\dfrac{n\pi x_0}{a} \cos\dfrac{m\pi y}{b} \cos\dfrac{l\pi z}{h}}{\left(\dfrac{n^2 k_x}{a^2} + \dfrac{m^2 k_y}{b^2} + \dfrac{l^2 k_z}{h^2} \right)}$$

$$\left\{ \left[\frac{\sin\left(\dfrac{\pi(-hmy_2 + bl(\hat{m}y_2 + \hat{c}))}{bh} \right)}{-hm\pi + bl\pi\hat{m}} + \frac{\sin\left(\dfrac{\pi(hmy_2 + bl(\hat{m}y_2 + \hat{c}))}{bh} \right)}{hm\pi + bl\pi\hat{m}} \right] \right.$$

$$\left. - \left[\frac{\sin\left(\dfrac{\pi(-hmy_1 + bl(\hat{m}y_1 + \hat{c}))}{bh} \right)}{-hm\pi + bl\pi\hat{m}} + \frac{\sin\left(\dfrac{\pi(hmy_1 + bl(\hat{m}y_1 + \hat{c}))}{bh} \right)}{hm\pi + bl\pi\hat{m}} \right] \right\} \right\} \tag{3.49}$$

We can write Eq. 3.49 in oil field unit as

$$p_R - p(x, y, z, t) = \left[\frac{887.53 B_o \mu_o q_o \left(\sqrt{1 + (\hat{m})^2} \right)}{abhL\alpha} \right]$$

$$\left\{ \frac{2\alpha a^2 (y_2 - y_1)}{\pi^2 k_x} \sum_{n=1}^{\infty} \cos\frac{n\pi x}{a} \cos\frac{n\pi x_0}{a} \right.$$

$$+ \frac{2\alpha b^3}{\pi^3 k_y} \sum_{m=1}^{\infty} \frac{\cos\dfrac{m\pi y}{b} \left(\sin\dfrac{m\pi y_2}{b} - \sin\dfrac{m\pi y_1}{b} \right)}{m^3}$$

$$+ \frac{2\alpha h^3}{\hat{m}\pi^3 k_z} \sum_{l=1}^{\infty} \frac{\cos\dfrac{l\pi z}{h} \left(\sin\dfrac{l\pi(\hat{m}y_2 + \hat{c})}{h} - \sin\dfrac{l\pi(\hat{m}y_1 + \hat{c})}{h} \right)}{l^3}$$

$$+ \frac{4\alpha h}{\hat{m}\pi^3} \sum_{l=1}^{\infty}\sum_{n=1}^{\infty} \frac{\cos\dfrac{n\pi x}{a} \cos\dfrac{n\pi x_0}{a} \cos\dfrac{l\pi z}{h} \left(\sin\dfrac{l\pi(\hat{m}y_2 + \hat{c})}{h} - \sin\dfrac{l\pi(\hat{m}y_1 + \hat{c})}{h} \right)}{l\left(\dfrac{l^2 k_z}{h^2} + \dfrac{n^2 k_x}{a^2} \right)}$$

$$+ \frac{4\alpha b}{\pi^3} \sum_{m=1}^{\infty}\sum_{n=1}^{\infty} \frac{\cos\dfrac{n\pi x}{a} \cos\dfrac{n\pi x_0}{a} \cos\dfrac{m\pi y}{b} \left(\sin\dfrac{m\pi y_2}{b} - \sin\dfrac{m\pi y_1}{b} \right)}{m\left(\dfrac{m^2 k_y}{b^2} + \dfrac{n^2 k_x}{a^2} \right)}$$

$$+ \frac{2\alpha bh}{\pi^2} \sum_{l=1}^{\infty}\sum_{m=1}^{\infty} \frac{\cos\dfrac{m\pi y}{b} \cos\dfrac{l\pi z}{h}}{\left(\dfrac{m^2 k_y}{b^2} + \dfrac{l^2 k_z}{h^2} \right)}$$

$$\left\{ \left[\frac{\sin\left(\dfrac{\pi(-hmy_2 + bl(\hat{m}y_2 + \hat{c}))}{bh} \right)}{-hm\pi + bl\pi\hat{m}} + \frac{\sin\left(\dfrac{\pi(hmy_2 + bl(\hat{m}y_2 + \hat{c}))}{bh} \right)}{hm\pi + bl\pi\hat{m}} \right] \right.$$

$$
-\left[\frac{sin\left(\dfrac{\pi\left(-hmy_1 + bl\left(\hat{m}y_1 + \hat{c}\right)\right)}{bh}\right)}{-hm\pi + bl\pi\hat{m}} + \frac{sin\left(\dfrac{\pi\left(hmy_1 + bl\left(\hat{m}y_1 + \hat{c}\right)\right)}{bh}\right)}{hm\pi + bl\pi\hat{m}}\right]\Bigg]\Bigg\}
$$

$$
+ \frac{4\alpha bh}{\pi^2}\sum_{l=1}^{\infty}\sum_{m=1}^{\infty}\sum_{n=1}^{\infty}\frac{\cos\dfrac{n\pi x}{a}\cos\dfrac{n\pi x_0}{a}\cos\dfrac{m\pi y}{b}\cos\dfrac{l\pi z}{h}}{\left(\dfrac{n^2 k_x}{a^2} + \dfrac{m^2 k_y}{b^2} + \dfrac{l^2 k_z}{h^2}\right)}
$$

$$
\Bigg\{\left[\frac{sin\left(\dfrac{\pi\left(-hmy_2 + bl\left(\hat{m}y_2 + \hat{c}\right)\right)}{bh}\right)}{-hm\pi + bl\pi\hat{m}} + \frac{sin\left(\dfrac{\pi\left(hmy_2 + bl\left(\hat{m}y_2 + \hat{c}\right)\right)}{bh}\right)}{hm\pi + bl\pi\hat{m}}\right]
$$

$$
-\left[\frac{sin\left(\dfrac{\pi\left(-hmy_1 + bl\left(\hat{m}y_1 + \hat{c}\right)\right)}{bh}\right)}{-hm\pi + bl\pi\hat{m}} + \frac{sin\left(\dfrac{\pi\left(hmy_1 + bl\left(\hat{m}y_1 + \hat{c}\right)\right)}{bh}\right)}{hm\pi + bl\pi\hat{m}}\right]\Bigg]\Bigg\}\Bigg\} \quad (3.50)
$$

where $\alpha = 158.73\phi\mu_o c_t$. By using Eq. 3.50, a slanted well performance can be evaluated. The inclined angle is calculated by

$$
\theta = tan^{-1}\left(\hat{m}\right) \tag{3.51}
$$

The line source model, Eq.3.50, is validated by comparing with a closed form model of slanted well presented by Besson[21] as shown in Fig. 3.16. The comparison shows that the productivity index obtained by the line source model agrees very well with that by the closed form model, which confirms that Eq. 3.49 can be used to calculate slanted well performance.

The slanted well performance is studied by using the data in Table 3.2. The slanted well fully penetrates from the top and the bottom of a box-shaped reservoir. The geometry of the slanted well is shown in Fig. 3.17. The flow rate profile and wellbore pressure profile are studied under different inner boundary condition.
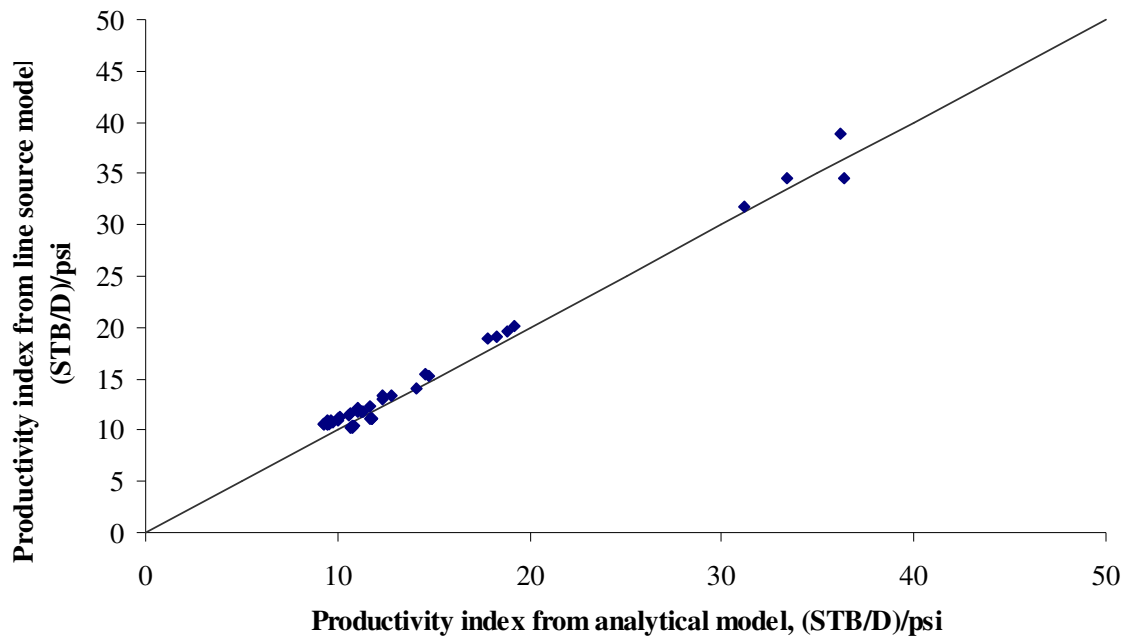
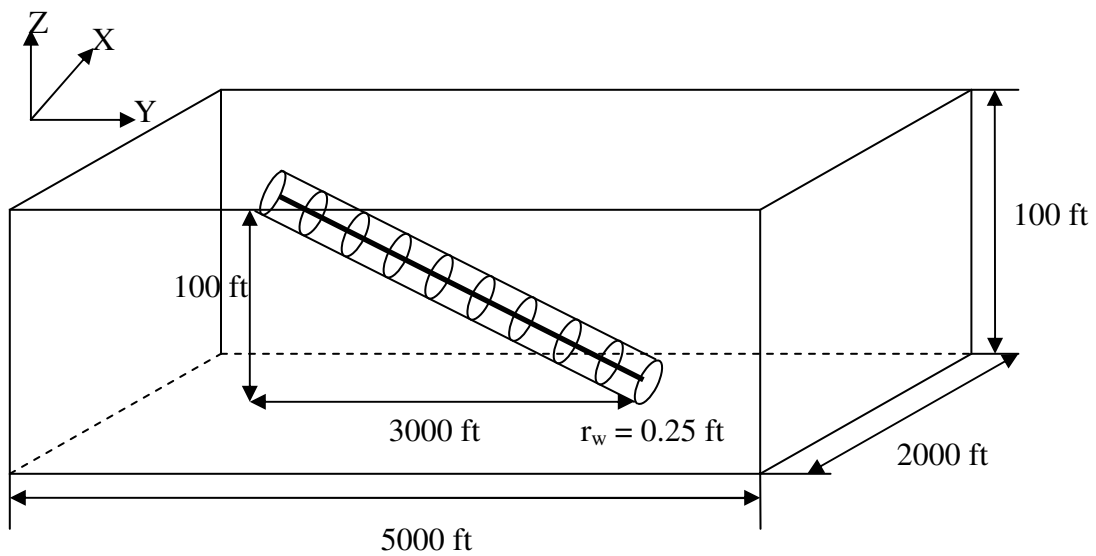**Fig. 3.16 Comparison line source model with closed form model for a slanted well.**

**Fig. 3.17 The geometry of the slanted well.**

First, we calculate the slanted well performance under the uniform flux inner boundary condition. When the well is assumed to have uniform flux as an inner boundary condition, the wellbore pressure will be varied along the wellbore. Fig. 3.18 shows the wellbore pressure profile along the slanted well under the uniform flux inner boundary condition. The profile shows that the wellbore pressure is the highest at the middle and lowest at the both ends of the wellbore. Since the top and the bottom of the well are close to the boundaries, the productivity at these locations is lower than other parts. High pressure drawdown is required to keep the well produces under uniform flux condition. However, usually the flow cannot occur under this wellbore pressure. In other words, the wellbore pressure profile under uniform flux implies that the inflow into the slanted well cannot be uniform.
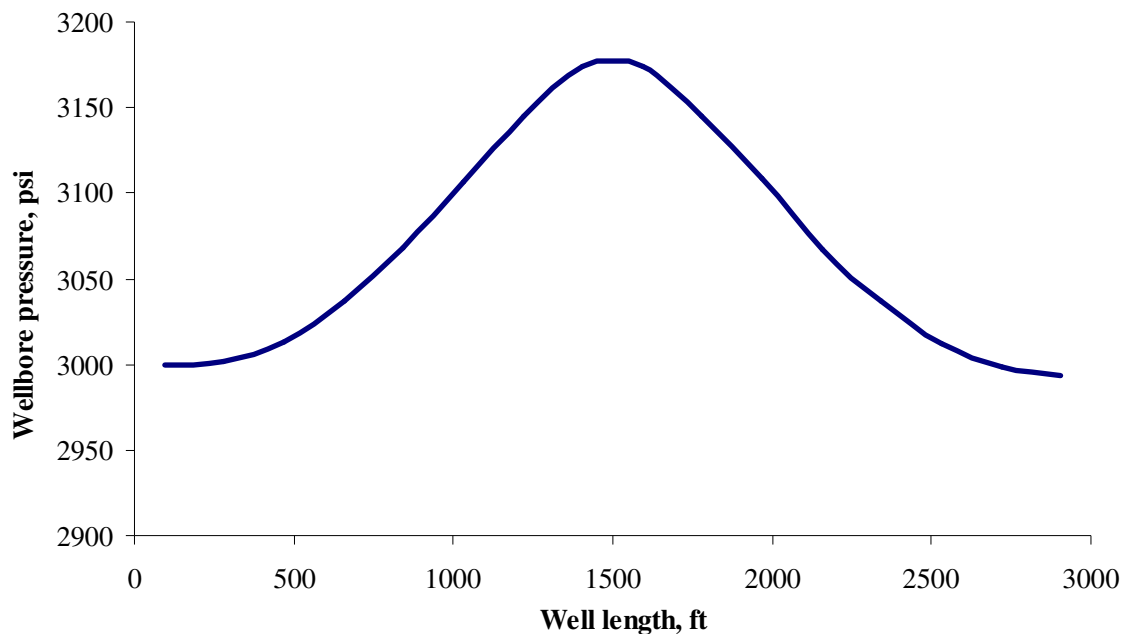
Fig. 3.18 Wellbore pressure profile under uniform flux boundary condition.

Next, we study the well performance under infinite conductivity boundary condition. Under this condition the productivity index is varied along the wellbore as shown in Fig. 3.19. Since the productivity is high at the middle and it decreases toward

the both ends, the flow rate is low at the tips of the well and increases toward the center of the well as a results of uniform wellbore pressure or constant pressure drawdown. We can see that when the wellbore produces under uniform flux, the highest wellbore pressure is at the middle. On the other hand, when the well produces at uniform wellbore pressure, the highest flow rate is at the middle. Both of them imply that the productivity is highest at the middle part because this part has least boundary effect.
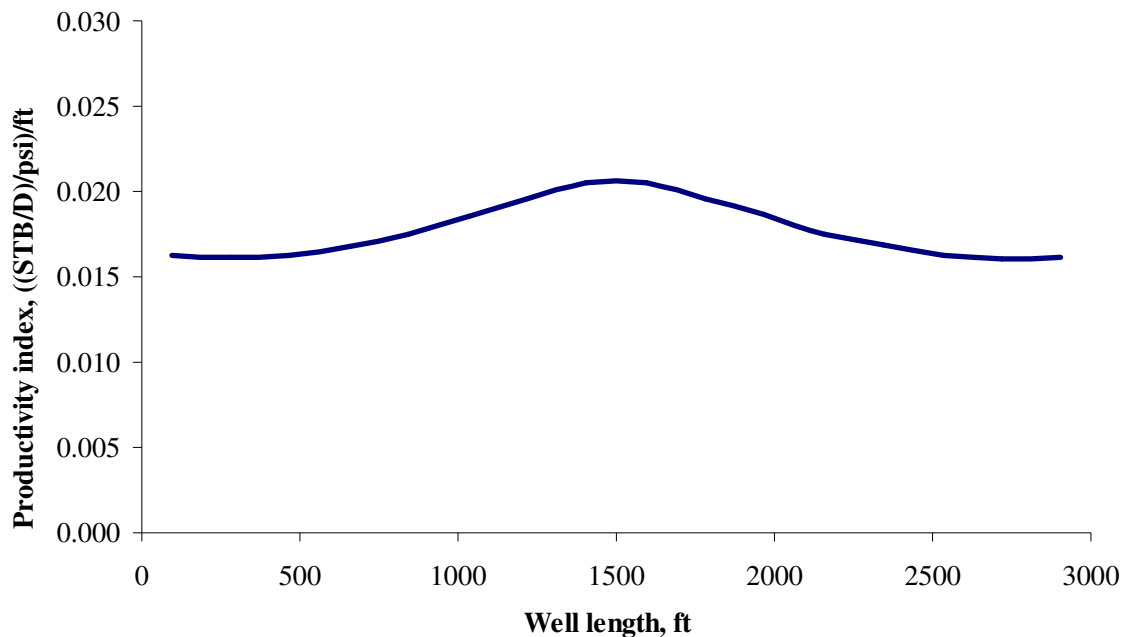
Fig. 3.19 Productivity index profile under infinite conductivity boundary condition.

If finite conductivity boundary condition is assumed, first we have to evaluate the well performance under infinite conductivity to obtain the wellbore inflow performance or flow rate into the wellbore. Then we couple the well inflow performance with the wellbore pressure drop to account for pressure drop along the wellbore. The wellbore pressure profile under finite conductivity inner boundary condition is shown in Fig. 3.20. It presents that the pressure decreases from the low-end to the high-end of the well. The pressure drop is caused by both frictional pressure drop and potential pressure drop. Since the wellbore pressure decreases from the bottom to the top of the well, the

pressure drawdown increases the same direction. The productivity index distribution is shown in Fig. 3.21. Because of the increasing pressure drawdown toward the top of the well, the flow rate is higher at the left side on Fig. 3.21.
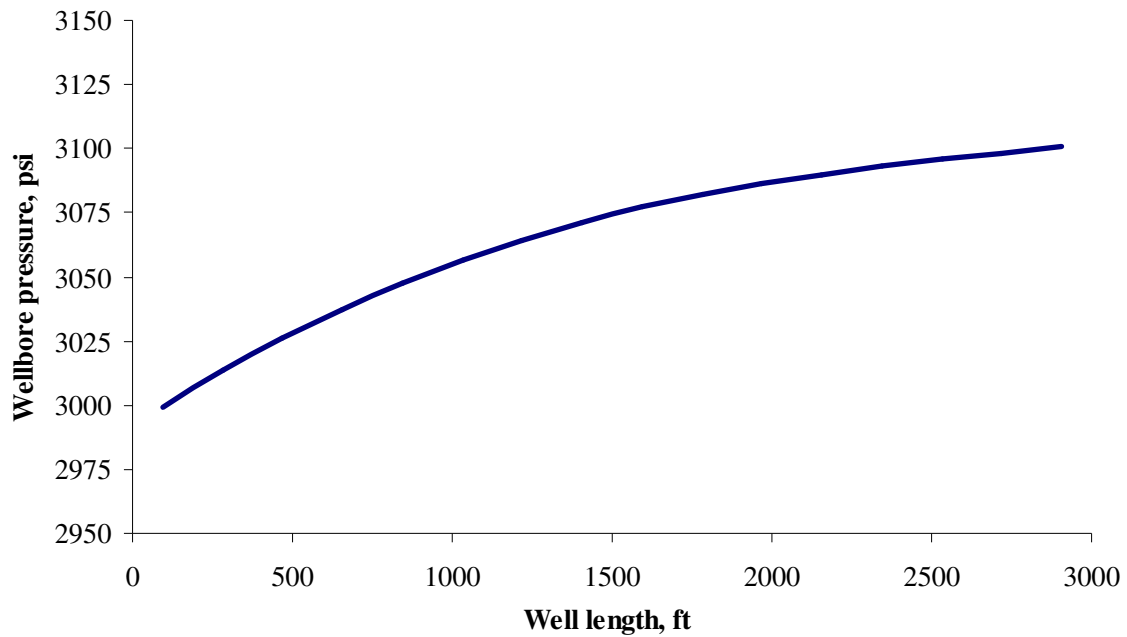
Fig. 3.20 Wellbore pressure profile under finite conductivity boundary condition.
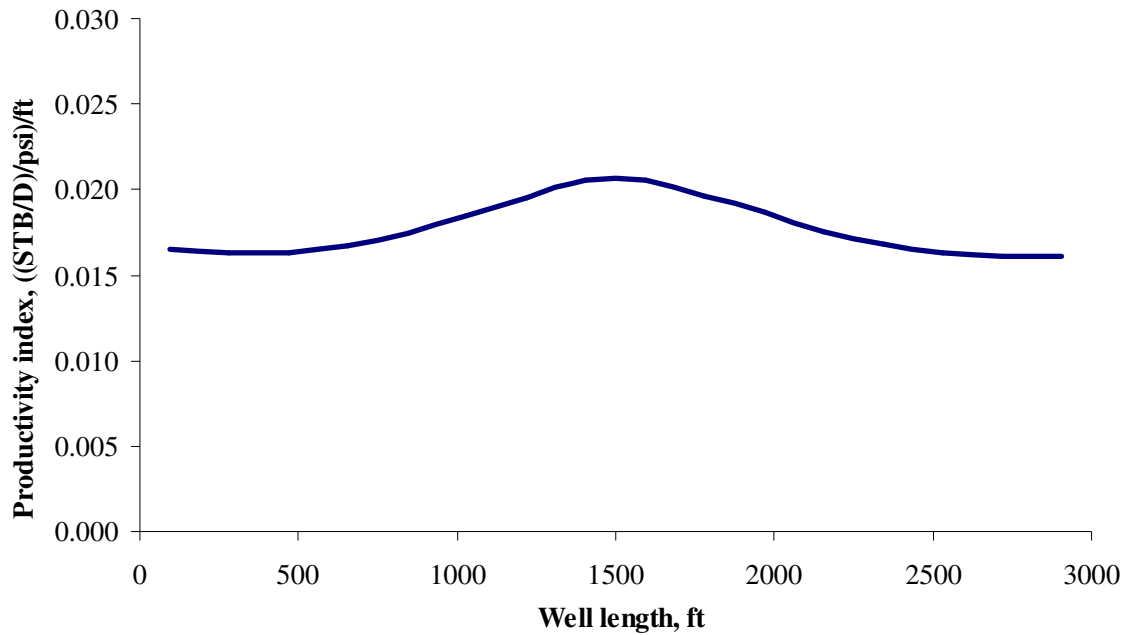
Fig. 3.21 Productivity index profile under finite conductivity boundary condition.

3.4 Summary

We present the line source solution for 2D wellbore in this chapter. The line source solution is very flexible and easy to use. The well trajectory can change in the y-direction and the z-direction, which allows the model to predict the performance of different types of wellbore trajectories. The model developed based on analytical approach, thus eliminates the numerical error from numerical process. By using this method, we can evaluate the wellbore performance under varieties of combinations of boundary conditions. The pressure drop along the wellbore can be accounted by coupling the line source model with the wellbore pressure drop model. Flow rate distribution and wellbore pressure distribution along wellbore can be investigated by the model.

CHAPTER IV

UNDULATING WELL PERFORMANCE

4.1 Introduction of Undulating Wells

Undulating wells are the wells that are not perfectly horizontal. We can divide undulating wells into two main categories, intentionally undulation and unintentionally undulation. In general, the unintentional undulating wells have various inclined angles. On the other hand, the intentional undulating wells have consistent angles.

4.1.1 Intentional Undulating Wells

Undulating wells are relatively new in reservoir development. The advantage of undulating wells is that they overcome some limitations of horizontal wells. When the vertical permeability of a formation is too low for horizontal wells to be economically attractive, undulating wells reduce the dependency of vertical permeability and can be used to produce from such a formation. When multiple thin layers involve in the formation, undulating wellbore can access these layers. If the formation is relatively thick, undulating wellbores have more formation contact area and can produce more effective than horizontal wells. Wellbores are designed with certain deviation angles to maximize production rate in different applications. However, the advantages of undulating wells are not always guaranteed especially for two-phase flow wells because of the complexity of wellbore structures and formation properties. The wellbore flow should be studied carefully when undulating wells are designed.

4.1.2 Unintentional Undulating Wells

Unintentional undulation occurs from drilling control or formation structure. Because of the difficulty in controlling directional drilling, undulation usually happens in horizontal wells. In fact, horizontal wells in the field are not perfectly horizontal. Undulating effect can cause problems in well completion and production. For example, if some parts of the

well are drilled too close to water-oil contact or gas-oil contact, these will cause early water-coning or gas-coning and decrease the well production. Another problem is unstable production at the surface because of slug flow. This problem will be discussed in section 4.4

We present two undulating well performance models, the closed form model and the line source model. Both methods can be used to evaluate well performance for single-phase and homogeneous reservoirs. The closed form model applies for two-phase system under some certain conditions.

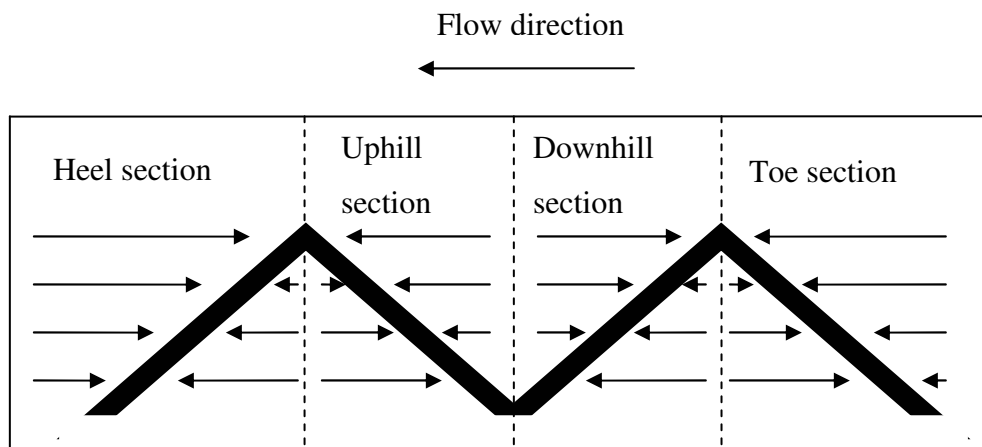## 4.2 Closed Form Model for Undulating Wells

For the undulating wells used in relatively low vertical permeability, we develop an analytical method to predict well performance. If we simply use a horizontal model, most likely we will underestimate the well performance since most horizontal well relies on vertical permeability to produce unlike undulating wells.

4.2.1 Model Description

We define an undulating well as a horizontal well that consists of uphill sections and downhill sections along the wellbore. The well trajectory can be defined by an inclined angle, θ_w, and a well height, h_w. Fig. 4.1 shows the physical well model used in this dissertation. One cycle is consisted of an uphill section and a downhill section. To develop a model for well performance, we assume that each cycle has the same height (h_w is a constant). An undulating well is divided into several sections, and the section number depends on number of well cycles. If an undulating well has n cycles, the drainage volume will be divided to 2n sections. In general, it is believed that undulating wells are predicted closer to horizontal wells, and the performance can be calculated by horizontal well models. However, if the undulating well is designed for relatively low vertical permeability formation, the dominant streamlines would be in the horizontal direction, as shown in Fig. 4.2.

Flow direction

Heel   Uphill   Downhill   Toe

h_w

θ_w
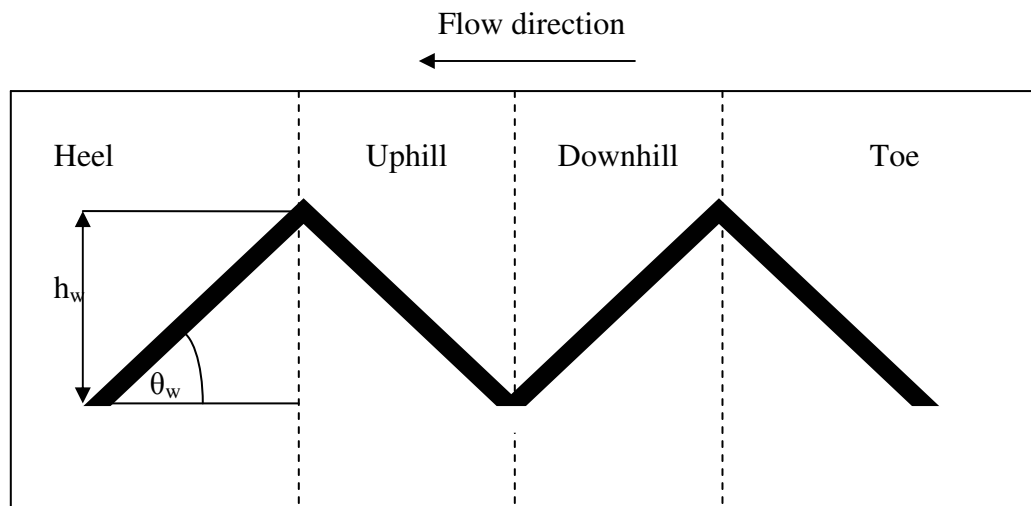
Fig. 4.1 Reservoir and well drainage region for a 2-cycle undulating well.

Flow direction

Heel section   Uphill section   Downhill section   Toe section

Fig. 4.2 Flow geometry of undulating well in low vertical permeability reservoir.

No-flow image boundaries can be assumed between sections. Fig. 4.3 presents the flow streamline in horizontal wells (Fig. 4.3a) and vertical wells (Fig. 4.3b). Comparing the flow streamlines in the undulating wells, Fig. 4.2, with that in horizontal

wells and vertical wells, it shows that the flow streamlines of an undulating well in a relatively low vertical permeability reservoir resemble to those of vertical wells. Thus, we will use vertical well models to predict undulating well performance in relatively low vertical permeability reservoirs with some modifications.
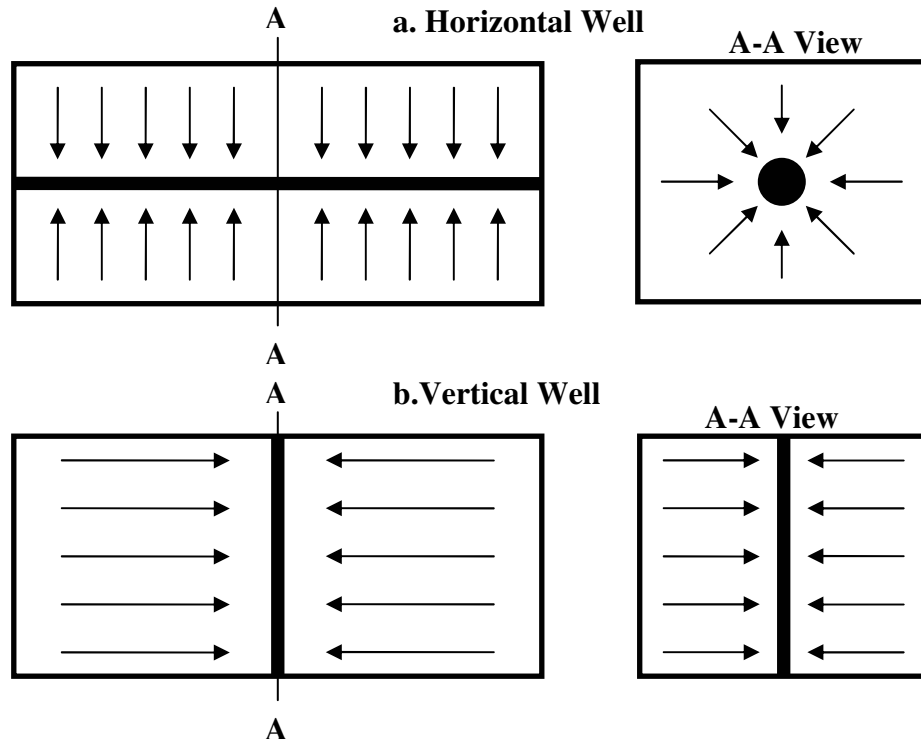
Fig. 4.3 Flow streams of horizontal wells and vertical wells.

The first modification for undulating well model is to account for the inclination of the wellbore. The inclination results in higher reservoir contact area than vertical wells, and a slanted skin, s_θ, is used to account for increasing reservoir contact area in undulating well. The second major modification for undulating well model is the approach to calculate wellbore pressure drop. The wellbore pressure drop can be calculated by dividing the wellbore in each section into many horizontal layers (notice, not vertical sections, as we do for horizontal wells in Chapter II) as shown in Fig. 4.4. Because the

well positions in each layer are different, a shape factor is used to count for the well segment location. The shape factor changes following the position of the segment along the wellbore. For the well that does not fully penetrating on the top and the bottom layers, we can use a partial penetrated skin factor to account for partially penetrating well segments in the wellbore.
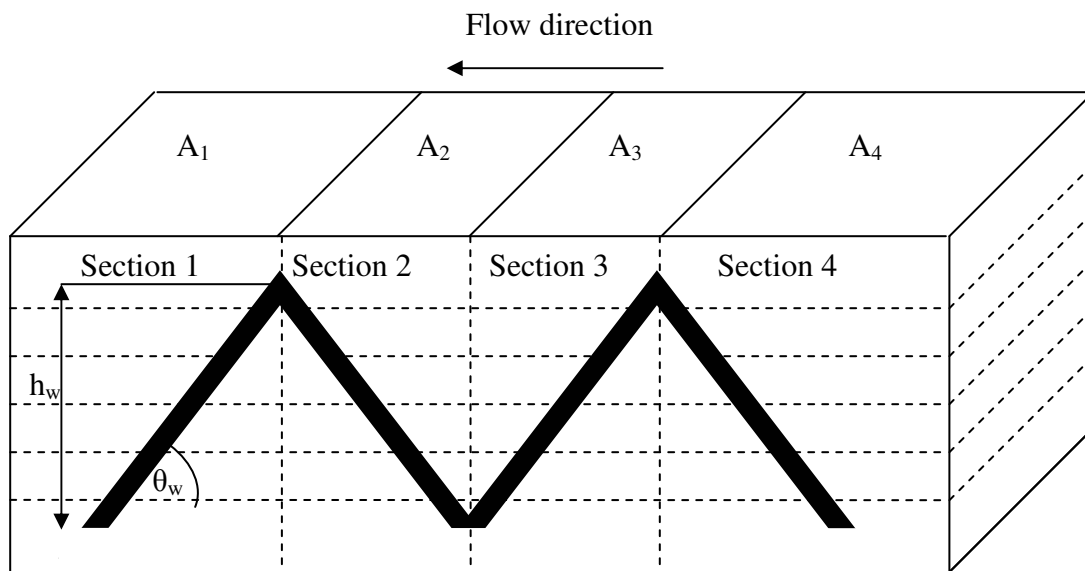
Fig. 4.4 Well and reservoir modeling for closed form model.

4.2.2 Equation Formulation

After we understand the flow streamlines behavior of undulating wells in relatively low vertical permeability reservoirs, we formulate the analytical inflow performance to estimate the well performance. The closed form model of inflow performance for undulating wells is

$$q_o = \frac{k_H h \Delta p}{141.2 B_o \mu_o \left[\frac{1}{2} \{ ln(4A) - ln(C_A) - ln(\gamma r_w^2) \} + s_\theta + s_p + s \right]}$$

(4.1)

where,

A = drainage area

$ln(C_A)$ = shape factor

s_θ = slanted skin factor

s_p = partial penetrated skin factor

s = damage skin factor.

Eq. 4.1 can be applied to each section in Fig. 4.4. For each segment, the drainage area varies depending on the inclined angle and the well height.

Because the position of the wellbore in each horizontal layer changes along the wellbore, the appropriate shape factor is required for the change. Earlougher[23] published a shape factor model for rectangular drainage area and his model has been used widely in the industry. However, his shape factor is only available for some certain ratio of the width and the length of the rectangular drainage area and the well has to be placed in some specific positions in the drainage area. To make the model flexible, we use Yaxley's model[24] to calculate the shape factor. This model is very flexible. The well can be in any positions in the rectangular drainage area and there is no limitation on the ratio of the width and the length of the rectangular drainage area. The comparison Yaxley's shape factor with Earlougher's shape factor is shown in Table 4.1 . We can see that the comparison shows excellent agreement. The Yaxley's shape factor model is

$$ln(C_A) = ln \left[\frac{16\pi^2 A \sin^2(\pi b_D)}{a^2} \right] - \frac{4\pi A}{a^2} \left(\frac{1}{3} - a_E d_E \right) - 2\alpha - ln(\gamma)$$

(4.2)

where,

$$\alpha = ln \left[(1-\varepsilon)^2 \{ (1-\varepsilon)^2 + 4\varepsilon \sin^2(\pi b_D) \} \right]^{-1/2}$$

(4.3)

$$\varepsilon = exp(-2\pi a_D)$$

(4.4)

$$b_D = \frac{a_i}{a} \tag{4.5}$$
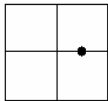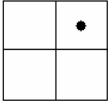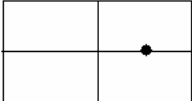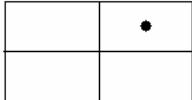
$$a_D = \frac{b_i}{a} \tag{4.6}$$

$$a_E = \frac{b_i}{b_{section}} \tag{4.7}$$

$$d_E = \frac{d_i}{b_{section}} \tag{4.8}$$

If the distance between the well and the nearest side of rectangular boundary is less than the width of the reservoir, Eq. 4.3 becomes zero. Fig. 4.5 shows the parameter definitions and geometries used in the shape factor calculation.

Table 4.1   Comparison of shape factor from Earlougher's model and Yaxley's model

Drainage Area	Earlougher Shape Factor	Yaxley Shape Factor
	2.56	2.56
	1.51	1.54
	1.51	1.51
	0.731	0.733
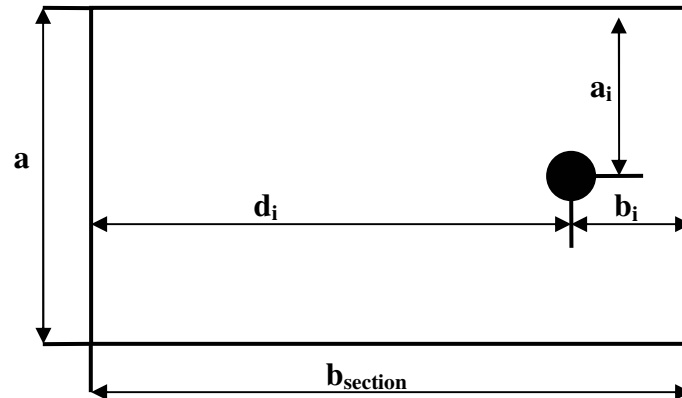
a_i = the distance between well and the nearest side of rectangular (ft)

b_i = the distance between well and the nearest end boundary of rectangular (ft)

d_i = the distance between well and the furthest end boundary of rectangular (ft)

Fig. 4.5 Geometry of the parameters for shape factor model.

The increasing of reservoir contact area in undulating wells is accounted by applying a slanted skin factor into the productivity model. The most well known slanted skin model is Cinco-ley's model[25]. However, Cinco-ley's model has been analyzed by many authors and the analysis shows that Cinco-ley's model should be modified when it is applied to anisotropic reservoirs. Even with the modification for anisotropic formations, this Cinco-ley's model can only be used at certain range of inclination ($\theta_w <$ 15°). To overcome the limitation, Besson[21] introduced a new slanted skin model in anisotropic formation and his model applies for inclination angle from 0 – 90°. Slanted skin factor model is written as,

$$s_\theta = ln\left[\frac{4r_w}{h_m}\frac{1}{\alpha\gamma}\right] + \frac{h}{\gamma h_m}ln\left[\frac{\sqrt{hh_m}}{4r_w}\frac{2\alpha\sqrt{\gamma}}{1+\frac{1}{\gamma}}\right] \qquad (4.9)$$

$$\alpha = \sqrt{k_H/k_V} \qquad (4.10)$$

$$\gamma = \sqrt{\frac{1}{\alpha^2} + \frac{h^2}{h_m^2}\left(1 - \frac{1}{\alpha^2}\right)}$$ (4.11)

where, h is vertical direction length of the well and h_m is the measured length of the well.

Since the model assumes there is no-flow between the layers, the reservoir drainage volume will be smaller than the original reservoir drainage volume when a well height is lower than the reservoir thickness. A partial penetrated skin can be used to account for partial penetrated layers. Papatzacos[26] presented a partial penetrated skin models as,

$$s_p = \left(\frac{1}{h_{pD}} - 1\right)ln\frac{\pi}{2r_D} + \frac{1}{h_{pD}}ln\left[\frac{h_{pD}}{2 + h_{pD}}\left(\frac{A-1}{B-1}\right)^{\frac{1}{2}}\right]$$ (4.12)

where,

$$h_{pD} = h_p/h_t$$ (4.13)

$$r_D = \frac{r_w}{h_t}\left(\frac{k_V}{k_H}\right)^{\frac{1}{2}}$$ (4.14)

$$h_{1D} = h_1/h_t$$ (4.15)

$$A = 1/\left(h_{1D} + h_{pD}/4\right)$$ (4.16)

$$B = 1/\left(h_{1D} + 3h_{pD}/4\right)$$ (4.17)
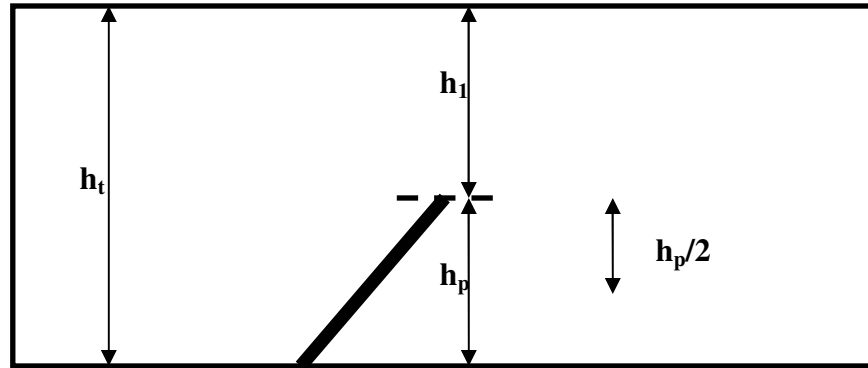
Fig. 4.6 Geometry and notation for partial penetrated skin calculation.

By applying this model, we can describe undulating well performance. The shape factor, the slanted skin factor, and the partial penetrated skin factor are calculated by Eq. 4.2, Eq. 4.9, and Eq. 4.12 respectively. An example is presented here, the well structure is shown in Fig. 4.4. The data in Table 4.2 is used to evaluate the well performance by the closed form model.

Before the productivity index is computed, the well and reservoir are divided into 2 uphill and 2 downhill sections. Then, the productivity index is calculation for the toe section. The well has a 5° inclination angle with 150 ft cycle height. The horizontal length for one section can be calculated from

$$b_{section} = \frac{curve\_height}{tan(\theta_w)} = \frac{h_w}{tan(\theta_w)} = \frac{150}{tan(5°)} = 1714.51 ft$$

The well has 2 cycles or 4 section so that the horizontal length (L_H) of the well is

$$L_H = number\_of\_curve \times 2 \times b_{section} = 2 \times 2 \times 1714.51 = 6858.03 ft$$

The reservoir length is 7500 and the horizontal well length is 6858.03 ft. The reservoir lengths for uphill and downhill section are 1714.51 ft ($b_{section}$). The well is at the center of the reservoir so the reservoir length for the heel and toe section can be calculated as the follows

Table 4.2   Parameters used in undulating well performance

Parameters	Data
Reservoir width, ft	3200
Reservoir length, ft	7500
Reservoir thickness, ft	150
Horizontal permeability, md	15
Vertical permeability, md	0.3
Cycle number	2
Well height, ft	150
Inclined angle, degree	5
Wellbore radius, ft	0.25
Damage skin	0
Oil formation volume factor, res bbl/STB	1
Oil viscosity, cp	1

$$b_{section,toe\&heel}\frac{(b)-(L_H)}{2}+(L_H)=\frac{7500-6858.03}{2}+1714.51=2038.49\,ft$$

Following the definition of b_i, which is the distance between the well and the nearest end of rectangular boundary, and d_i, which is the distance between the well and the furthest end of rectangular boundary, b_i is always less than d_i. For this case, b_i is 492.44 ft and d_i is 1546.05 ft. If we divide each section into 5 layers, the thickness of each layer is 30 ft. For the toe section of the first layer is calculated the shape factor by Eq. 4.2-Eq. 4.8 shown below,

$$a_E=\frac{b_{i,1}}{b_{section}}=\frac{492.44}{2038.49}=0.24$$

$$d_E = \frac{d_{i,1}}{b_{section}} = \frac{1543.06}{2038.49} = 0.76$$

$$a_D = \frac{b_{i,1}}{a} = \frac{492.44}{3200} = 0.15$$

Because the well is in the center of the reservoir and b_D is 0.5, we obtain

$$\varepsilon = exp(-2\pi a_D) = exp(-2\pi 0.15) = 0.39$$

$$\alpha = ln\left[(1-0.39)^2\left\{(1-0.39)^2 + 4(0.39)sin^2(\pi 0.5)\right\}\right]^{-1/2} = 0.16$$

$$A = ab_{section} = 3200 \times 2038.49 = 6.52 \times 10^6 \ ft^2$$

$$ln(C_A) = ln\left[\frac{16\pi^2 A \ sin^2(\pi b_D)}{a^2}\right] - \frac{4\pi A}{a^2}\left(\frac{1}{3} - a_E d_E\right) - 2\alpha - ln(\gamma) = 2.83$$

The slanted skin factor is calculated by Eq. 4.9-Eq. 4.11

$$\alpha = \sqrt{k_H/k_V} = \sqrt{15/0.3} = 7.07$$

$$h_m = \frac{h}{sin(\theta_w)} = \frac{30}{sin(5)} = 344.21$$

$$\gamma = \sqrt{\frac{1}{\alpha^2} + \frac{h^2}{h_m^2}\left(1 - \frac{1}{\alpha^2}\right)} = 0.17$$

$$s_\theta = ln\left[\frac{4r_w}{h_m}\frac{1}{\alpha\gamma}\right] + \frac{h}{\gamma h_m}ln\left[\frac{\sqrt{hh_m}}{4r_w}\frac{2\alpha\sqrt{\gamma}}{1+1/\gamma}\right] = -3.51$$

The well is fully penetrating so we do not have to calculate the partial penetrated skin. The productivity of this layer is calculated by

$$JB_o\mu_o = \frac{k_H h}{141.2\left[\frac{1}{2}\left\{ln(4A) - ln(C_A) - ln(\gamma r_w^2)\right\} + s_\theta + s_{partial} + s\right]}$$

$$JB_o\mu_o = 0.73\frac{STB}{day \bullet psi}$$

The productivity index of the next layer is determined by the same procedure. The pressure drop along the well can be calculated by coupling the inflow model with the

wellbore pressure drop model as shown in Chapter II. Fig. 4.7 and Fig. 4.8 show the productivity index profiles and wellbore pressure profile along the undulating well respectively. Fig. 4.7 reveals that the top and the bottom segments of the well have lower productivity than the middle segments have because of the boundary effect. The total productivity index of the undulating well is 13.6 (STB/D)/psi. Fig. 4.8 shows that the wellbore pressure profile reflects the wellbore trajectory because the potential pressure drop dominates the total pressure drop over the frictional pressure drop in the wellbore.
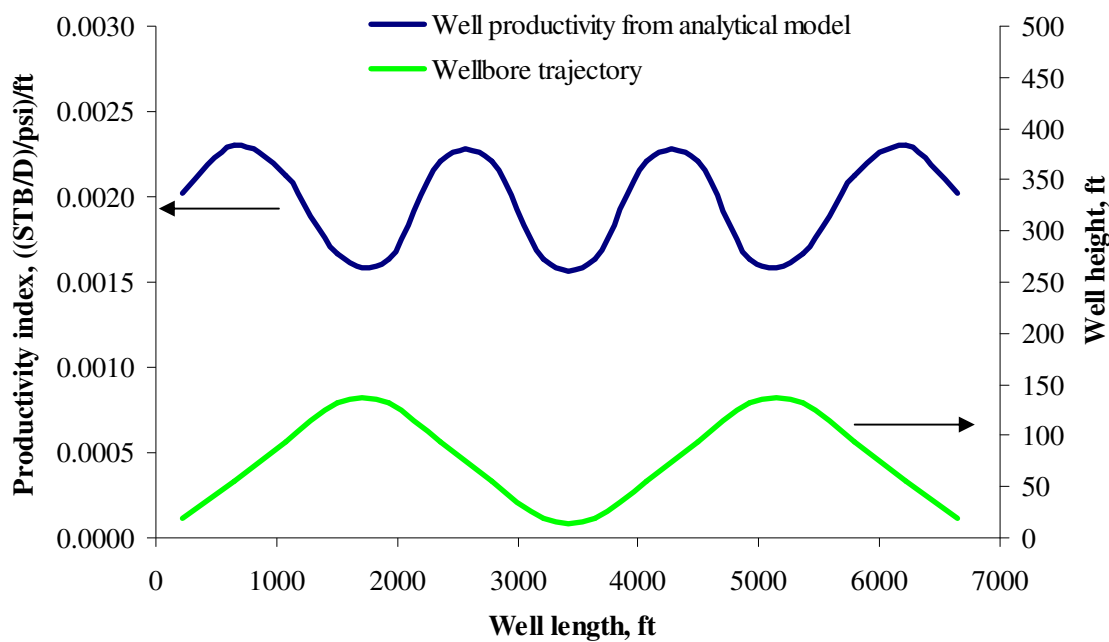
Fig. 4.7 Productivity index profile from closed form model.
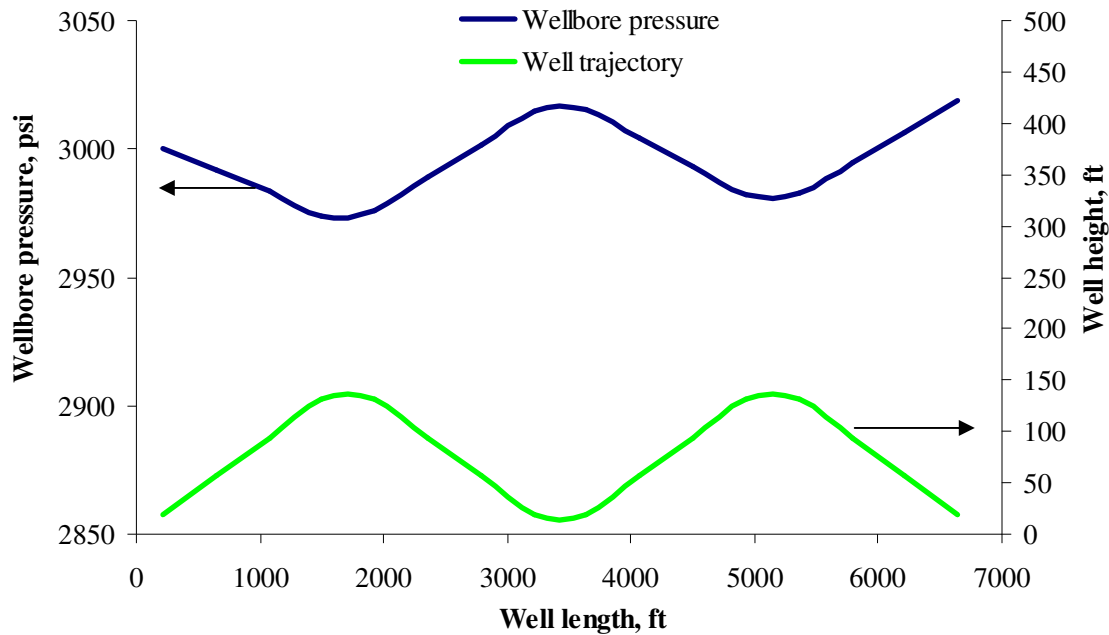
Fig. 4.8 Wellbore pressure profile from closed form model.

4.2.3 Field Application

The closed form model was used to predict the performance of an undulating well designed for Cosmopolitan project. Cosmopolitan project is in Cook Inlet field in Alaska, USA. The initial oil in place is over 800 million barrel of oil and the oil gravity is about 24-27 API. Oil viscosity is about 7 cp. The previous studies show that the permeability of the formation depends on the drawdown and vertical permeability is much lower than horizontal permeability. Undulating wells are planed to drill in the field since high productivity wells are required to make the project economically attractive. In general, horizontal well is one option to increase well productivity. However, horizontal well is usually a good candidate for high vertical permeability formation and/or in thin bed of reservoir. Since Hemlock formation has low vertical permeability, undulating wells are interested and might be more effective than horizontal wells. To make a decision, the well performance of undulating is evaluated by the closed form model. Fig. 4.9 shows the evaluation result of undulating well in Hemlock formation.

The comparison among the analytical undulating well models, the analytical horizontal well model and the reservoir simulation model shows that the undulating well model gives comparable results with simulation results. On the other hand, the results from the analytical horizontal well underestimate the performance of undulating well. If we use analytical horizontal well model with modified vertical permeability to be the same as horizontal permeability, the model overestimates the performance of undulating well. Therefore, to evaluate the undulating well performance, the analytical undulating well model should be used for more accurate results.
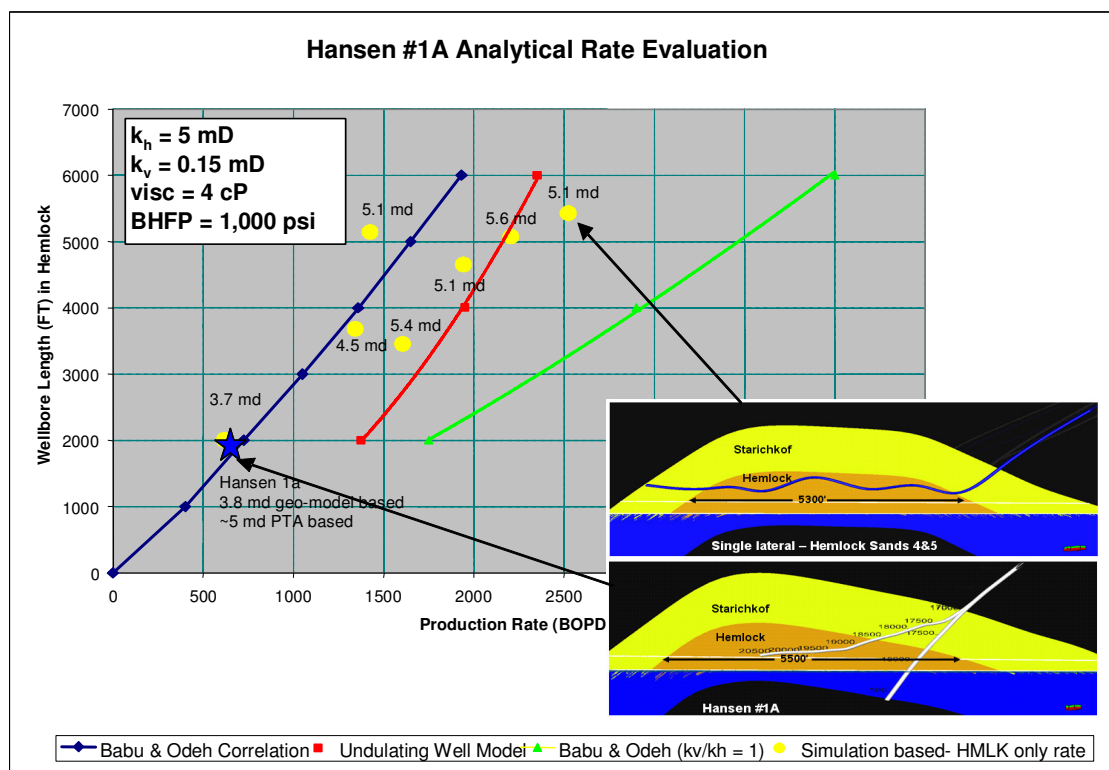

Fig. 4.9 Undulating well evaluation.

4.3 Line Source Model

For more accurate results, the performance of undulating wells can be modeled by the line source solution described in Chapter III. It needs to point out that analytical

approach assumes that vertical permeability does not contribute to the well productivity. This assumption may not be valid, especially when undulating is unintentional undulation. It may involve significant error when the anisotropic ratio of a formation is relatively high. To apply the line source approach, the well is divided into several segments. On each segment, it is assumed that the inclined angle is constant. The inclined angle can be different among segments. The wellbore segments are connected using the superposition principle. From this method, we generate a set of linear equation, as presented in Chapter III. Then, the undulating well performance is evaluated by the line source solution. For the closed box-shaped reservoir, we can use the slanted well model in Chapter III to calculate the performance of each segment in undulating well model. The slanted well performance at stabilized flow or late time in oil field unit is

$$p_R - p(x,y,z,t) = \left[\frac{887.53 B_o \mu_o q_o \left(\sqrt{1+(\hat{m})^2} \right)}{abhL\alpha} \right]$$

$$\left\{ \frac{2\alpha a^2 (y_2 - y_1)}{\pi^2 k_x} \sum_{n=1}^{\infty} \cos \frac{n\pi x}{a} \cos \frac{n\pi x_0}{a} \right.$$

$$+ \frac{2\alpha b^3}{\pi^3 k_y} \sum_{m=1}^{\infty} \frac{\cos \frac{m\pi y}{b} \left(\sin \frac{m\pi y_2}{b} - \sin \frac{m\pi y_1}{b} \right)}{m^3}$$

$$+ \frac{2\alpha h^3}{\hat{m}\pi^3 k_z} \sum_{l=1}^{\infty} \frac{\cos \frac{l\pi z}{h} \left(\sin \frac{l\pi(\hat{m}y_2 + \hat{c})}{h} - \sin \frac{l\pi(\hat{m}y_1 + \hat{c})}{h} \right)}{l^3}$$

$$+ \frac{4\alpha h}{\hat{m}\pi^3} \sum_{l=1}^{\infty} \sum_{n=1}^{\infty} \frac{\cos \frac{n\pi x}{a} \cos \frac{n\pi x_0}{a} \cos \frac{l\pi z}{h} \left(\sin \frac{l\pi(\hat{m}y_2 + \hat{c})}{h} - \sin \frac{l\pi(\hat{m}y_1 + \hat{c})}{h} \right)}{l \left(\frac{l^2 k_z}{h^2} + \frac{n^2 k_x}{a^2} \right)}$$

$$+\frac{4\alpha b}{\pi^3}\sum_{m=1}^{\infty}\sum_{n=1}^{\infty}\frac{\cos\dfrac{n\pi x}{a}\cos\dfrac{n\pi x_0}{a}\cos\dfrac{m\pi y}{b}\left(\sin\dfrac{m\pi y_2}{b}-\sin\dfrac{m\pi y_1}{b}\right)}{m\left(\dfrac{m^2 k_y}{b^2}+\dfrac{n^2 k_x}{a^2}\right)}$$

$$+\frac{2\alpha bh}{\pi^2}\sum_{l=1}^{\infty}\sum_{m=1}^{\infty}\frac{\cos\dfrac{m\pi y}{b}\cos\dfrac{l\pi z}{h}}{\left(\dfrac{m^2 k_y}{b^2}+\dfrac{l^2 k_z}{h^2}\right)}$$

$$\left\{\left[\frac{\sin\left(\dfrac{\pi\left(-hmy_2+bl(\hat{m}y_2+\hat{c})\right)}{bh}\right)}{-hm\pi+bl\pi\hat{m}}+\frac{\sin\left(\dfrac{\pi\left(hmy_2+bl(\hat{m}y_2+\hat{c})\right)}{bh}\right)}{hm\pi+bl\pi\hat{m}}\right]\right.$$

$$\left.-\left[\frac{\sin\left(\dfrac{\pi\left(-hmy_1+bl(\hat{m}y_1+\hat{c})\right)}{bh}\right)}{-hm\pi+bl\pi\hat{m}}+\frac{\sin\left(\dfrac{\pi\left(hmy_1+bl(\hat{m}y_1+\hat{c})\right)}{bh}\right)}{hm\pi+bl\pi\hat{m}}\right]\right\}$$

$$+\frac{4\alpha bh}{\pi^2}\sum_{l=1}^{\infty}\sum_{m=1}^{\infty}\sum_{n=1}^{\infty}\frac{\cos\dfrac{n\pi x}{a}\cos\dfrac{n\pi x_0}{a}\cos\dfrac{m\pi y}{b}\cos\dfrac{l\pi z}{h}}{\left(\dfrac{n^2 k_x}{a^2}+\dfrac{m^2 k_y}{b^2}+\dfrac{l^2 k_z}{h^2}\right)}$$

$$\left\{\left[\frac{\sin\left(\dfrac{\pi\left(-hmy_2+bl(\hat{m}y_2+\hat{c})\right)}{bh}\right)}{-hm\pi+bl\pi\hat{m}}+\frac{\sin\left(\dfrac{\pi\left(hmy_2+bl(\hat{m}y_2+\hat{c})\right)}{bh}\right)}{hm\pi+bl\pi\hat{m}}\right]\right.$$

$$\left.-\left[\frac{\sin\left(\dfrac{\pi\left(-hmy_1+bl(\hat{m}y_1+\hat{c})\right)}{bh}\right)}{-hm\pi+bl\pi\hat{m}}+\frac{\sin\left(\dfrac{\pi\left(hmy_1+bl(\hat{m}y_1+\hat{c})\right)}{bh}\right)}{hm\pi+bl\pi\hat{m}}\right]\right\}\right\} \tag{4.18}$$

where $\alpha = 158.73\phi\mu_o c_t$. The line source model for undulating wells is shown in Fig. 4.10. From the figure, we use Eq. 4.18 to evaluate the well performance of each segment. Then, we solve the linear equations by using either wellbore pressure or flow rate constraint.

Using the line source model, we can calculate the well productivity of undulating wells. The data in Table 4.2 shown in section 4.2 are used in this example. The productivity index distribution and the wellbore pressure distribution of the undulating wells are shown in Fig. 4.11 and Fig. 4.12 respectively similar to the results from the analytical method. The productivity index is low at the top and bottom segments since the well segments are close to the reservoir boundary. The total productivity index of the undulating well is 14.5 (STB/D)/psi. Since the potential pressure drop is much higher than the frictional pressure drop, the wellbore pressure profile reflects the well trajectory.
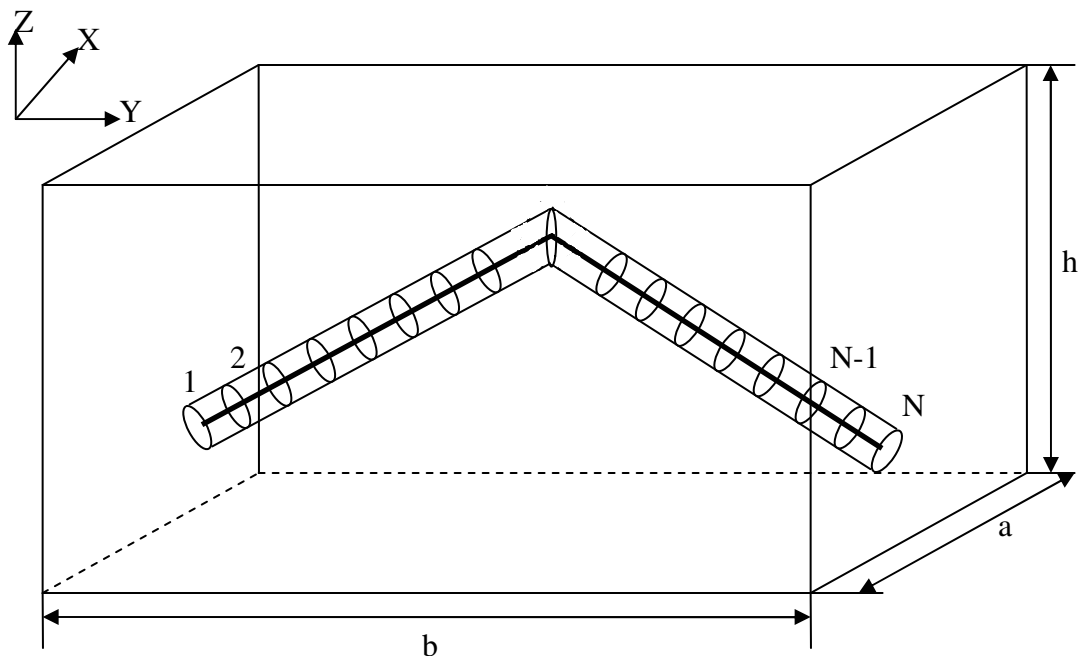
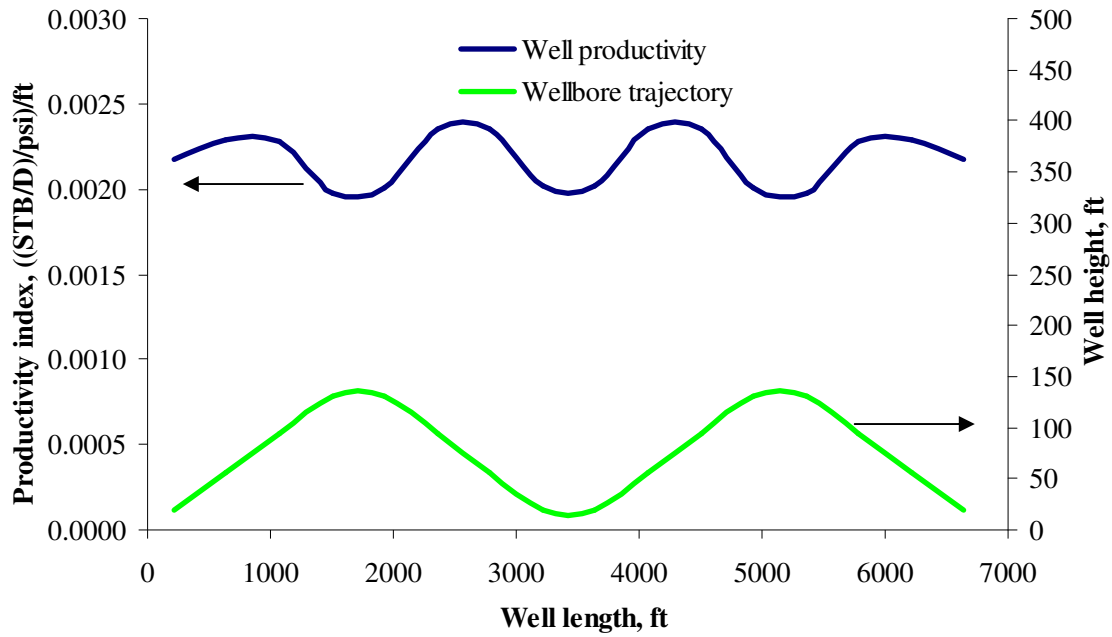**Fig. 4.10 Undulating well trajectory in a box-shaped reservoir.**

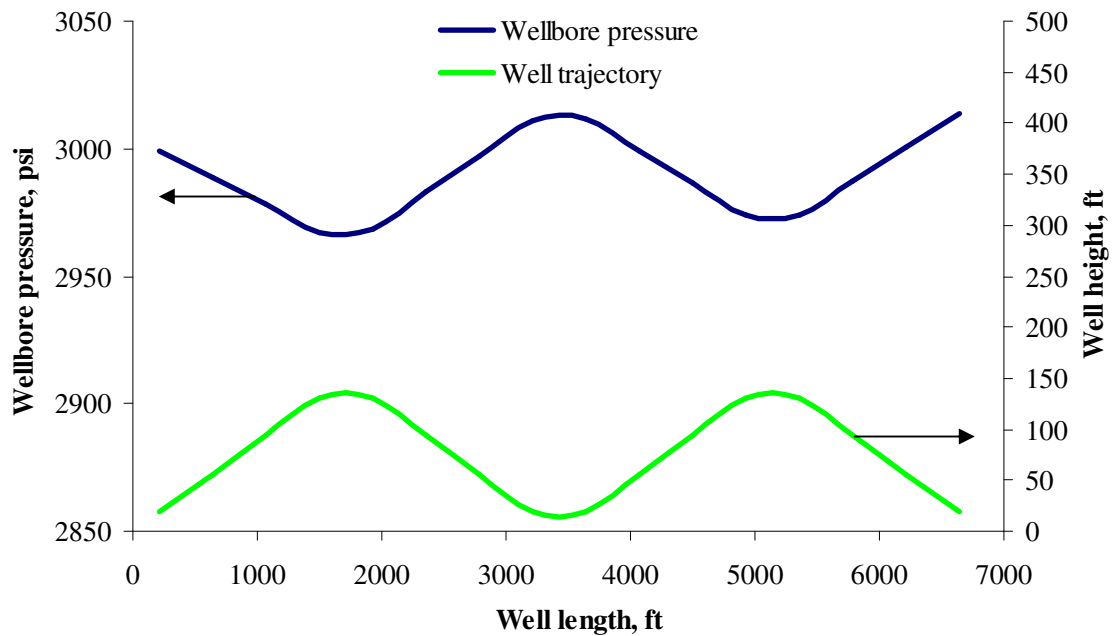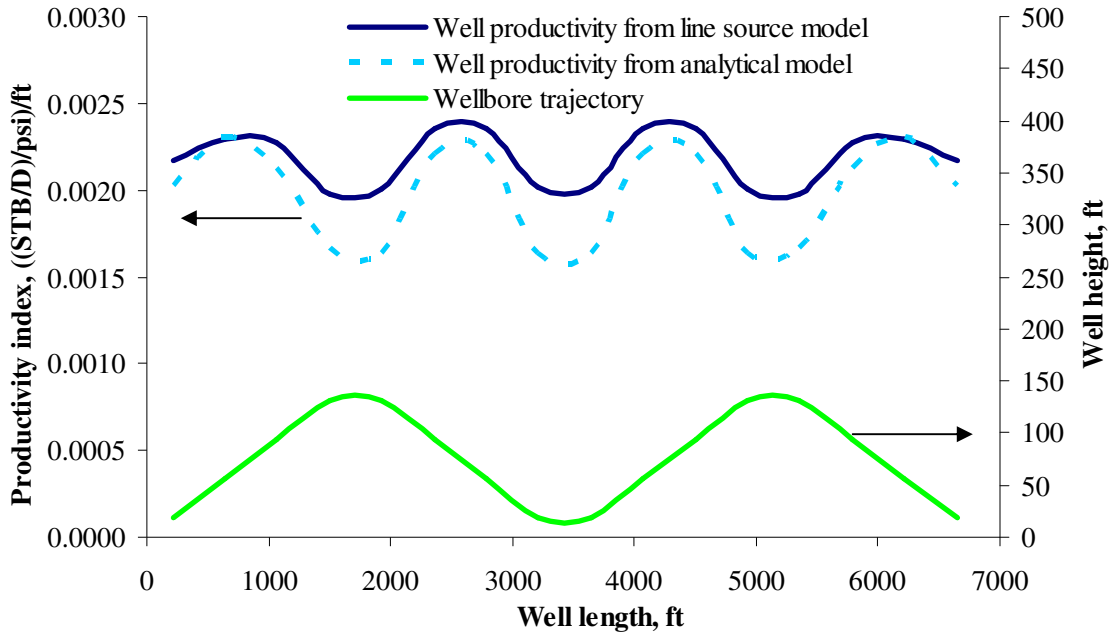**Fig. 4.11 Productivity profile from the line source model.**

Fig. 4.12 Wellbore pressure profile from line source model.

4.4 Model Comparison

The productivity index profile and the wellbore pressure profile of the undulating well in Table 4.2 obtained by the closed form model are compared with the ones obtained by the line source method. The comparison of the productivity profile is shown in Fig. 4.13. It reveals that the productivity index obtained by the closed form model is slightly lower than that obtained by the line source model. The total productivity index from closed form model is 13.6 STB/D/psi and the total productivity index from the line source model is 14.5 STB/D/psi. The difference is about 6%. The wellbore pressure profile along the undulating well is shown in Fig. 4.14. Both wellbore pressure profiles reflect the wellbore trajectory. Since the productivity index obtained by the closed form model is slightly lower that that obtained by the line source model, the flow rate from the closed form model is lower than that from the line source model. Therefore the wellbore pressure profile from the closed form model is slightly higher than that from the line source model. The most significant advantage of the line source approach is that the model does not assume non-vertical permeability (streamline is horizontal), but the closed form model is simple and easy to be applied.

4.5 Wellbore Pressure Drop

The wellbore pressure drop in undulating wells is critical to well performance especially in two-phase flow systems. Slug flow; which causes unstable production, and may result in the damages to the wellbore and the surface facility, can be occurred when the well is produced at a low flow rate. In two-phase flow system, liquid usually flows along the bottom part of the well and gas flows at the top part of the wellbore. For undulating wells, the liquid tends to accumulate at the bottom of the downward part and blocks the flow in the wellbore. The well can flow again when the gas behind the liquid builds up enough pressure to push the liquid through the well. Therefore, the wellbore pressure distribution is very sensitive to the well trajectory in undulating wells.

Fig. 4.13 Comparison the productivity profile from closed form model with line source model.
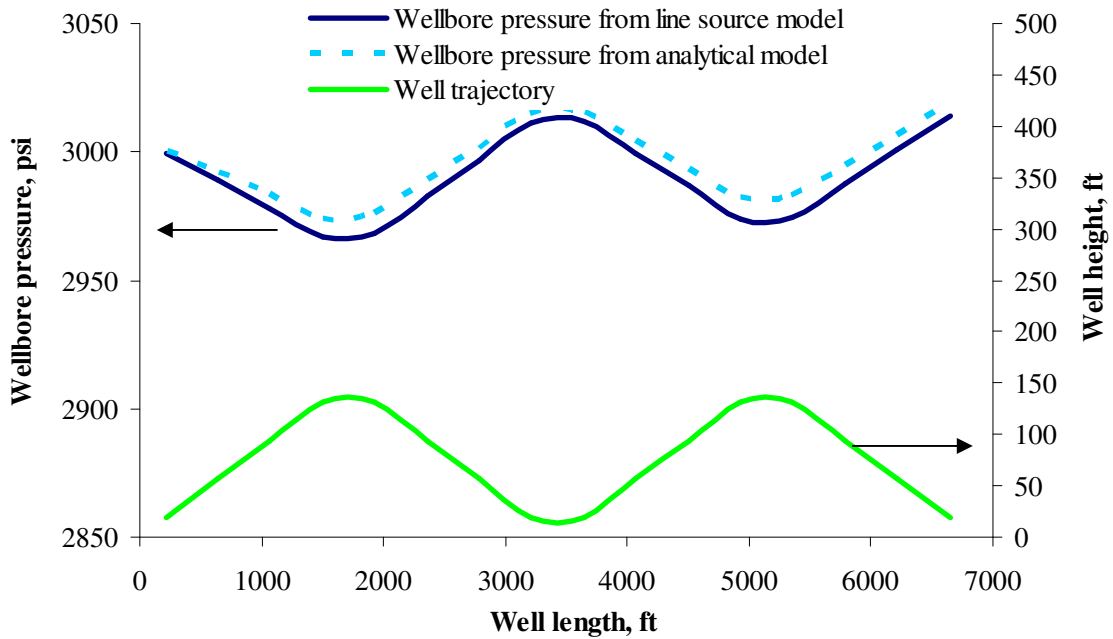
Fig. 4.14 Wellbore profile from closed form model and line source model.

Well design is the key to prevent slug flow problem in undulating wells. Because slug flow happens at low rate, we do not have to worry about this problem for high production wells. When the flow rate is low, the wellbore pressure profile reflects the well trajectory. The potential pressure drop is higher than the frictional pressure drop. On the other hand, at high flow rate the friction pressure may balance the potential pressure drop so that the wellbore pressure decreases from the toe to the heel. To minimize the potential pressure, we can decrease the height of the well. Fig. 4.15 shows the wellbore pressure profile under different wellbore pressure constraints. One well produces at constant wellbore pressure of 3000 psi at the heel, and another well produces at constant pressure of 200 psi at the heel. Since the flow rate of the first well is low, the wellbore pressure profile reflects the well trajectory. Conversely at high flow rate, the wellbore pressure profile shows that the wellbore pressure decreases from the toe to the heel, with a much lower pressure at the heel.
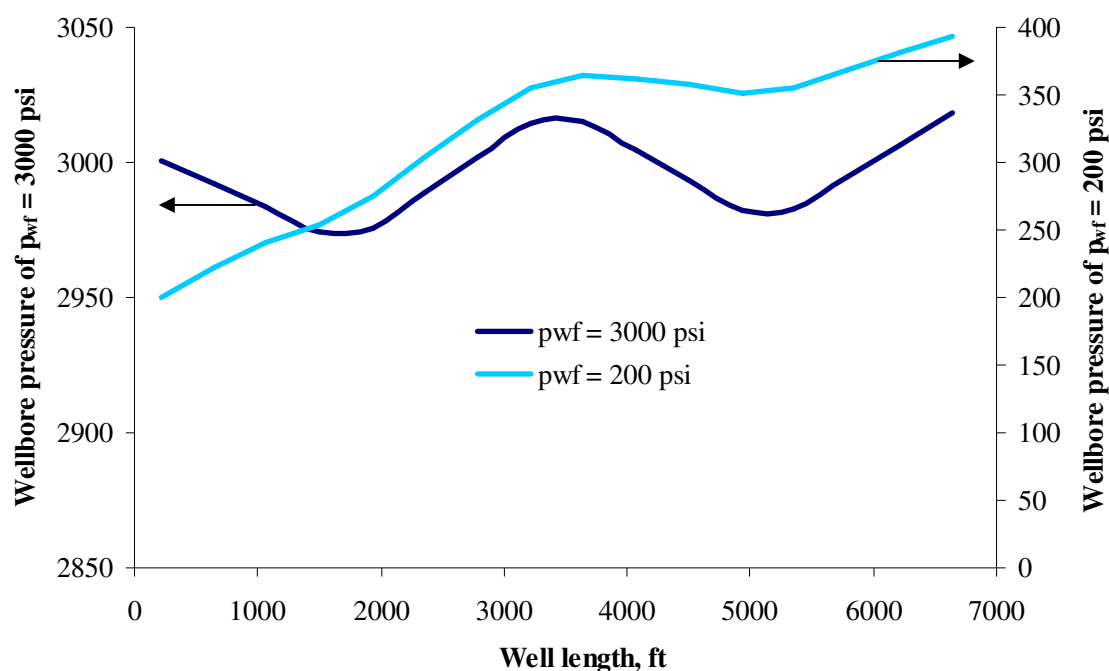
Fig. 4.15 Wellbore pressure profiles at different production conditions.

To study the effect of well trajectory on pressure distribution for the well and reservoir data in Table 4.2, we can alter the well trajectory by decreasing the well height from 150 ft to 100 ft and 75 ft with the same 5° of inclination. The well with the height of 100 ft has 3 cycles and the well with 75 ft has 4 cycles. All three well trajectories have the same measurement length. The productivity per foot profiles and wellbore pressure profile of the 3-cycle trajectory well are shown in Fig. 4.16 and Fig. 4.17 respectively and the productivity profile and wellbore pressure profile of the 4-cycle well trajectory are presented in Fig. 4.18 and Fig. 4.19 respectively.
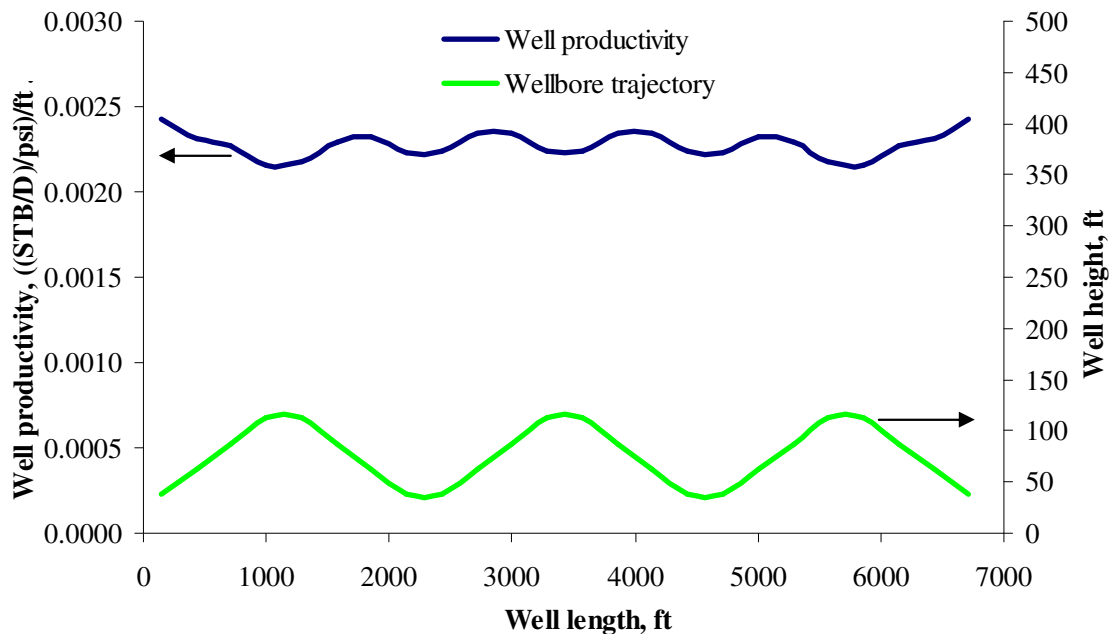
Fig. 4.16 Well productivity profile of the 3-cycle well trajectory.
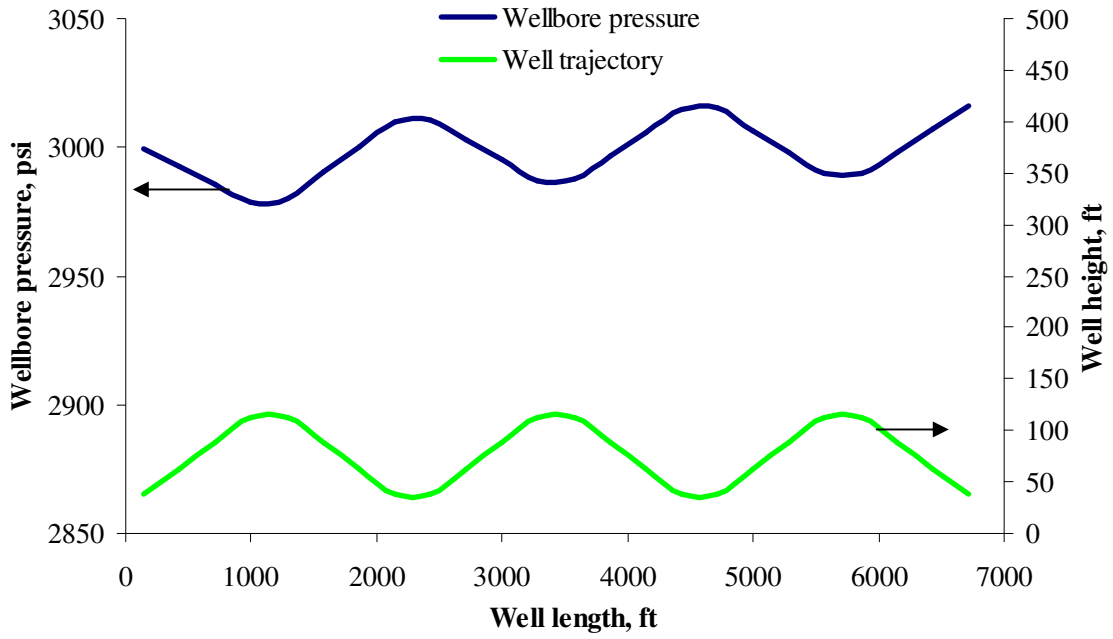
Fig. 4.17 Wellbore pressure profile of the 3-cycle well trajectory.
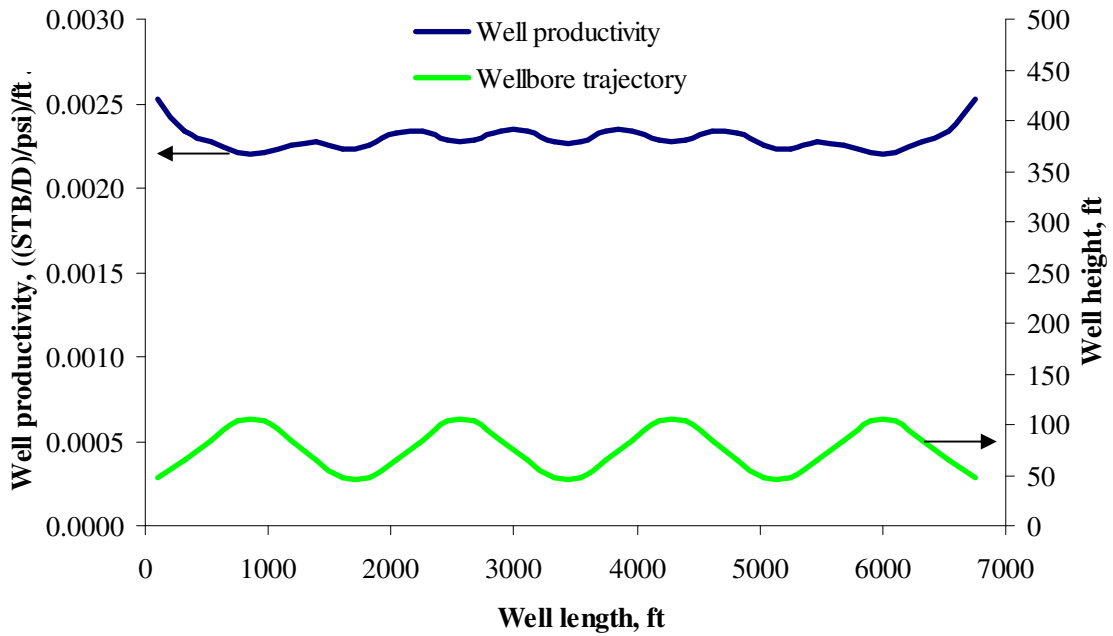
Fig. 4.18 Well productivity profile of the 4-cycle well trajectory.
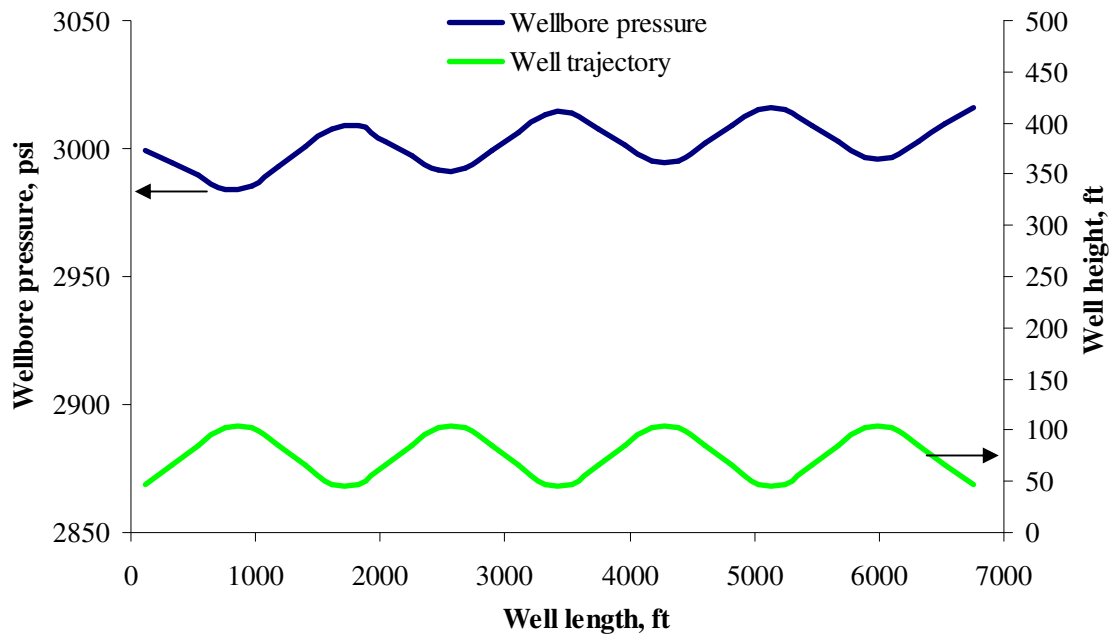
Fig. 4.19 Wellbore pressure profile of the 4-cycle well trajectory.

From Fig. 4.16 and Fig. 4.18, the productivity profile is almost uniform. The well is placed in the middle of the reservoir and away from the reservoir boundary. Therefore, these well do not affect by the reservoir boundary. Fig. 4.20 shows the pressure profiles of 2, 3 and 4 cycles of undulating. Form Fig. 4.20, we observe that the lower the well height, the lower the fluctuation in the pressure profile. To minimize the chance of slug-flow in the wellbore, reducing the fluctuation in the wellbore pressure profile results in a smoother production of the well, and also reduces the slug flow in undulating wells.
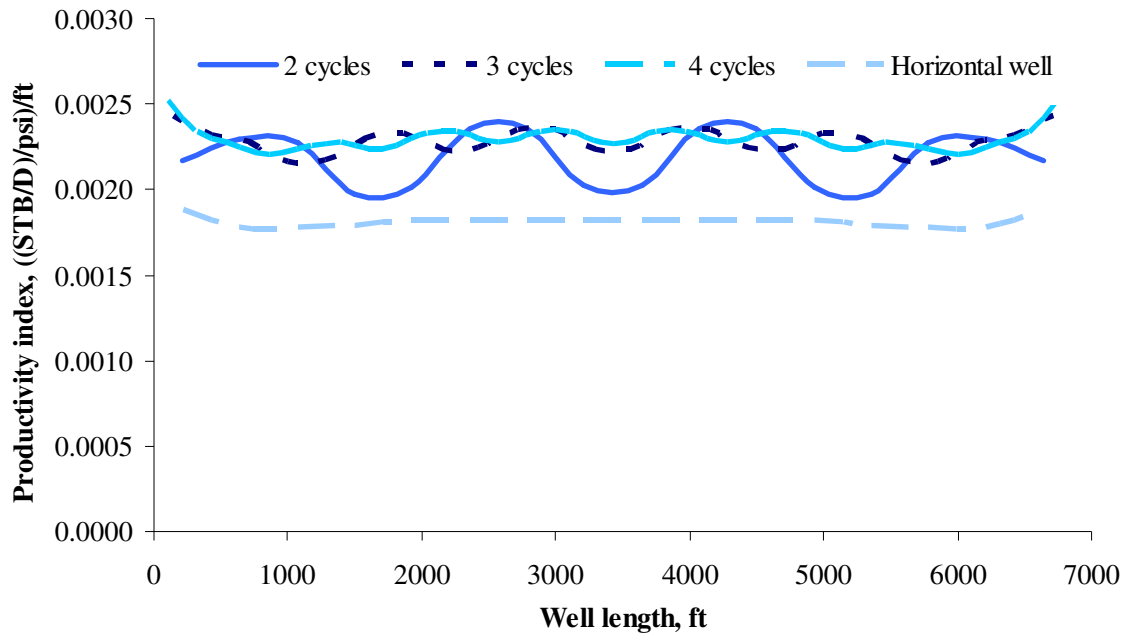
Fig. 4.20 Comparison wellbore pressure profiles of different well trajectories.

To optimize the wellbore performance, we compare the well productivity of each type of the well trajectory. The total productivity index for each well is presented in Table 4.3 and the well productivity profile is shown in Fig. 4.21.

Table 4.3   Well productivity data of different well trajectories

Well trajectory	Well height, ft	Well productivity index, STB/D/psi
4-cycle	75	15.8
3-cycle	100	15.6
2-cycle	150	14.5
Horizontal well	-	12.4
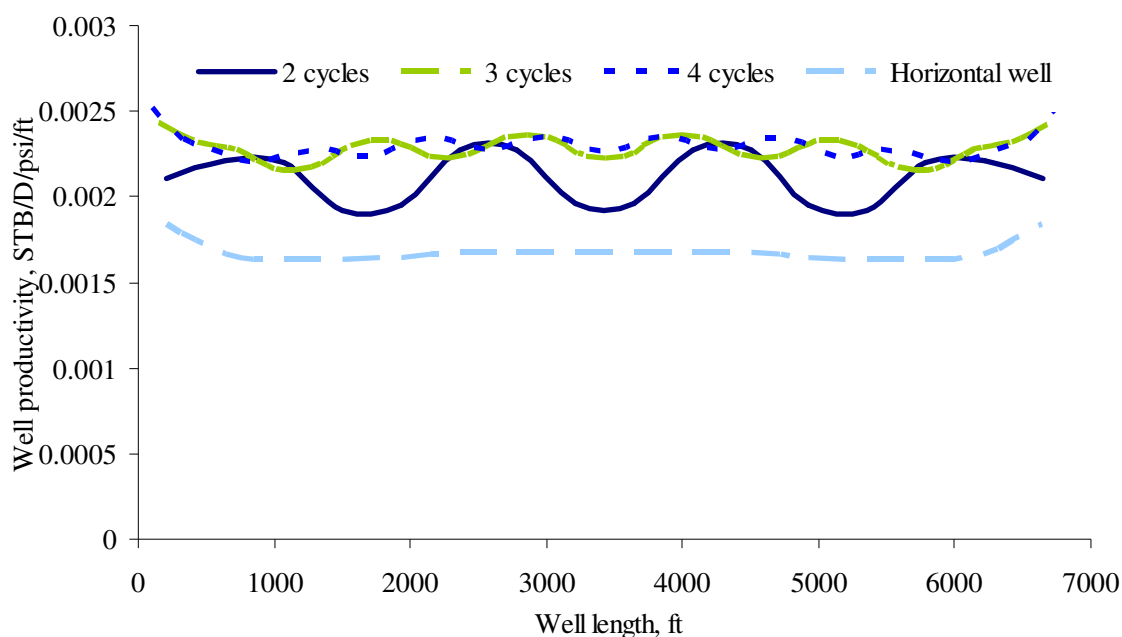
Fig. 4.21 Well productivity of different well trajectories.

The comparison shows that the productivity index of 4-cycle well is the highest yield flow rate for the well. Moreover, the fluctuation of the wellbore pressure profile is the lowest. The stable production in undulating well is a self-controlled problem when the height of undulating well decreases, the production rate increases, and the possibility of slug flow decreases.

However, decreasing the well height does not always increase the well productivity. For the extremely low vertical permeability formation, we can assume that the flow in the vertical direction is zero. In this case, the drainage volume depends on the well height. Thus the well productivity increases as the well height increase as shown in Table 4.4. The productivity of different well trajectories is calculated by using the input data in Table 4.2 with 0.00001 md vertical permeability. The results show that 2-cycle well trajectory, which the well height is the same as the reservoir thickness, has the highest productivity.

Table 4.4   Well productivity of different well trajectories in the extremely low vertical permeability formation

Well trajectory	Well height, ft	Well productivity index, STB/D/psi
4-cycle	75	6.75
3-cycle	100	7.48
2-cycle	150	8.25
Horizontal well	-	0.17

4.6 Summary

Two undulating well performance models are presented in this chapter. The first model is a closed form model which can predict the performance of undulating wells in relatively low vertical permeability formation. The closed form model applies to both single-phase and two-phase flow system in homogeneous reservoirs. The reservoir can be either isotropic or anisotropic. The model is easy to use with reasonable accuracy. The second model is the line source model. Although the line source only applies for single-phase flow system, this model can predict the undulating well performance in any vertical permeability conditions in homogeneous reservoirs. Because wellbore pressure drop is one of the major concerns in undulating well, our study shows that the undulating models can be used to optimize the undulating performance by increasing the productivity of the wells and decreasing the fluctuation of wellbore pressure along the wellbore.

CHAPTER V

MULTILATERAL WELL PERFORMANCE

In this chapter, we present multilateral well performance models. We first present the closed form model to evaluate multilateral well performance in single-phase and two-phase systems. Then we present the methodology to model multilateral well by using line source solution. After that we conduct the sensitivity study of different parameters on two-phase model. The cross flow phenomenon in multilateral wells is also discussed in this chapter.

5.1 Introduction

Multilateral wells are defined as the well that has at least two laterals connected to the same main wellbore. The production from each lateral can be commingled at the main wellbore to increase the productivity per well or it can be produced separately. For the well that the production non-commingles at the main wellbore, the well performance can be evaluated the same as a horizontal well performance. On the other hand, the evaluation of the multilateral well performance that the production from each lateral is commingled in the main wellbore is more complex than that of a single horizontal well. The pressure in the main wellbore has to meet the flow condition of each lateral connected to the junction. Otherwise, the production from one lateral can flow into other laterals, and causes low productivity in multilateral wells. To prevent this problem, the performance of multilateral wells is necessary. The well deliverability model of multilateral wells presents as the relationship of well head pressure and the total production from the wells, as well as production from each lateral.

5.2 Closed Form Model of Two-Phase Multilateral Wells

A closed form model of multilateral wells was presented by Zhu *et al.*[27] in 2002. The

model can be applied to single-phase oil reservoirs. This single-phase closed form model for multilateral well deliverability was developed to evaluate and optimize well performance. Instead of generating the relationship between wellbore pressure and flow rate, for multilateral wells, the relationship of surface pressure versus lateral total flow rates was established to describe well deliverability. The well performance was coupled with wellbore pressure drop model. The previous study showed that multilateral well performance strongly depends on the pressure distribution in the well system especially for commingled production. Sometimes fluid from one lateral may flow into other laterals instead of flowing to the surface (crossflow), which greatly reduces the surface production.

Based on the horizontal well introduced in Chapter II and the single-phase multilateral well model, the deliverability models of multilateral wells for other fluid systems rather than single-phase oil well is readily developed. We introduce two-phase correlation for two-phase system of multilateral well performance, and gas well model for multilateral wells in gas formations.

5.2.1 Model Assumptions

In order to apply the closed form model to predict multilateral well performance, we have to make some assumptions. These assumptions are,

- Each lateral produces from different reservoir and the reservoir compartments are isolated from each other.
- The laterals are assumed to be horizontal such that gravity effect is neglected.
- Inflow effect on wellbore pressure drop is comparatively small and negligible.
- Each lateral is connected to the main wellbore by a build section which has no contact with reservoir (non-producing).

5.2.2 Model Description

To calculate well deliverability, we divide each lateral into several segments as shown in

Fig. 5.1. Pressure and flow rate are solved from the wellbore inflow performance model and the wellbore pressure drop model simultaneously over each segment as described in Chapter II. By applying the first and second assumptions (isolated reservoir and perfectly horizontal wellbore), we can evaluate the wellbore performance model by the horizontal performance model. For two-phase flows, we use the modified Vogel's correlation to evaluate the wellbore performance presented in Chapter II. With the third assumption, we apply the pressure drop correlation for fluid flowing in a pipe to calculate the pressure drop along the wellbore. Since the build sections are non-producing, according to the fourth assumption, we can calculate the pressure drop along the build sections by the pressure drop correlations. Because the junction connects each lateral to the main wellbore, we have to match the pressure from each lateral in the main wellbore to meet the flow condition. This process required iteration. Once the equilibrium condition at the junction is established, we calculate the pressure drop along the main wellbore by using the correlation[28] to obtain the surface pressure.
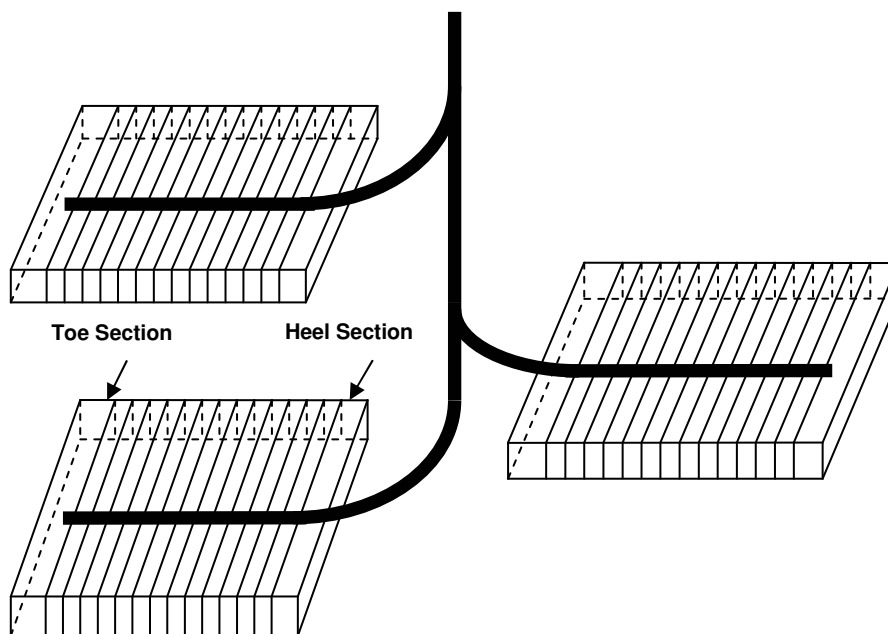
Fig. 5.1 Schematic of physical closed form model.

5.2.3 Calculation Procedure

The model consists of two main parts. The first part is producing part or the lateral part. In this part we couple the well performance model with the pressure drop model. The second part is non-producing part or the junction and the main wellbore parts. The junction and the main wellbore are non-producing part so we can calculate the pressure profile along these sections by using a pressure calculation methods. One important step in the well deliverability calculation for multilateral wells is to find an equilibrium pressure at junction. The proper pressure at the junction allows all of the laterals in the system to produce, and this requires the iteration. Once a flow condition is established, surface pressure is easily evaluated by pressure drop correlation. A multilateral well deliverability curve can be generated by changing a different drawdown pressure and repeating the calculation. The procedure is summarized as

1. Dividing reservoir and well into several segments (Fig. 5.1) and calculating the productivity index of each segment in the bottom-most lateral from the inflow performance model. (Section 2.2 for gas and Section 2.3 for two-phase system)

2. Assuming the wellbore pressure for the toe segment and multiplying the pressure drawdown to the productivity index of the toe segment to obtain the flow rate for this segment. (Section 2.5)

3. Calculating the wellbore pressure drop over this segment and obtain the new flowing bottomhole pressure and drawdown for the next segment. (Section 2.5)

4. Calculating the flow rate for the next segment with the new drawdown. (Section 2.5)

5. Repeating Steps 3 and 4 until reach the heel segment.

6. Calculating the pressure drop in the build section to obtain the pressure at Junction 1.

7. Moving upwards and repeating Steps 1-4 for Lateral 2 and calculating the pressure drop in build section 2 to obtain the pressure at Junction 1 for Lateral 2

8. Comparing two junction pressure from Lateral 1 and Lateral 2, if they are different, repeating Step 7 with different flowing bottomhole pressure until the junction pressure from two laterals agree.

9. Moving upwards and repeating the calculation for all laterals.

10. Calculating the pressure drop between the top-most junction and the surface.

This procedure can be repeated to generate a curve on deliverability plot for multilateral wells by changing the wellbore pressure at the lower lateral.

5.2.4 Comparison of Single-Phase Model with Two-Phase Model

Normally, the single-phase models are used to predict well performance for multilateral wells regardless of reservoir pressures. When the reservoir pressure is below bubble-point pressure, single-phase model deviates from the predicted flow condition. This is very critical in multilateral wells because the production from different lateral is sensitive to the pressure distribution in the wellbore system. Mis-predicted pressure distribution can cause significant error in flow rate distribution. In this section, we compare the results of production rate in a single-phase model and a two-phase model. In the single-phase model, original Babu and Odeh's model was used for wellbore performance, Ouyang's model[29] was used to calculate wellbore pressure drop, and the procedure in section 5.2.3 was applied for the calculation procedure. For the two-phase model, we applied the modified Vogel's correlation to calculate the wellbore performance and Begg and Brill's correlation to evaluate the pressure drop along the wellbore with the same procedure presented in the previous section. A two-lateral well is used in the comparison. The reservoir, well, and fluid information are presented in Table 5.1 and the well trajectory is shown in Fig. 5.2.

Table 5.1　　　Reservoir, lateral and fluid property data of dual lateral well

Properties	Reservoir and Lateral Data	
	1	2
Length, ft	3400	2800
Width, ft	2000	2000
Height, ft	80	58
k_x, md	375	225
k_y, md	375	225
k_z, md	38	23
p_R, psi	3200	2800
L_w, ft	3000	2400
r_w, inch	1.8	1.8
s	10	10
Gas Gravity	0.7	0.7
Oil Gravity (API°)	25	25
GOR (Scf/STB)	1200	1000

Main wellbore
TVL = 2500 ft
MDL = 2500 ft

Build section 2
TVL = 2500 ft
MDL = 2800 ft

Build section 1
TVL = 3000 ft
MDL = 3400 ft

Lateral 2
Lateral length = 2400 ft

Lateral 1
Lateral length = 3000 ft
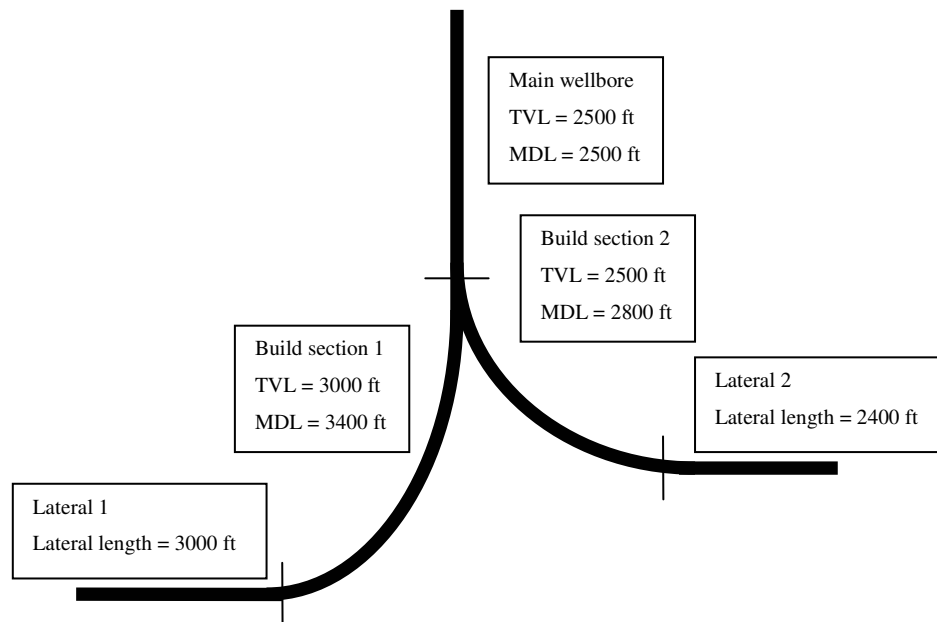
Fig. 5.2 Dual lateral well.

We first compare the wellbore pressure distribution and flow rate distribution along both laterals generated by the single-phase model and the two-phase model. Next, we study the wellbore pressure distribution by fixing the wellbore pressure at the heel of the laterals. Fig. 5.3 presents the pressure distribution along the two laterals.
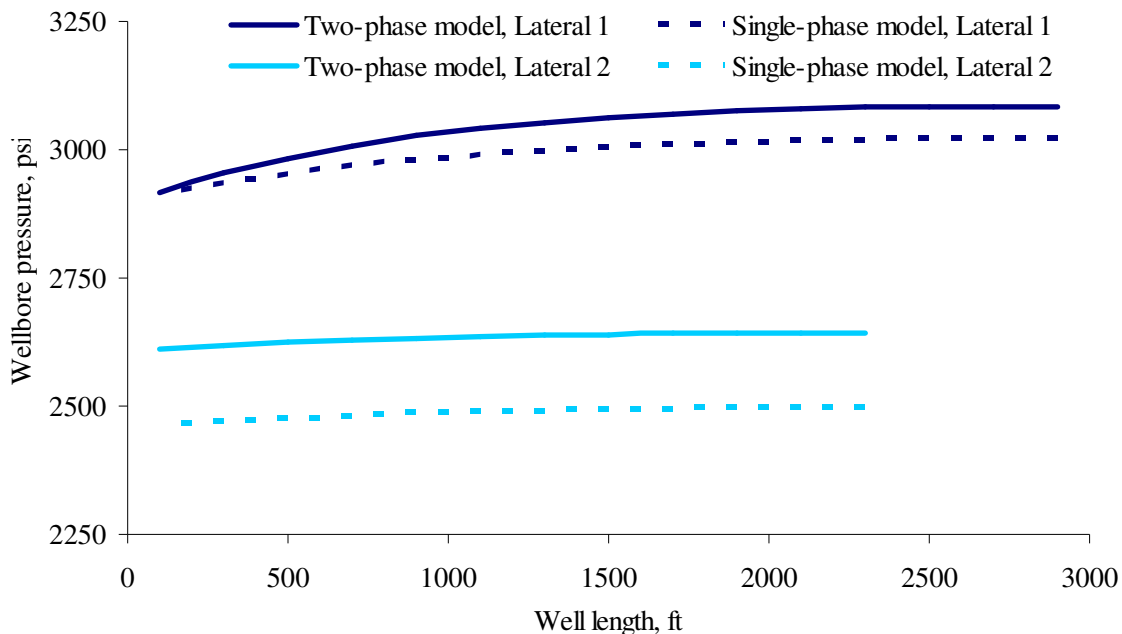
Fig. 5.3 Wellbore pressure distribution along the wellbore.

It shows clearly on Fig. 5.3 that for a giving wellbore pressure at the heel, the two-phase model predicts higher wellbore pressure distribution along the lateral for both laterals than the single-phase model does. The figure shows that the pressure drop along the laterals estimated by two-phase model is higher than that predicted by the single-phase model though the single-phase model predicted higher production rate than the two-phase model. This is because of a higher frictional pressure drop caused by the gas flow with much higher velocity in the laterals. As a result of higher wellbore pressure predicted by the two-phase model, the drawdown pressure of the two-phase model is smaller than that from single-phase model resulting a lower flow rate.

Fig. 5.4 shows the inflow distribution along lateral 1 and lateral 2. This distribution is important information for well control and well optimization. From the figure, we can see that the single-phase model predict higher oil inflow rate than the two-phase model since the single-phase model predicts higher pressure drawdown than the two-phase model. Moreover, the single-phase model does not account for relative permeability so the well productivity index predicted by the single-phase model is higher than that by the two-phase model. In general, the single-phase model will overestimate the well performance of multilateral well when the reservoir pressure and/or when the wellbore pressure is below the bubble point pressure.
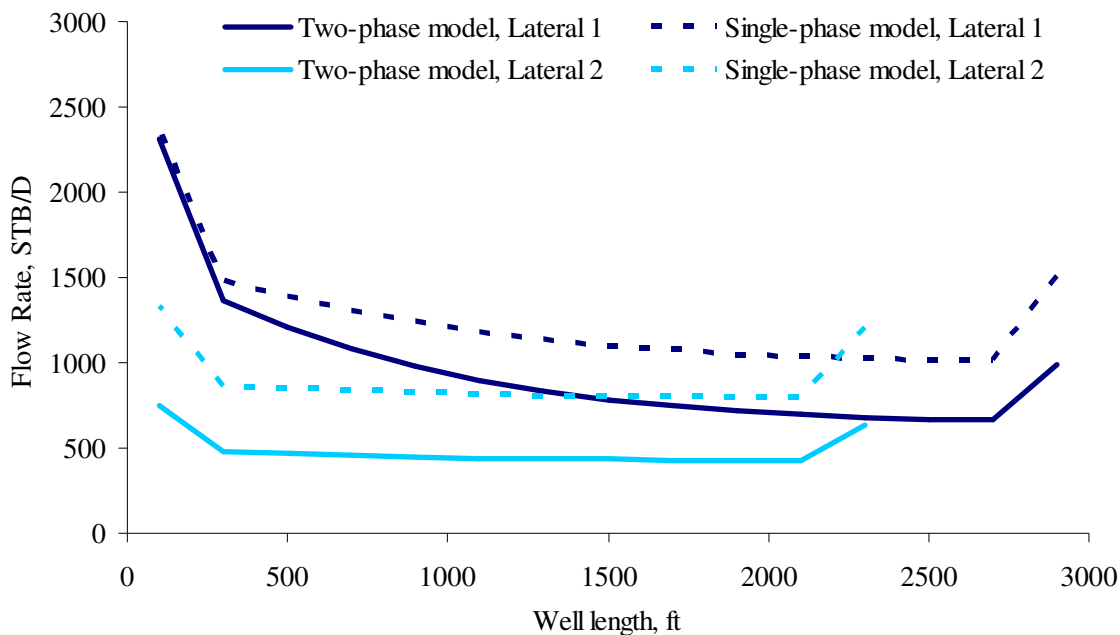
Fig. 5.4 Inflow rate distribution along the lateral.

The well deliverability of multilateral well is presented by plotting the wellhead pressure versus the total production rate of the well. The well deliverability is shown in Fig. 5.5. The figure shows that the well deliverability obtained by two-phase model is different from that by the single-phase model. The difference increases when the well is operated at low wellhead pressure. At low wellhead pressure, wellbore pressure is low

but gas flow rate is high. Therefore the difference between the two-phase model and the single-phase model is more pronounced at low wellhead pressure. From the figure we can see that if the single-phase inflow is used for two-phase system, the oil flow rate can be overestimate. The error in this case is about 10%.
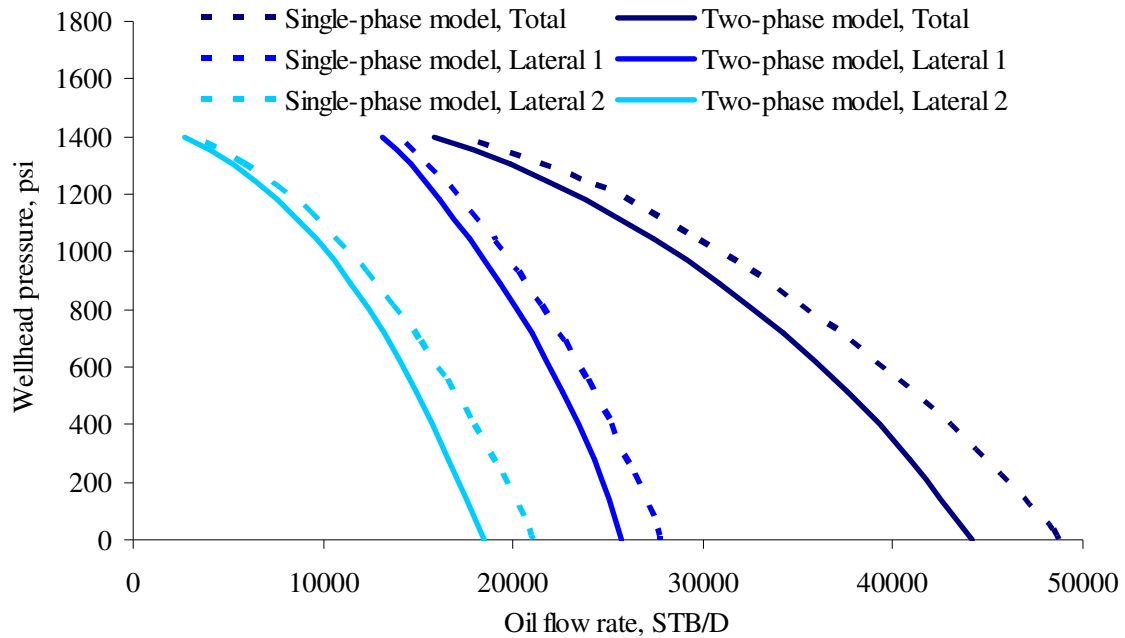
Fig. 5.5 Comparing multilateral well deliverability from single-phase model with two-phase model.

5.3 Line Source Model

Line source model can be used to model multilateral well performance. The models are available for single-phase reservoir only. Although the line source model do not apply for two-phase system, this model can be used to estimate the multilateral well performance when laterals are not perfectly horizontal or when build sections have communication with reservoirs (considering as a producing part). Each lateral can produce from the same reservoir or from different reservoirs.

5.3.1 Calculation Procedure

The line source solution is used to model multilateral well. We divide multilateral wells into two main parts, producing part and non-producing part. We only apply the line source model to the producing part. Then, we calculate the inflow along the part and couple with the wellbore pressure drop model to account for the pressure drop along the wellbore (finite conductivity inner boundary condition). For non-producing part we apply the pressure drop model to calculate the pressure drop along this part. The procedure can be summarized as,

1. Dividing the well into producing part and non-producing part.
2. For producing-part, we divide the producing part into several segments by assuming each segment can be represented by a linear equation (Eq. 3.25).
3. Applying Eq. 3.30 to calculate the pressure drop at the middle of well circumstance of each segment as a result of the production into individual segment. The source solution can be any combination depending on reservoir boundaries. If the reservoir is sealed, Eq. 3.34, Eq. 3.35 can be used for every segment.
4. After complete the calculation in Step 3, a set of linear function is created as Eq. 3.44.
5. The well can be controlled by either the wellbore pressure or the maximum flow rate. Then we can solve the set of linear equation created in step 4.
6. The flow rate is flow through non-producing part and we can use this flow rate to calculate pressure drop along the non-production part to obtain the pressure at the surface.

We repeat this procedure by changing the well constraint in Step 5 to obtain a relationship between the well flow rate and wellhead pressure. Then, we can obtain the well deliverability of multilateral wells.

5.4 Parametric Study

Crossflow is one of the main causes of low productivity in multilateral wells. Crossflow in multilateral wells is defined as the flow rate produced from one lateral flowing into other laterals. Crossflow can occur either from the lower lateral to the top lateral or from top lateral to the lower lateral. However, we can prevent this problem by correctly predicting and controlling the pressure and flow rate in the well system.

5.4.1 Effects of Gas Oil Ratio

Gas oil ratio (GOR) is very essential in two-phase flow calculation because it controls the amount of free gas in the well. As the ratio of oil and gas changes, the pressure drop inside wellbore will change. More importantly, the flow regime of two-phase flow in the wellbore may vary with GOR, and this will significantly affect the pressure drop in the laterals, build section and the main wellbore. We studied the effects of GOR on well deliverability and flow rate distribution. The total flow rates versus the wellhead pressure for different GOR are shown in Fig. 5.6 with GOR varied from 500 SCF/STB to 1800 SCF/STB. The figure shows that the slope or the derivative of the wellhead pressure with respect to the total flow rate increases as GOR increases. The slope represents how quick the flow rate increases when lower the wellhead pressure. The lower the GOR, the smaller the slope; and thereafter, the faster increase in the flow rate. As a result, at low wellhead pressure, the high GOR well produces less oil, but at high wellhead pressure, the high GOR well will produce more oil.
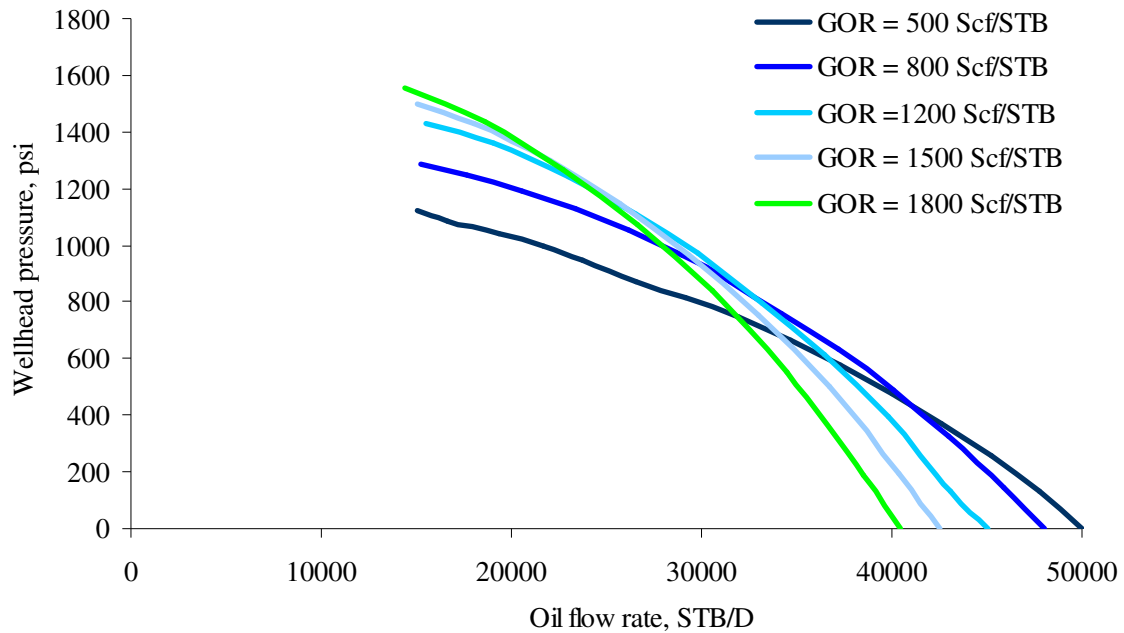
Fig. 5.6 Effect of GOR on well deliverability.

5.4.2 Effect of Oil Gravity

Oil gravity is one of the important parameters that affect the well deliverability. We studied the effect of oil gravity on the multilateral well performance by varying the oil gravity from 15 API to 35 API. From Fig. 5.7, the oil gravity changes the well deliverability dramatically. At low oil gravity, the total production rate is much lower than the production rate at high oil gravity. For example, at 8900 psi wellhead pressure the total production of 35 API case is about 40,000 STB/Day and the total production rate of 15 API case is about 20,000 STB/Day. In other words, the total production of 35 API case is approximately double of the total production of 15 API case because at low oil gravity, oil viscosity is high. Since well productivity index is inversely proportional to the viscosity of the fluid, the lower the oil gravity, the lower the well productivity index.
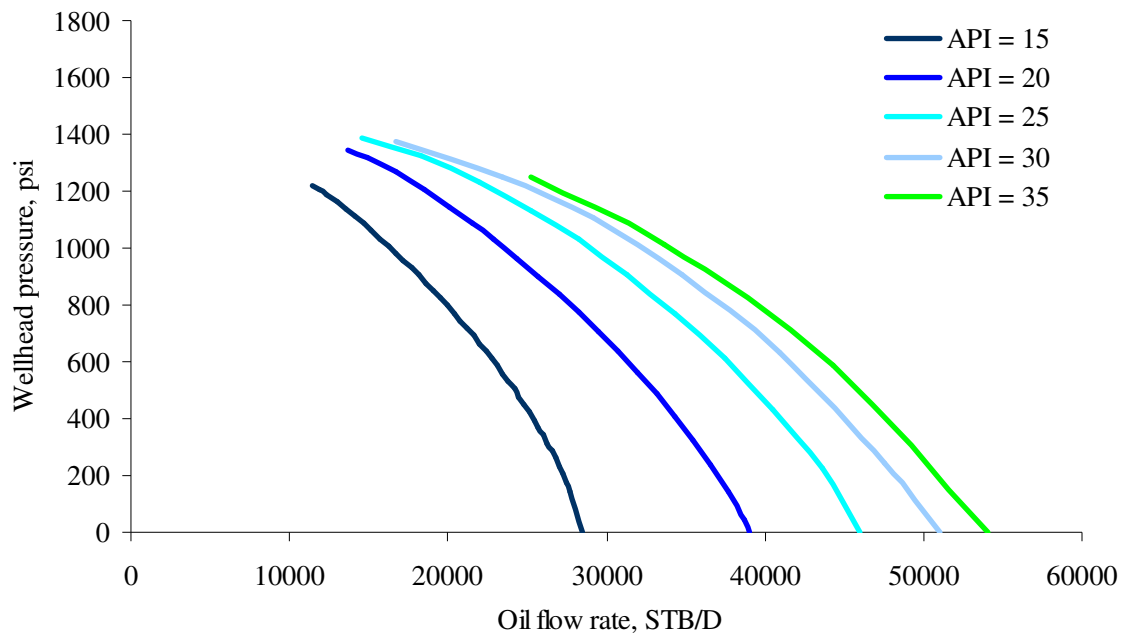
Fig. 5.7 Effect of oil gravity on well deliverability.

CHAPTER VI

CONCLUSIONS

Complex wells (horizontal wells, undulating wells, and multilateral wells) have been used widely today in the oil and gas industry to develop conventional and unconventional fields. In general, these wells offer high productivity. However, predicting well performance becomes much more difficult compared with conventional vertical wells because of the complexity of well structures. In order to evaluate well performance, we need new robust models. This dissertation presents well performance models of horizontal wells, undulating wells, and multilateral wells. The models are divided into two main categories, the closed form model and the line source model. These models can be used to generate inflow performance relationships, study parameter sensitivity, and optimize well designs.

This study modifies and summarizes the systematic analytical equations for horizontal wells in single-phase oil, single-phase gas, and two-phase oil and gas formations for steady-state and pseudosteady-state boundary condition. It also presents the line source solution of 2D wellbore for horizontal wells, inclined wells, and undulating wells. The effects of important parameters, such as permeability, well structures, and reservoir conditions, on well productivity are discussed. Wellbore pressure distribution is addressed in detail in this study because of its critical role in complex well performance. Based on the study, we can present the following conclusions and recommendations.

6.1 Conclusions

The conclusions can be summarized as following.

1. The systematic table of horizontal well inflow performance models is created to summarize the models. The models are categorized by the fluid systems and

boundary conditions. Each model should be used appropriately to obtain accurate results.

2. A line source model of 2D well structures is presented and tested. The well trajectory can change in two directions which makes the model very practical. The model applies for vertical wells, horizontal wells and inclined wells for single-phase system and homogeneous formations.

3. The study of flow distribution and pressure distribution in horizontal wells shows that the productivity distribution along horizontal well has w-shape when the well length is relatively long comparing with the reservoir length. When the well length is relatively short comparing with the reservoir length, the productivity distribution becomes u-shape.

4. The closed form model of undulating wells in relatively low vertical permeability formation is presented and tested. The model applies for both single-phase and two-phase systems. This model can be used to evaluate undulating well performance with reasonable results when vertical permeability is very low and the flow is dominated by horizontal permeability. The developed undulating model overcomes the problem of underestimated production performance by the horizontal well model, and avoids missing the economic value of develop low vertical permeability reservoir with undulating wells.

5. A line source model of undulating wells is presented. This model applied for single-phase system in homogeneous reservoirs. The model can be used to predict the undulating well performance under different boundary conditions including steady-steady condition, pseudosteady-state condition and mixed-boundary condition. In addition to the flexibility and accuracy of the model comparing with the analytical undulating well model, it can be used for both intentional and unintentional undulating well structures.

6. Wellbore pressure and fluid distribution are extremely important in undulating wells, especially in two-phase systems. If the well structure is not designed

carefully, unstable production may occur. Using the developed models can help to optimize undulating well performance.

7. The closed form model used for predicting two-phase flow in multilateral well is presented. The model is fast and easy to use. It also applies for the multilateral wells that each lateral produces from different reservoirs and each reservoir does not connect to each other. Incorporating with a wellbore hydrodynamic model, production at the surface from a commingled multilateral well can be optimized

6.2 Recommendations

Based on the results of this study, it is recommended that

1. A comprehensive two-phase well flow model should be integrated to the line source model for accurate prediction of slugging in undulating wells. This will explain the necessary of drilling control in well trajectory.

2. A 3D line source model needs to be developed to relax the assumption of well structures in horizontal and undulating wells.

NOMENCLATURE

Symbol	Description
A	drainage area
a	reservoir width
B	formation volume factor
b	reservoir length
D	wellbore diameter
h	reservoir thickness
f_f	friction factor with wall flux
J	productivity index
k	permeability
L	well length
N_{Re}	Reynolds number
p	pressure
q	flow rate
r	radius
s	skin factor
T	temperature

Greek

ε	relative pipe roughness
Φ	flow potential
ϕ	porosity
θ	wellbore inclination
μ	viscosity
ρ	density

τ	time

Subscripts

0	damaged
d	damaged
g	gas
I	inflow
o	oil
R	reservoir
w	wellbore
wf	wellbore flowing
x	x-direction
y	y-direction
z	z-direction

REFERENCES

1. Joshi, S.D.: "Augmentation of Well Productivity with Slant and Horizontal Wells," *JPT* (June 1988) 729.

2. Economides, M.J., Deimbacher, F.X., Brand, C.W., and Heinemann, Z.E.: "Comprehensive Simulation of Horizontal Well Performance," *SPEFE* (December 1991) 418.

3. Butler, R.M.: Horizontal Wells for the Recovery of Oil, Gas and Bitumen, Petroleum Monograph, Petroleum Society of CIM (1994) 2.

4. Furui, K., Zhu, D. and Hill, A.D.: "A Rigorous Formation Damage Skin Factor and Reservoir Inflow Model for a Horizontal Well," *SPEPF* (August 2003) 151.

5. Babu, D.K. and Odeh A.S.: "Productivity of a Horizontal Well," *SPE Reservoir Engineering* (November 1989) 417.

6. Goktas, B. and Ertekin, T.: "Performances of Openhole Completed and Cased Horizontal/Undulating Wells in Thin-Bedded, Tight Sand Gas Reservoirs," paper SPE 65619 presented at the 2000 SPE Eastern Regional Meeting, Morgantown, West Virginia, 17-19 October.

7. Al-Mohannadi, N., Ozkan, E., and Kazemi, H.: "Pressure-Transient Responses of Horizontal and Curved Wells in Anticlines and Domes," paper SPE 84378 presented at the 2003 SPE Annual Technical Conference and Exhibition, Denver, 5-8 October.

8. Azar-Nejad, F., Tortike, W.S., and Farouq Ali, S.M.: "Performance of Horizontal Wells with Irregular Geometry," paper SPE 36550 presented at the 1998 SPE Annual Technical Conference and Exhibition, Denver, 6-9 October.

9. Peters, J. E.: *Theory and Applications of Reservoir Transient*, Spring, University of Texas at Austin, TX (2003).

10. Goode, P.A. and Thambynayagam, R.K.M.: "Pressure Drawdown and Build up Analysis for Horizontal Wells in Anisotropic Media," *SPEFE* (December 1987) 683.

11. Yildiz, T. and Ozkan, E.: "Transient Pressure Behavior of Selectivity Completed Horizontal Wells," paper SPE 28388 presented at the 1994 SPE Annual Technical Conference and Exhibition, New Orleans, LA, 25-28 September.

12. Al-Hussainy, R.R. et al.: "The Flow of Real Gases Through Porous Media," *JPT* (May 1966) 624.

13. Economides, M.J., Hill, A.D. and Economides, C.E.: *Petroleum Production Systems*, Practice-Hall Inc., Upper Saddle River, NJ (1993).

14. Thomas, L.K. et al.: "Horizontal Well IPR Calculation," paper SPE 36753 presented at the 1996 SPE Annual Technical Conference and Exhibition, Denver, CO, 6-9 October.

15. Vogel, J. V.: "Inflow Performance Relationships for Solution-Gas Drive Wells," *JPT* (January 1968) 83.

16. Hill, A. D. and Zhu, D.: "The Relative Important of Wellbore Pressure Drop and Formation Damage in Horizontal Wells," paper SPE 100207 presented at the SPE Europec/EAGE Annual Conference and Exhibition, Vienna, Austria, 12-15 June.

17. Economides, M.J., Brand, C.W., and Frick, T.P.: "Well Configurations in Anisotropic Reservoirs," *SPEFE* (December 1996) 257.

18. Penmatcha, V.R. and Aziz K.: "Comprehensive Reservoir/Wellbore Model for Horizontal Wells," *SPEJ* (September 1999) 224.

19. Ouyang, L.B. and Aziz, K.: "A General Single-Phase Wellbore/Reservoir Coupling Model for Multilateral Wells," *SPEREE* (August 2001) 327.

20. Brigham, W.E.: "Discussion of Productivity of a Horizontal Well," *SPE Reservoir Engineering* (May 1990) 254.

21. Besson, J.: "Performance of Slated and Horizontal Wells on an Anisotropic Medium," paper SPE 20965 presented at 1990 Europac, Hague, The Netherlands, 22-24 October.

22. Gringarten, A. C. and Ramey, H. J.: "The Use of Source and Green's Functions in Solving Unsteady-Flow Problems in Reservoirs," *SPEJ* (October 1973) 285.

23. Earlougher, R.C..: "Estimating Drainage Shapes from Reservoir Limit Tests," *JPT* (October 1971) 1266.

24. Yaxley, L.M.: "New Stabilized Inflow Equations for Rectangular and Wedge Shaped Drainage System," Manuscript SPE paper 17082.

25. Cinco, H., Miller, F.G. and Ramey, H.J.: "Unsteady-State Pressure Distribution Created by a Directionally Drilled Well," *JPT* (November 1975) 1392.

26. Papatzacos, P.: "Approximate Partial-Penetration Pseudoskin for Infinite-Conductivity Wells," *SPE Reservoir Engineering* (May 1987) 227.

27. Zhu, D., Hill, A.D. and Landrum, W.R.: "Evaluation of Crossflow Effects in Multilateral Wells," paper SPE 75250 presented at the SPE /DOE Thirteen Symposium on Improved Oil Recovery, Tulsa, Oklahoma, 13-17 April.

28. Beggs, H.D and Brill, J. P.: "A Study of Two-Phase Flow in Inclined Pipes," *JPT* (May 1973) 607.

29. Ouyang, L.B. and Aziz, K.: "A General Single-Phase Wellbore/Reservoir Coupling Model for Multilateral Wells," *SPEREE* (August 2001) 327.

APPENDIX A

STEADY STATE HORIZONTAL WELL MODEL

The horizontal well model under steady-state condition is derived in this appendix. The diffusivity of single-phase incompressible fluid is solved by the instantaneous source/sink function in a homogeneous box-shaped reservoir. The formation is either isotropic or anisotropic. The initial boundary condition is constant pressure in the reservoir and the boundary condition in the X-direction is constant pressure boundary and no-flow boundary in the Y- and Z- direction. The inner boundary condition is uniform flux along the reservoir.

The line source represents a horizontal well and the well can be located anywhere in the reservoir parallel to the Y-axis. Assuming the source or the horizontal well is located at (x_0, y_0, z_0). The toe and the heel are at (x_0, y_1, z_0) and (x_0, y_2, z_0) respectively. The pressure drop at any locations in the reservoir is estimated by

$$p_{init} - p(x, y, z, t) = \left[\frac{B_o \mu_o q_o}{L\alpha} \right] \int\limits_0^t \int\limits_{y_1}^{y_2} (S_x S_y S_z) dy_0 d\tau \tag{A-1}$$

where,

$$S_x = S(x, x_0, \tau) = \frac{2}{a} \sum_{n=1}^{\infty} \sin \frac{n\pi x}{a} \sin \frac{n\pi x_0}{a} \exp\left[-\frac{n^2 \pi^2 k_x \tau}{\alpha a^2} \right] \tag{A-2}$$

$$S_y = S(y, y_0, \tau) = \frac{1}{b} \left(1 + 2 \sum_{m=1}^{\infty} \cos \frac{m\pi y}{b} \cos \frac{m\pi y_0}{b} \exp\left[-\frac{m^2 \pi^2 k_y \tau}{\alpha b^2} \right] \right) \tag{A-3}$$

$$S_z = S(z, z_0, \tau) = \frac{1}{h} \left(1 + 2 \sum_{l=1}^{\infty} \cos \frac{l\pi z}{h} \cos \frac{l\pi z_0}{h} \exp\left[-\frac{l^2 \pi^2 k_z \tau}{\alpha h^2} \right] \right) \tag{A-4}$$

$$\alpha = \phi \mu c_t \tag{A-5}$$

First, we start from integrate along a horizontal well

$$\int\limits_{y_1}^{y_2} (S_x S_y S_x) dy_0 = \frac{1}{abh} \left\{ \int\limits_{y_1}^{y_2} \left\{ \left\{ 2 \sum_{n=1}^{\infty} \sin \frac{n\pi x}{a} \sin \frac{n\pi x_0}{a} \exp\left[-\frac{n^2 \pi^2 k_x \tau}{\alpha a^2} \right] \right] \right\} \right\}$$

$$\left\{1 + 2\sum_{m=1}^{\infty} \cos\frac{m\pi y}{b} \cos\frac{m\pi y_0}{b} \exp\left[-\frac{m^2\pi^2 k_y\tau}{\alpha b^2}\right]\right\}$$

$$\left\{1 + 2\sum_{l=1}^{\infty} \cos\frac{l\pi z}{h} \cos\frac{l\pi z_0}{h} \exp\left[-\frac{l^2\pi^2 k_z\tau}{\alpha h^2}\right]\right\}\right\} dy_0\right\} \tag{A-6}$$

Rewriting Eq. A-6

$$\int_{y1}^{y2}\left(S_x S_y S_x\right) dy_0 = \frac{1}{abh}\left\{\left\{2\sum_{n=1}^{\infty} \sin\frac{n\pi x}{a} \sin\frac{n\pi x_0}{a} \exp\left[-\frac{n^2\pi^2 k_x\tau}{\alpha a^2}\right]\right\}\right.$$

$$\left\{1 + 2\sum_{l=1}^{\infty} \cos\frac{l\pi z}{h} \cos\frac{l\pi z_0}{h} \exp\left[-\frac{l^2\pi^2 k_z\tau}{\alpha h^2}\right]\right\}$$

$$\int_{y1}^{y2}\left\{1 + 2\sum_{m=1}^{\infty} \cos\frac{m\pi y}{b} \cos\frac{m\pi y_0}{b} \exp\left[-\frac{m^2\pi^2 k_y\tau}{\alpha b^2}\right]\right\} dy_0\right\} \tag{A-7}$$

Considering the integral term on the right hand side in Eq. A-7

$$\int_{y1}^{y2}\left\{1 + 2\sum_{m=1}^{\infty} \cos\frac{m\pi y}{b} \cos\frac{m\pi y_0}{b} \exp\left[-\frac{m^2\pi^2 k_y\tau}{\alpha b^2}\right]\right\} dy_0 =$$

$$y\Big|_{y1}^{y2} + 2\frac{b}{m\pi}\sum_{m=1}^{\infty} \cos\frac{m\pi y}{b}\left[\sin\frac{m\pi y_0}{b}\right]\exp\left[-\frac{m^2\pi^2 k_y\tau}{\alpha b^2}\right]\Bigg|_{y1}^{y2} \tag{A-8}$$

Eq. A-8 becomes

$$\int_{y1}^{y2}\left\{1 + 2\sum_{m=1}^{\infty} \cos\frac{m\pi y}{b} \cos\frac{m\pi y_0}{b} \exp\left[-\frac{m^2\pi^2 k_y\tau}{\alpha b^2}\right]\right\} dy_0 =$$

$$\left(y_2 - y_1\right) + \frac{2b}{\pi}\sum_{m=1}^{\infty} \frac{\cos\dfrac{m\pi y}{b}\left[\sin\dfrac{m\pi y_2}{b} - \sin\dfrac{m\pi y_1}{b}\right]}{m}\exp\left[-\frac{m^2\pi^2 k_y\tau}{\alpha b^2}\right] \tag{A-9}$$

We can rewritten Eq. A-7 as,

$$\int_{y_1}^{y_2}\left(S_x S_y S_x\right)dy_0 = \frac{1}{abh}\left\{\left\{2\sum_{n=1}^{\infty}\sin\frac{n\pi x}{a}\sin\frac{n\pi x_0}{a}\exp\left[-\frac{n^2\pi^2 k_x\tau}{\alpha a^2}\right]\right\}\right.$$

$$\left\{1+2\sum_{l=1}^{\infty}\cos\frac{l\pi z}{h}\cos\frac{l\pi z_0}{h}\exp\left[-\frac{l^2\pi^2 k_z\tau}{\alpha h^2}\right]\right\}$$

$$\left.\left\{(y_2-y_1)+\frac{2b}{\pi}\sum_{m=1}^{\infty}\frac{\cos\frac{m\pi y}{b}\left[\sin\frac{m\pi y_2}{b}-\sin\frac{m\pi y_1}{b}\right]}{m}\exp\left[-\frac{m^2\pi^2 k_y\tau}{\alpha b^2}\right]\right\}\right\}$$

$$\text{(A-10)}$$

Then, we multiply the right hand side of Eq. A-10

$$\int_{y_1}^{y_2}\left(S_x S_y S_x\right)dy_0 = \frac{1}{abh}\left\{2(y_2-y_1)\sum_{n=1}^{\infty}\sin\frac{n\pi x}{a}\sin\frac{n\pi x_0}{a}\exp\left[-\frac{n^2\pi^2 k_x\tau}{\alpha a^2}\right]\right.$$

$$+4(y_2-y_1)\sum_{l=1}^{\infty}\sum_{n=1}^{\infty}\sin\frac{n\pi x}{a}\sin\frac{n\pi x_0}{a}\cos\frac{l\pi z}{h}\cos\frac{l\pi z_0}{h}$$

$$\exp\left[-\left(\frac{\pi^2\tau}{\alpha}\right)\left(\frac{l^2 k_z}{h^2}+\frac{n^2 k_x}{a^2}\right)\right]$$

$$+\frac{4b}{\pi}\sum_{m=1}^{\infty}\sum_{n=1}^{\infty}\frac{\sin\frac{n\pi x}{a}\sin\frac{n\pi x_0}{a}\cos\frac{m\pi y}{b}\left(\sin\frac{m\pi y_2}{b}-\sin\frac{m\pi y_1}{b}\right)}{m}$$

$$\exp\left[-\left(\frac{\pi^2\tau}{\alpha}\right)\left(\frac{m^2 k_y}{b^2}+\frac{n^2 k_x}{a^2}\right)\right]$$

$$+\frac{8b}{\pi}\sum_{l=1}^{\infty}\sum_{m=1}^{\infty}\sum_{n=1}^{\infty}\frac{\sin\frac{n\pi x}{a}\sin\frac{n\pi x_0}{a}\cos\frac{l\pi z}{h}\cos\frac{l\pi z_0}{h}\cos\frac{m\pi y}{b}}{m}$$

$$\left.\left[\sin\frac{m\pi y_2}{b}-\sin\frac{m\pi y_1}{b}\right]\exp\left[-\left(\frac{\pi^2\tau}{\alpha}\right)\left(\frac{m^2 k_y}{b^2}+\frac{l^2 k_z}{h^2}+\frac{n^2 k_x}{a^2}\right)\right]\right\} \quad \text{(A-11)}$$

To obtain the continuous line source solution, we integrate over time interval

$$\int_0^t \int_{y_1}^{y_2} \left(S_x S_y S_x \right) dy_0 d\tau = \frac{1}{abh} \int_0^t \left\{ 2(y_2 - y_1) \sum_{n=1}^{\infty} \sin \frac{n\pi x}{a} \sin \frac{n\pi x_0}{a} \exp\left[-\frac{n^2 \pi^2 k_x \tau}{\alpha a^2} \right] \right. $$

$$+ 4(y_2 - y_1) \sum_{l=1}^{\infty} \sum_{n=1}^{\infty} \sin \frac{n\pi x}{a} \sin \frac{n\pi x_0}{a} \cos \frac{l\pi z}{h} \cos \frac{l\pi z_0}{h}$$

$$\exp\left[-\left(\frac{\pi^2 \tau}{\alpha} \right) \left(\frac{l^2 k_z}{h^2} + \frac{n^2 k_x}{a^2} \right) \right]$$

$$+ \frac{4b}{\pi} \sum_{m=1}^{\infty} \sum_{n=1}^{\infty} \frac{\sin \frac{n\pi x}{a} \sin \frac{n\pi x_0}{a} \cos \frac{m\pi y}{b} \left(\sin \frac{m\pi y_2}{b} - \sin \frac{m\pi y_1}{b} \right)}{m}$$

$$\exp\left[-\left(\frac{\pi^2 \tau}{\alpha} \right) \left(\frac{m^2 k_y}{b^2} + \frac{n^2 k_x}{a^2} \right) \right]$$

$$+ \frac{8b}{\pi} \sum_{l=1}^{\infty} \sum_{m=1}^{\infty} \sum_{n=1}^{\infty} \frac{\sin \frac{n\pi x}{a} \sin \frac{n\pi x_0}{a} \cos \frac{l\pi z}{h} \cos \frac{l\pi z_0}{h} \cos \frac{m\pi y}{b}}{m}$$

$$\left[\sin \frac{m\pi y_2}{b} - \sin \frac{m\pi y_1}{b} \right] \exp\left[-\left(\frac{\pi^2 \tau}{\alpha} \right) \left(\frac{m^2 k_y}{b^2} + \frac{l^2 k_z}{h^2} + \frac{n^2 k_x}{a^2} \right) \right] \right\} d\tau \quad \text{(A-12)}$$

After integrating Eq. A-12, we have

$$\int_0^t \int_{y_1}^{y_2} \left(S_x S_y S_x \right) dy_0 d\tau = \frac{1}{abh}$$

$$\left\{ -\frac{2\alpha a^2 (y_2 - y_1)}{\pi^2 k_x} \sum_{n=1}^{\infty} \frac{\sin \frac{n\pi x}{a} \sin \frac{n\pi x_0}{a}}{n^2} \exp\left[-\frac{n^2 \pi^2 k_x \tau}{\alpha a^2} \right] \right|_0^t$$

$$-\frac{4\alpha (y_2 - y_1)}{\pi^2} \sum_{l=1}^{\infty} \sum_{n=1}^{\infty} \frac{\sin \frac{n\pi x}{a} \sin \frac{n\pi x_0}{a} \cos \frac{l\pi z}{h} \cos \frac{l\pi z_0}{h}}{\left(\frac{l^2 k_z}{h^2} + \frac{n^2 k_x}{a^2} \right)}$$

$$exp\left[-\left(\frac{\pi^2\tau}{\alpha}\right)\left(\frac{l^2k_z}{h^2}+\frac{n^2k_x}{a^2}\right)\right]\Bigg|_0^t$$

$$-\frac{4\alpha b}{\pi^3}\sum_{m=1}^{\infty}\sum_{n=1}^{\infty}\frac{\sin\dfrac{n\pi x}{a}\sin\dfrac{n\pi x_0}{a}\cos\dfrac{l\pi y}{b}\left(\sin\dfrac{m\pi y_2}{b}-\sin\dfrac{m\pi y_1}{b}\right)}{m\left(\dfrac{m^2k_y}{b^2}+\dfrac{n^2k_x}{a^2}\right)}$$

$$exp\left[-\left(\frac{\pi^2\tau}{\alpha}\right)\left(\frac{m^2k_y}{b^2}+\frac{n^2k_x}{a^2}\right)\right]\Bigg|_0^t$$

$$-\frac{8\alpha b}{\pi^3}\sum_{l=1}^{\infty}\sum_{m=1}^{\infty}\sum_{n=1}^{\infty}\frac{\sin\dfrac{n\pi x}{a}\sin\dfrac{n\pi x_0}{a}\cos\dfrac{l\pi z}{h}\cos\dfrac{l\pi z_0}{h}\cos\dfrac{m\pi y}{b}}{m\left(\dfrac{m^2k_y}{b^2}+\dfrac{l^2k_z}{h^2}+\dfrac{n^2k_x}{a^2}\right)}$$

$$\left.\left[\sin\frac{m\pi y_2}{b}-\sin\frac{m\pi y_1}{b}\right]exp\left[-\left(\frac{\pi^2\tau}{\alpha}\right)\left(\frac{m^2k_y}{b^2}+\frac{l^2k_z}{h^2}+\frac{n^2k_x}{a^2}\right)\right]\Bigg|_0^t\right\}\qquad\text{(A-13)}$$

Eq. A-13 can be written as

$$\int_0^t\int_{y_1}^{y_2}\left(S_xS_yS_x\right)dy_0\,d\tau=\frac{1}{abh}\left\{\frac{2\alpha a^2\left(y_2-y_1\right)}{\pi^2 k_x}\frac{\sum\limits_{n=1}^{\infty}\sin\dfrac{n\pi x}{a}\sin\dfrac{n\pi x_0}{a}}{n^2}\right.$$

$$\left(1-exp\left[-\frac{n^2\pi^2k_x\tau}{\alpha a^2}\right]\right)$$

$$+\frac{4\alpha\left(y_2-y_1\right)}{\pi^2}\sum_{l=1}^{\infty}\sum_{n=1}^{\infty}\frac{\sin\dfrac{n\pi x}{a}\sin\dfrac{n\pi x_0}{a}\cos\dfrac{l\pi z}{h}\cos\dfrac{l\pi z_0}{h}}{\left(\dfrac{l^2k_z}{h^2}+\dfrac{n^2k_x}{a^2}\right)}$$

$$\left(1-exp\left[-\left(\frac{\pi^2\tau}{\alpha}\right)\left(\frac{l^2k_z}{h^2}+\frac{n^2k_x}{a^2}\right)\right]\right)$$

$$+\frac{4\alpha b}{\pi^3}\sum_{m=1}^{\infty}\sum_{n=1}^{\infty}\frac{\sin\dfrac{n\pi x}{a}\sin\dfrac{n\pi x_0}{a}\cos\dfrac{m\pi y}{b}\left(\sin\dfrac{m\pi y_2}{b}-\sin\dfrac{m\pi y_1}{b}\right)}{m\left(\dfrac{m^2 k_y}{b^2}+\dfrac{n^2 k_x}{a^2}\right)}$$

$$\left(1-exp\left[-\left(\frac{\pi^2\tau}{\alpha}\right)\left(\frac{m^2 k_y}{b^2}+\frac{n^2 k_x}{a^2}\right)\right]\right)$$

$$+\frac{8\alpha b}{\pi^3}\sum_{l=1}^{\infty}\sum_{m=1}^{\infty}\sum_{n=1}^{\infty}\frac{\sin\dfrac{n\pi x}{a}\sin\dfrac{n\pi x_0}{a}\cos\dfrac{l\pi z}{h}\cos\dfrac{l\pi z_0}{h}\cos\dfrac{m\pi y}{b}}{m\left(\dfrac{m^2 k_y}{b^2}+\dfrac{l^2 k_z}{h^2}+\dfrac{n^2 k_x}{a^2}\right)}$$

$$\left[\sin\frac{m\pi y_2}{b}-\sin\frac{m\pi y_1}{b}\right]\left[1-exp\left[-\left(\frac{\pi^2\tau}{\alpha}\right)\left(\frac{m^2 k_y}{b^2}+\frac{l^2 k_z}{h^2}+\frac{n^2 k_x}{a^2}\right)\right]\right]\Bigg\}\quad\text{(A-14)}$$

Substituting Eq. A-14 into Eq. A-1 gives

$$p_{init}-p(x,y,z,t)=\left[\frac{B_o\mu_o q_o}{abhL\alpha}\right]\left\{\frac{2\alpha a^2(y_2-y_1)}{\pi^2 k_x}\frac{\sum_{n=1}^{\infty}\sin\dfrac{n\pi x}{a}\sin\dfrac{n\pi x_0}{a}}{n^2}\right.$$

$$\left(1-exp\left[-\frac{n^2\pi^2 k_x\tau}{\alpha a^2}\right]\right)$$

$$+\frac{4\alpha(y_2-y_1)}{\pi^2}\sum_{l=1}^{\infty}\sum_{n=1}^{\infty}\frac{\sin\dfrac{n\pi x}{a}\sin\dfrac{n\pi x_0}{a}\cos\dfrac{l\pi z}{h}\cos\dfrac{l\pi z_0}{h}}{\left(\dfrac{l^2 k_z}{h^2}+\dfrac{n^2 k_x}{a^2}\right)}$$

$$\left(1-exp\left[-\left(\frac{\pi^2\tau}{\alpha}\right)\left(\frac{l^2 k_z}{h^2}+\frac{n^2 k_x}{a^2}\right)\right]\right)$$

$$
+ \frac{4\alpha b}{\pi^3} \sum_{m=1}^{\infty} \sum_{n=1}^{\infty} \frac{\sin \frac{n\pi x}{a} \sin \frac{n\pi x_0}{a} \cos \frac{m\pi y}{b} \left(\sin \frac{m\pi y_2}{b} - \sin \frac{m\pi y_1}{b} \right)}{m \left(\frac{m^2 k_y}{b^2} + \frac{n^2 k_x}{a^2} \right)}
$$

$$
\left(1 - \exp\left[-\left(\frac{\pi^2 \tau}{\alpha} \right) \left(\frac{m^2 k_y}{b^2} + \frac{n^2 k_x}{a^2} \right) \right] \right)
$$

$$
+ \frac{8\alpha b}{\pi^3} \sum_{l=1}^{\infty} \sum_{m=1}^{\infty} \sum_{n=1}^{\infty} \frac{\sin \frac{n\pi x}{a} \sin \frac{n\pi x_0}{a} \cos \frac{l\pi z}{h} \cos \frac{l\pi z_0}{h} \cos \frac{m\pi y}{b}}{m \left(\frac{m^2 k_y}{b^2} + \frac{l^2 k_z}{h^2} + \frac{n^2 k_x}{a^2} \right)}
$$

$$
\left[\sin \frac{m\pi y_2}{b} - \sin \frac{m\pi y_1}{b} \right] \left[1 - \exp\left[-\left(\frac{\pi^2 \tau}{\alpha} \right) \left(\frac{m^2 k_y}{b^2} + \frac{l^2 k_z}{h^2} + \frac{n^2 k_x}{a^2} \right) \right] \right] \right\} \quad \text{(A-15)}
$$

Eq. A-15 can be used to evaluate the flow performance of a fully or partially penetrating horizontal well under steady-state condition with uniform flux, q, along the well. At late time, the exponential term becomes zero. We rewrite Eq. A-15 as

$$
p_{init} - p(x,y,z,t) = \left[\frac{B_o \mu_o q_o}{abhL\alpha} \right] \left\{ \frac{2\alpha a^2 (y_2 - y_1)}{\pi^2 k_x} \sum_{n=1}^{\infty} \frac{\sin \frac{n\pi x}{a} \sin \frac{n\pi x_0}{a}}{n^2} \right.
$$

$$
+ \frac{4\alpha(y_2 - y_1)}{\pi^2} \sum_{l=1}^{\infty} \sum_{n=1}^{\infty} \frac{\sin \frac{n\pi x}{a} \sin \frac{n\pi x_0}{a} \cos \frac{l\pi z}{h} \cos \frac{l\pi z_0}{h}}{\left(\frac{l^2 k_z}{h^2} + \frac{n^2 k_x}{a^2} \right)}
$$

$$
+ \frac{4\alpha b}{\pi^3} \sum_{m=1}^{\infty} \sum_{n=1}^{\infty} \frac{\sin \frac{n\pi x}{a} \sin \frac{n\pi x_0}{a} \cos \frac{m\pi y}{b} \left(\sin \frac{m\pi y_2}{b} - \sin \frac{m\pi y_1}{b} \right)}{m \left(\frac{m^2 k_y}{b^2} + \frac{n^2 k_x}{a^2} \right)}
$$

$$+\frac{8\alpha b}{\pi^3}\sum_{l=1}^{\infty}\sum_{m=1}^{\infty}\sum_{n=1}^{\infty}\frac{\sin\dfrac{n\pi x}{a}\sin\dfrac{n\pi x_0}{a}\cos\dfrac{l\pi z}{h}\cos\dfrac{l\pi z_0}{h}\cos\dfrac{m\pi y}{b}}{m\left(\dfrac{m^2 k_y}{b^2}+\dfrac{l^2 k_z}{h^2}+\dfrac{n^2 k_x}{a^2}\right)}$$

$$\left[\sin\frac{m\pi y_2}{b}-\sin\frac{m\pi y_1}{b}\right]\Bigg\}$$

(A-16)

For a fully penetrated well, the third and the finally terms on the right hand side of Eq. A-16 becomes zero. Therefore, a fully penetrating horizontal well can be presented as,

$$p_{init}-p(x,y,z,t)=\left[\frac{B_o\mu_o q_o}{abhL\alpha}\right]\Bigg\{\frac{2\alpha a^2(y_2-y_1)}{\pi^2 k_x}\sum_{n=1}^{\infty}\frac{\sin\dfrac{n\pi x}{a}\sin\dfrac{n\pi x_0}{a}}{n^2}$$

$$+\frac{4\alpha(y_2-y_1)}{\pi^2}\sum_{l=1}^{\infty}\sum_{n=1}^{\infty}\frac{\sin\dfrac{n\pi x}{a}\sin\dfrac{n\pi x_0}{a}\cos\dfrac{l\pi z}{h}\cos\dfrac{l\pi z_0}{h}}{\left(\dfrac{l^2 k_z}{h^2}+\dfrac{n^2 k_x}{a^2}\right)}$$

(A-17)

APPENDIX B

PSEUDOSTEADY STATE HORIZONTAL WELL MODEL

In this appendix, we derive the horizontal well performance under pseudosteady state condition. The model is introduced by Babu and Odeh in 1989 based on the use of the instantaneous Green's function. This model is available for a single-phase and incompressible fluid in a box-shaped reservoir and the well is parallel to the Y-axis. The location of the well can be anywhere in the homogenous reservoir. The reservoir can be either an isotropic or an anisotropic reservoir.

The line source represents the wellbore located parallel to the Y-axis. The heel of the well locates at (x_0, y_1, z_0) and the toe of the well locates at (x_0, y_2, z_0). The pressure drop as a result of a constant production into the well is calculated by Eq. B-1.

$$p_{init} - p(x,y,z,t) = \left[\frac{B_o \mu_o q_o}{L\alpha}\right] \int_0^t \int_{y_1}^{y_2} \left(S_x S_y S_z\right) dy_0 d\tau \tag{B-1}$$

where

$$S_x = S(x,x_0,\tau) = \frac{1}{a}\left(1 + 2\sum_{n=1}^{\infty} \cos\frac{n\pi x}{a}\cos\frac{n\pi x_0}{a}\exp\left[-\frac{n^2\pi^2 k_x \tau}{\alpha a^2}\right]\right) \tag{B-2}$$

$$S_y = S(y,y_0,\tau) = \frac{1}{b}\left(1 + 2\sum_{m=1}^{\infty} \cos\frac{m\pi y}{b}\cos\frac{m\pi y_0}{b}\exp\left[-\frac{m^2\pi^2 k_y \tau}{\alpha b^2}\right]\right) \tag{B-3}$$

$$S_z = S(z,z_0,\tau) = \frac{1}{h}\left(1 + 2\sum_{l=1}^{\infty} \cos\frac{l\pi z}{h}\cos\frac{l\pi z_0}{h}\exp\left[-\frac{l^2\pi^2 k_z \tau}{\alpha h^2}\right]\right) \tag{B-4}$$

$$\alpha = \phi\mu c_t \tag{B-5}$$

First, we start from integrate along a horizontal well from y_1 to y_2.

$$\int_{y_1}^{y_2}\left(S_x S_y S_x\right) dy_0 = \frac{1}{abh}\left\{\int_{y_1}^{y_2}\left\{\left\{1 + 2\sum_{n=1}^{\infty}\cos\frac{n\pi x}{a}\cos\frac{n\pi x_0}{a}\exp\left[-\frac{n^2\pi^2 k_x \tau}{\alpha a^2}\right]\right\}\right.\right.$$

$$\left\{1+2\sum_{m=1}^{\infty}\cos\frac{m\pi y}{b}\cos\frac{m\pi y_0}{b}\exp\left[-\frac{m^2\pi^2 k_y\tau}{\alpha b^2}\right]\right\}$$

$$\left\{1+2\sum_{l=1}^{\infty}\cos\frac{l\pi z}{h}\cos\frac{l\pi z_0}{h}\exp\left[-\frac{l^2\pi^2 k_z\tau}{\alpha h^2}\right]\right\}\right\}dy_0\right\} \tag{B-6}$$

Rewriting Eq. B-6, we have

$$\int_{y1}^{y2}\left(S_x S_y S_x\right)dy_0 = \frac{1}{abh}\left\{\left\{1+2\sum_{n=1}^{\infty}\cos\frac{n\pi x}{a}\cos\frac{n\pi x_0}{a}\exp\left[-\frac{n^2\pi^2 k_x\tau}{\alpha a^2}\right]\right\}\right.$$

$$\left\{1+2\sum_{l=1}^{\infty}\cos\frac{l\pi z}{h}\cos\frac{l\pi z_0}{h}\exp\left[-\frac{l^2\pi^2 k_z\tau}{\alpha h^2}\right]\right\}$$

$$\int_{y1}^{y2}\left\{1+2\sum_{m=1}^{\infty}\cos\frac{m\pi y}{b}\cos\frac{m\pi y_0}{b}\exp\left[-\frac{m^2\pi^2 k_y\tau}{\alpha b^2}\right]\right\}dy_0\right\} \tag{B-7}$$

Considering the integral term on the right hand side of Eq. B-7

$$\int_{y1}^{y2}\left\{1+2\sum_{m=1}^{\infty}\cos\frac{m\pi y}{b}\cos\frac{m\pi y_0}{b}\exp\left[-\frac{m^2\pi^2 k_y\tau}{\alpha b^2}\right]\right\}dy_0 =$$

$$y\Big|_{y1}^{y2} +2\frac{b}{m\pi}\sum_{m=1}^{\infty}\cos\frac{m\pi y}{b}\left[\sin\frac{m\pi y_0}{b}\right]\exp\left[-\frac{m^2\pi^2 k_y\tau}{\alpha b^2}\right]\Bigg|_{y1}^{y2} \tag{B-8}$$

Rewriting Eq. B-8 as

$$\int_{y1}^{y2}\left\{1+2\sum_{m=1}^{\infty}\cos\frac{m\pi y}{b}\cos\frac{m\pi y_0}{b}\exp\left[-\frac{m^2\pi^2 k_y\tau}{\alpha b^2}\right]\right\}dy_0 =$$

$$\left(y_2 - y_1\right)+\frac{2b}{\pi}\sum_{m=1}^{\infty}\frac{\cos\frac{m\pi y}{b}\left[\sin\frac{m\pi y_2}{b} - \sin\frac{m\pi y_1}{b}\right]}{m}\exp\left[-\frac{m^2\pi^2 k_y\tau}{\alpha b^2}\right] \tag{B-9}$$

Substituting Eq. B-9 into Eq. B-6

$$\int_{y1}^{y2}\left(S_x S_y S_x\right)dy_0 = \frac{1}{abh}\left\{\left\{1+2\sum_{n=1}^{\infty}\cos\frac{n\pi x}{a}\cos\frac{n\pi x_0}{a}\exp\left[-\frac{n^2\pi^2 k_x\tau}{\alpha a^2}\right]\right\}\right.$$

$$\left\{1+2\sum_{l=1}^{\infty}\cos\frac{l\pi z}{h}\cos\frac{l\pi z_0}{h}\exp\left[-\frac{l^2\pi^2 k_z\tau}{\alpha h^2}\right]\right\}$$

$$\left.\left\{(y_2-y_1)+\frac{2b}{\pi}\sum_{m=1}^{\infty}\frac{\cos\frac{m\pi y}{b}\left[\sin\frac{m\pi y_2}{b}-\sin\frac{m\pi y_1}{b}\right]}{m}\exp\left[-\frac{m^2\pi^2 k_y\tau}{\alpha b^2}\right]\right\}\right\}$$

(B-10)

Then, we multiply the right hand side of Eq. B-10

$$\int_{y1}^{y2}\left(S_x S_y S_x\right)dy_0 = \frac{1}{abh}\left\{(y_2-y_1)+2(y_2-y_1)\sum_{l=1}^{\infty}\cos\frac{l\pi z}{h}\cos\frac{l\pi z_0}{h}\exp\left[-\frac{l^2\pi^2 k_z\tau}{\alpha h^2}\right]\right.$$

$$+\frac{2b}{\pi}\sum_{m=1}^{\infty}\frac{\cos\frac{m\pi y}{b}\left[\sin\frac{m\pi y_2}{b}-\sin\frac{m\pi y_1}{b}\right]}{m}\exp\left[-\frac{m^2\pi^2 k_y\tau}{\alpha b^2}\right]$$

$$+\frac{4b}{\pi}\sum_{m=1}^{\infty}\sum_{l=1}^{\infty}\frac{\cos\frac{l\pi z}{h}\cos\frac{l\pi z_0}{h}\cos\frac{m\pi y}{b}}{m}$$

$$\left[\sin\frac{m\pi y_2}{b}-\sin\frac{m\pi y_1}{b}\right]\exp\left[-\frac{m^2\pi^2 k_y\tau}{\alpha b^2}-\frac{l^2\pi^2 k_z\tau}{\alpha h^2}\right]$$

$$+2(y_2-y_1)\sum_{n=1}^{\infty}\cos\frac{n\pi x}{a}\cos\frac{n\pi x_0}{a}\exp\left[-\frac{n^2\pi^2 k_x\tau}{\alpha a^2}\right]$$

$$+4(y_2-y_1)\sum_{l=1}^{\infty}\sum_{n=1}^{\infty}\cos\frac{n\pi x}{a}\cos\frac{n\pi x_0}{a}\cos\frac{l\pi z}{h}\cos\frac{l\pi z_0}{h}$$

$$\exp\left[-\frac{l^2\pi^2 k_z\tau}{\alpha h^2}-\frac{n^2\pi^2 k_x\tau}{\alpha a^2}\right]$$

$$+\frac{4b}{\pi}\sum_{m=1}^{\infty}\sum_{n=1}^{\infty}\frac{\cos\dfrac{n\pi x}{a}\cos\dfrac{n\pi x_0}{a}\cos\dfrac{m\pi y}{b}}{m}$$

$$\left[\sin\frac{m\pi y_2}{b}-\sin\frac{m\pi y_1}{b}\right]\exp\left[-\frac{m^2\pi^2 k_y\tau}{\alpha b^2}-\frac{n^2\pi^2 k_x\tau}{\alpha a^2}\right]$$

$$+\frac{8b}{\pi}\sum_{l=1}^{\infty}\sum_{m=1}^{\infty}\sum_{n=1}^{\infty}\frac{\cos\dfrac{n\pi x}{a}\cos\dfrac{n\pi x_0}{a}\cos\dfrac{l\pi z}{h}\cos\dfrac{l\pi z_0}{h}\cos\dfrac{m\pi y}{b}}{m}$$

$$\left[\sin\frac{m\pi y_2}{b}-\sin\frac{m\pi y_1}{b}\right]\exp\left[-\frac{m^2\pi^2 k_y\tau}{\alpha b^2}-\frac{l^2\pi^2 k_z\tau}{\alpha h^2}-\frac{n^2\pi^2 k_x\tau}{\alpha a^2}\right]\Bigg\}\qquad\text{(B-11)}$$

To obtain the continuous line source solution, we integrate over the time interval.

$$\int_0^t\int_{y_1}^{y_2}\left(S_x S_y S_x\right)dy_0\,d\tau=\frac{1}{abh}\left\{\int_0^t\left\{(y_2-y_1)\right.\right.$$

$$+2(y_2-y_1)\sum_{l=1}^{\infty}\cos\frac{l\pi z}{h}\cos\frac{l\pi z_0}{h}\exp\left[-\frac{l^2\pi^2 k_z\tau}{\alpha h^2}\right]$$

$$+\frac{2b}{\pi}\sum_{m=1}^{\infty}\frac{\cos\dfrac{m\pi y}{b}\left[\sin\dfrac{m\pi y_2}{b}-\sin\dfrac{m\pi y_1}{b}\right]}{m}\exp\left[-\frac{m^2\pi^2 k_y\tau}{\alpha b^2}\right]$$

$$+\frac{4b}{\pi}\sum_{m=1}^{\infty}\sum_{l=1}^{\infty}\frac{\cos\dfrac{l\pi z}{h}\cos\dfrac{l\pi z_0}{h}\cos\dfrac{m\pi y}{b}}{m}$$

$$\left[\sin\frac{m\pi y_2}{b}-\sin\frac{m\pi y_1}{b}\right]\exp\left[-\frac{m^2\pi^2 k_y\tau}{\alpha b^2}-\frac{l^2\pi^2 k_z\tau}{\alpha h^2}\right]$$

$$+2(y_2-y_1)\sum_{n=1}^{\infty}\cos\frac{n\pi x}{a}\cos\frac{n\pi x_0}{a}\exp\left[-\frac{n^2\pi^2 k_x\tau}{\alpha a^2}\right]$$

$$\exp\left[-\frac{l^2\pi^2 k_z\tau}{\alpha h^2}-\frac{n^2\pi^2 k_x\tau}{\alpha a^2}\right]$$

$$+\frac{4b}{\pi}\sum_{m=1}^{\infty}\sum_{n=1}^{\infty}\frac{\cos\dfrac{n\pi x}{a}\cos\dfrac{n\pi x_0}{a}\cos\dfrac{m\pi y}{b}}{m}$$

$$\left[\sin\frac{m\pi y_2}{b}-\sin\frac{m\pi y_1}{b}\right]\exp\left[-\frac{m^2\pi^2 k_y\tau}{\alpha b^2}-\frac{n^2\pi^2 k_x\tau}{\alpha a^2}\right]$$

$$+\frac{8b}{\pi}\sum_{l=1}^{\infty}\sum_{m=1}^{\infty}\sum_{n=1}^{\infty}\frac{\cos\dfrac{n\pi x}{a}\cos\dfrac{n\pi x_0}{a}\cos\dfrac{l\pi z}{h}\cos\dfrac{l\pi z_0}{h}\cos\dfrac{m\pi y}{b}}{m}$$

$$\left.\left[\sin\frac{m\pi y_2}{b}-\sin\frac{m\pi y_1}{b}\right]\exp\left[-\frac{m^2\pi^2 k_y\tau}{\alpha b^2}-\frac{l^2\pi^2 k_z\tau}{\alpha h^2}-\frac{n^2\pi^2 k_x\tau}{\alpha a^2}\right]\right]\right\}d\tau\right\}$$

(B-12)

Rewriting Eq. B-12

$$\int_0^t\int_{y_1}^{y_2}(S_xS_yS_x)dy_0\,d\tau=\frac{1}{abh}\left\{(y_2-y_1)\tau\Big|_0^t\right.$$

$$-\frac{2\alpha h^2(y_2-y_1)}{\pi^2 k_z}\sum_{l=1}^{\infty}\frac{\cos\dfrac{l\pi z}{h}\cos\dfrac{l\pi z_0}{h}}{l^2}\exp\left[-\frac{l^2\pi^2 k_z\tau}{\alpha h^2}\right]\Bigg|_0^t$$

$$-\frac{2\alpha b^3}{\pi^3 k_y}\sum_{m=1}^{\infty}\frac{\cos\dfrac{m\pi y}{b}\left[\sin\dfrac{m\pi y_2}{b}-\sin\dfrac{m\pi y_1}{b}\right]}{m^3}\exp\left[-\frac{m^2\pi^2 k_y\tau}{\alpha b^2}\right]\Bigg|_0^t$$

$$-\frac{4b\alpha}{\pi^3}\sum_{m=1}^{\infty}\sum_{l=1}^{\infty}\frac{\cos\dfrac{l\pi z}{h}\cos\dfrac{l\pi z_0}{h}\cos\dfrac{m\pi y}{b}}{m\left(\dfrac{m^2 k_y}{b^2}+\dfrac{l^2 k_z}{h^2}\right)}$$

$$\left.\left[\sin\frac{m\pi y_2}{b}-\sin\frac{m\pi y_1}{b}\right]\exp\left[-\frac{\pi^2\tau}{\alpha}\left(\frac{m^2 k_y}{b^2}+\frac{l^2 k_z}{h^2}\right)\right]\right|_0^t$$

$$-\frac{2\alpha a^2\left(y_2-y_1\right)}{\pi^2 k_x}\sum_{n=1}^{\infty}\frac{\cos\dfrac{n\pi x}{a}\cos\dfrac{n\pi x_0}{a}}{n^2}\,exp\left[-\frac{n^2\pi^2 k_x\tau}{\alpha a^2}\right]\Bigg|_0^t$$

$$-\frac{4\alpha\left(y_2-y_1\right)}{\pi^2}\sum_{l=1}^{\infty}\sum_{n=1}^{\infty}\frac{\cos\dfrac{n\pi x}{a}\cos\dfrac{n\pi x_0}{a}\cos\dfrac{l\pi z}{h}\cos\dfrac{l\pi z_0}{h}}{\left(\dfrac{l^2 k_z}{h^2}+\dfrac{n^2 k_x}{a^2}\right)}$$

$$exp\left[-\frac{\pi^2\tau}{\alpha}\left(\frac{l^2 k_z}{h^2}+\frac{n^2 k_x}{a^2}\right)\right]\Bigg|_0^t$$

$$-\frac{4b\alpha}{\pi^3}\sum_{m=1}^{\infty}\sum_{n=1}^{\infty}\frac{\cos\dfrac{n\pi x}{a}\cos\dfrac{n\pi x_0}{a}\cos\dfrac{m\pi y}{b}}{m\left(\dfrac{m^2 k_y}{b^2}+\dfrac{n^2 k_x}{a^2}\right)}$$

$$\left[\sin\frac{m\pi y_2}{b}-\sin\frac{m\pi y_1}{b}\right]exp\left[-\frac{\pi^2\tau}{\alpha}\left(\frac{m^2 k_y}{b^2}+\frac{n^2 k_x}{a^2}\right)\right]\Bigg|_0^t$$

$$-\frac{8b\alpha}{\pi^3}\sum_{l=1}^{\infty}\sum_{m=1}^{\infty}\sum_{n=1}^{\infty}\frac{\cos\dfrac{n\pi x}{a}\cos\dfrac{n\pi x_0}{a}\cos\dfrac{l\pi z}{h}\cos\dfrac{l\pi z_0}{h}\cos\dfrac{m\pi y}{b}}{m\left(\dfrac{m^2 k_y}{b^2}+\dfrac{l^2 k_z}{h^2}+\dfrac{n^2 k_x}{a^2}\right)}$$

$$\left[\sin\frac{m\pi y_2}{b}-\sin\frac{m\pi y_1}{b}\right]exp\left[-\frac{\pi^2\tau}{\alpha}\left(\frac{m^2 k_y}{b^2}+\frac{l^2 k_z}{h^2}+\frac{n^2 k_x}{a^2}\right)\right]\Bigg|_0^t\Bigg\} \qquad (B\text{-}13)$$

Eq. B-13 becomes

$$\int_0^t\int_{y_1}^{y_2}\left(S_x S_y S_x\right)dy_0 d\tau=\frac{1}{abh}\Big\{\left(y_2-y_1\right)t$$

$$+\frac{2\alpha h^2\left(y_2-y_1\right)}{\pi^2 k_z}\sum_{l=1}^{\infty}\frac{\cos\dfrac{l\pi z}{h}\cos\dfrac{l\pi z_0}{h}}{l^2}\left(1-exp\left[-\frac{l^2\pi^2 k_z\tau}{\alpha h^2}\right]\right)$$

$$+\frac{2\alpha b^3}{\pi^3 k_y}\sum_{m=1}^{\infty}\frac{\cos\dfrac{m\pi y}{b}\left[\sin\dfrac{m\pi y_2}{b}-\sin\dfrac{m\pi y_1}{b}\right]}{m^3}\left(1-exp\left[-\frac{m^2\pi^2 k_y\tau}{\alpha b^2}\right]\right)$$

$$+\frac{4b\alpha}{\pi^3}\sum_{m=1}^{\infty}\sum_{l=1}^{\infty}\frac{\cos\dfrac{l\pi z}{h}\cos\dfrac{l\pi z_0}{h}\cos\dfrac{m\pi y}{b}}{m\left(\dfrac{m^2 k_y}{b^2}+\dfrac{l^2 k_z}{h^2}\right)}$$

$$\left[\sin\frac{m\pi y_2}{b}-\sin\frac{m\pi y_1}{b}\right]\left(1-exp\left[-\frac{\pi^2\tau}{\alpha}\left(\frac{m^2 k_y}{b^2}+\frac{l^2 k_z}{h^2}\right)\right]\right)$$

$$+\frac{2\alpha a^2(y_2-y_1)}{\pi^2 k_x}\sum_{n=1}^{\infty}\frac{\cos\dfrac{n\pi x}{a}\cos\dfrac{n\pi x_0}{a}}{n^2}\left(1-exp\left[-\frac{n^2\pi^2 k_x\tau}{\alpha a^2}\right]\right)$$

$$+\frac{4\alpha(y_2-y_1)}{\pi^2}\sum_{l=1}^{\infty}\sum_{n=1}^{\infty}\frac{\cos\dfrac{n\pi x}{a}\cos\dfrac{n\pi x_0}{a}\cos\dfrac{l\pi z}{h}\cos\dfrac{l\pi z_0}{h}}{\left(\dfrac{l^2 k_z}{h^2}+\dfrac{n^2 k_x}{a^2}\right)}$$

$$\left(1-exp\left[-\frac{\pi^2\tau}{\alpha}\left(\frac{l^2 k_z}{h^2}+\frac{n^2 k_x}{a^2}\right)\right]\right)$$

$$+\frac{4b\alpha}{\pi^3}\sum_{m=1}^{\infty}\sum_{n=1}^{\infty}\frac{\cos\dfrac{n\pi x}{a}\cos\dfrac{n\pi x_0}{a}\cos\dfrac{m\pi y}{b}}{m\left(\dfrac{m^2 k_y}{b^2}+\dfrac{n^2 k_x}{a^2}\right)}$$

$$\left[\sin\frac{m\pi y_2}{b}-\sin\frac{m\pi y_1}{b}\right]\left(1-exp\left[-\frac{\pi^2\tau}{\alpha}\left(\frac{m^2 k_y}{b^2}+\frac{n^2 k_x}{a^2}\right)\right]\right)$$

$$+\frac{8b\alpha}{\pi^3}\sum_{l=1}^{\infty}\sum_{m=1}^{\infty}\sum_{n=1}^{\infty}\frac{\cos\dfrac{n\pi x}{a}\cos\dfrac{n\pi x_0}{a}\cos\dfrac{l\pi z}{h}\cos\dfrac{l\pi z_0}{h}\cos\dfrac{m\pi y}{b}}{m\left(\dfrac{m^2 k_y}{b^2}+\dfrac{l^2 k_z}{h^2}+\dfrac{n^2 k_x}{a^2}\right)}$$

$$\left[\sin\frac{m\pi y_2}{b}-\sin\frac{m\pi y_1}{b}\right]\left(1-exp\left[-\frac{\pi^2\tau}{\alpha}\left(\frac{m^2 k_y}{b^2}+\frac{l^2 k_z}{h^2}+\frac{n^2 k_x}{a^2}\right)\right]\right)\right\} \quad \text{(B-14)}$$

Since $(y_2-y_1)=L$ and we can substitute equation (B-14) into equation (B-1), we rewritten equation (B-1) as,

$$p_{init}-p(x,y,z,t)=\left[\frac{B_o\mu_o q_o}{abh\alpha}\right]$$

$$\left\{t+\frac{2\alpha h^2}{\pi^2 k_z}\sum_{l=1}^{\infty}\frac{\cos\frac{l\pi z}{h}\cos\frac{l\pi z_0}{h}}{l^2}\left(1-exp\left[-\frac{l^2\pi^2 k_z\tau}{\alpha h^2}\right]\right)\right.$$

$$+\frac{2\alpha b^3}{\pi^3 k_y(y_2-y_1)}\sum_{m=1}^{\infty}\frac{\cos\frac{m\pi y}{b}\left[\sin\frac{m\pi y_2}{b}-\sin\frac{m\pi y_1}{b}\right]}{m^3}\left(1-exp\left[-\frac{m^2\pi^2 k_y\tau}{\alpha b^2}\right]\right)$$

$$+\frac{4b\alpha}{\pi^3(y_2-y_1)}\sum_{m=1}^{\infty}\sum_{l=1}^{\infty}\frac{\cos\frac{l\pi z}{h}\cos\frac{l\pi z_0}{h}\cos\frac{m\pi y}{b}}{m\left(\frac{m^2 k_y}{b^2}+\frac{l^2 k_z}{h^2}\right)}$$

$$\left[\sin\frac{m\pi y_2}{b}-\sin\frac{m\pi y_1}{b}\right]\left(1-exp\left[-\frac{\pi^2\tau}{\alpha}\left(\frac{m^2 k_y}{b^2}+\frac{l^2 k_z}{h^2}\right)\right]\right)$$

$$+\frac{2\alpha a^2}{\pi^2 k_x}\sum_{n=1}^{\infty}\frac{\cos\frac{n\pi x}{a}\cos\frac{n\pi x_0}{a}}{n^2}\left(1-exp\left[-\frac{n^2\pi^2 k_x\tau}{\alpha a^2}\right]\right)$$

$$+\frac{4\alpha}{\pi^2}\sum_{l=1}^{\infty}\sum_{n=1}^{\infty}\frac{\cos\frac{n\pi x}{a}\cos\frac{n\pi x_0}{a}\cos\frac{l\pi z}{h}\cos\frac{l\pi z_0}{h}}{\left(\frac{l^2 k_z}{h^2}+\frac{n^2 k_x}{a^2}\right)}$$

$$\left(1-exp\left[-\frac{\pi^2\tau}{\alpha}\left(\frac{l^2 k_z}{h^2}+\frac{n^2 k_x}{a^2}\right)\right]\right)$$

$$+\frac{4b\alpha}{\pi^3\left(y_2-y_1\right)}\sum_{m=1}^{\infty}\sum_{n=1}^{\infty}\frac{\cos\dfrac{n\pi x}{a}\cos\dfrac{n\pi x_0}{a}\cos\dfrac{m\pi y}{b}}{m\left(\dfrac{m^2 k_y}{b^2}+\dfrac{n^2 k_x}{a^2}\right)}$$

$$\left[\sin\frac{m\pi y_2}{b}-\sin\frac{m\pi y_1}{b}\right]\left(1-\exp\left[-\frac{\pi^2\tau}{\alpha}\left(\frac{m^2 k_y}{b^2}+\frac{n^2 k_x}{a^2}\right)\right]\right)$$

$$+\frac{8b\alpha}{\pi^3\left(y_2-y_1\right)}\sum_{l=1}^{\infty}\sum_{m=1}^{\infty}\sum_{n=1}^{\infty}\frac{\cos\dfrac{n\pi x}{a}\cos\dfrac{n\pi x_0}{a}\cos\dfrac{l\pi z}{h}\cos\dfrac{l\pi z_0}{h}\cos\dfrac{m\pi y}{b}}{m\left(\dfrac{m^2 k_y}{b^2}+\dfrac{l^2 k_z}{h^2}+\dfrac{n^2 k_x}{a^2}\right)}$$

$$\left.\left[\sin\frac{m\pi y_2}{b}-\sin\frac{m\pi y_1}{b}\right]\left(1-\exp\left[-\frac{\pi^2\tau}{\alpha}\left(\frac{m^2 k_y}{b^2}+\frac{l^2 k_z}{h^2}+\frac{n^2 k_x}{a^2}\right)\right]\right)\right\}\quad\text{(B-15)}$$

At late time, the exponential term becomes zero and Eq. B-15 becomes

$$p_{init}-p(x,y,z,t)=\left[\frac{B_o\mu_o q_o}{abh\alpha}\right]\left\{t+\frac{2\alpha h^2}{\pi^2 k_z}\sum_{l=1}^{\infty}\frac{\cos\dfrac{l\pi z}{h}\cos\dfrac{l\pi z_0}{h}}{l^2}\right.$$

$$+\frac{2\alpha b^3}{\pi^3 k_y\left(y_2-y_1\right)}\sum_{m=1}^{\infty}\frac{\cos\dfrac{m\pi y}{b}\left[\sin\dfrac{m\pi y_2}{b}-\sin\dfrac{m\pi y_1}{b}\right]}{m^3}$$

$$+\frac{4b\alpha}{\pi^3\left(y_2-y_1\right)}\sum_{m=1}^{\infty}\sum_{l=1}^{\infty}\frac{\cos\dfrac{l\pi z}{h}\cos\dfrac{l\pi z_0}{h}\cos\dfrac{m\pi y}{b}}{m\left(\dfrac{m^2 k_y}{b^2}+\dfrac{l^2 k_z}{h^2}\right)}\left[\sin\frac{m\pi y_2}{b}-\sin\frac{m\pi y_1}{b}\right]$$

$$+\frac{2\alpha a^2}{\pi^2 k_x}\sum_{n=1}^{\infty}\frac{\cos\dfrac{n\pi x}{a}\cos\dfrac{n\pi x_0}{a}}{n^2}$$

$$+ \frac{4\alpha}{\pi^2} \sum_{l=1}^{\infty} \sum_{n=1}^{\infty} \frac{\cos\dfrac{n\pi x}{a} \cos\dfrac{n\pi x_0}{a} \cos\dfrac{l\pi z}{h} \cos\dfrac{l\pi z_0}{h}}{\left(\dfrac{l^2 k_z}{h^2} + \dfrac{n^2 k_x}{a^2}\right)}$$

$$+ \frac{4b\alpha}{\pi^3 (y_2 - y_1)} \sum_{m=1}^{\infty} \sum_{n=1}^{\infty} \frac{\cos\dfrac{n\pi x}{a} \cos\dfrac{n\pi x_0}{a} \cos\dfrac{m\pi y}{b}}{m\left(\dfrac{m^2 k_y}{b^2} + \dfrac{n^2 k_x}{a^2}\right)} \left[\sin\frac{m\pi y_2}{b} - \sin\frac{m\pi y_1}{b}\right]$$

$$+ \frac{8b\alpha}{\pi^3 (y_2 - y_1)} \sum_{l=1}^{\infty} \sum_{m=1}^{\infty} \sum_{n=1}^{\infty} \frac{\cos\dfrac{n\pi x}{a} \cos\dfrac{n\pi x_0}{a} \cos\dfrac{l\pi z}{h} \cos\dfrac{l\pi z_0}{h} \cos\dfrac{m\pi y}{b}}{m\left(\dfrac{m^2 k_y}{b^2} + \dfrac{l^2 k_z}{h^2} + \dfrac{n^2 k_x}{a^2}\right)}$$

$$\left[\sin\frac{m\pi y_2}{b} - \sin\frac{m\pi y_1}{b}\right]\Bigg\} \qquad\qquad (B-16)$$

VITA

Rungtip Kamkom received her Bachelor of Engineering in chemical engineering from King Mongkut's University of Technology Thonburi in 1998. She attended the Environmental program at New York Institute of Technology in 1999 and graduated with Master of Science degree in 2001. After that, she entered in the engineering school at University of Texas at Austin and received the Master of Science in petroleum engineering in 2004. She continued her educated at Texas A&M University and completed her Ph.D. in petroleum engineering in 2007.

Rungtip Kamkom can be reached at DeGolyer and MacNaughton, 5001 Spring Valley Road, Suite 800 East Dallas, Texas 75244.